ABSTRACT

Title of Thesis:	A QUANTITATIVE FRAMEWORK FOR UNDERSTANDING THE COMPLEX INTERACTIONS OF COMPETING INTERFACIAL PROCESSES AND IN-SITU BIODEGRADATION
	Mark Adam Johnson, Master of Science, 2004
Thesis Directed By:	Associate Professor Eric A. Seagren, Department of Civil and Environmental Engineering

In Situ bioremediation of contaminated groundwater is made technologically challenging by the physically, chemically, and biologically heterogeneous subsurface environment. Subsurface heterogeneities are important because of influences on interfacial mass transfer processes which impact the availability of substrates to microorganisms. The goal was to develop a quantitative understanding of the impact of interfacial heterogeneities effecting contaminant biodegradation. A quantitative framework of dimensionless parameters was developed to capture the effects of competing physiochemical and biokinetic processes. Two numerical modeling experiments were completed, demonstrating the framework, and how it can be used to determine what engineered enhancements will alleviate the rate-limiting process. Baseline conditions were established to examine intrinsic biodegradation with a set rate-limiting process (either dispersion or biokinetics). Three different engineering controls were then examined. In each case, the control predicted to be appropriate based on the quantitative framework more successfully alleviated the limitation and enhanced biodegradation more than the alternative enhancements.

A QUANTITATIVE FRAMEWORK FOR UNDERSTANDING THE COMPLEX INTERACTIONS OF COMPETING INTERFACIAL PROCESSES AND IN-SITU BIODEGRADATION

By

Mark Adam Johnson

Thesis submitted to the Faculty of the Graduate School of the
University of Maryland, College Park, in partial fulfillment
of the requirements for the degree of
Masters of Science
2004

Advisory Committee:
Associate Professor Eric A. Seagren, Chair
Professor Allen P. Davis
Assistant Professor Jennifer G. Becker

DEDICATION

For Jennifer and Hadley

ACKNOWLEDGEMENTS

First I would like to thank the Department of Civil and Environmental Engineering, and the Graduate Enrollment Management Services for having patience and understanding to allow me to continue on with this research over the last few years. I would especially like to thank Al Santos, for his guidance, and assistance in making sure that I could continue working, even in the face of looming deadlines! I would also like to thank fellow student Xin Song for her assistance and cooperation in this effort.

I would like to thank my advisory committee, Drs. Davis and Becker for their time in reviewing and improving this manuscript, and in assisting me to complete the long journey. I am especially grateful and indebted to Dr. Seagren for his encouragement, enthusiasm, and guidance. In particular, his patience in understanding the need to juggle a professional career and graduate studies has allowed me to continue on with this research (albeit with a time extension or two!). I have learned a great deal on this topic, and on research in general from him, and look forward to continuing in collaboration on future efforts.

Lastly, I would like to thank my wife, Jennifer, without whom, I may not have made it this far. Her love, encouragement, and support has kept me on track, boosting my morale at times, and keeping me focused at others. From simple tasks such as proof-reading, to "being on duty" with our daughter, Hadley, while I worked away in the office, her sacrifices have imparted on me an even greater sense of accomplishment.

TABLE OF CONTENTS

LIST OF TABLES

LIST OF FIGURES

1.0 INTRODUCTION

In situ bioremediation is rapidly becoming a dominant technology utilized by environmental practitioners concerned with remediating subsurface contamination as an alternative to traditional pump-and-treat systems. Data compiled by the US Environmental Protection Agency (USEPA, 1996) indicates that the percentage of Superfund sites for which bioremediation was the selected remedial action technology increased from 13% in fiscal year 1989 to over 37% in fiscal year 1994. Further, since 1991, the percentage of bioremediation projects performed *ex situ* has decreased while the percentage of projects performed *in situ* has increased (USEPA, 2001). For example, in fiscal year 1991, only 35% of the bioremediation remedial action projects at Superfund sites were *in situ* versus 53% in fiscal year 1999 (USEPA, 2001).

Although the practice of *in situ* bioremediation has grown considerably in the past decade through innovations in technologies such as biosparging, bioventing, and oxygen/nutrient releasing compounds, quantitative understanding of the limitations of this complex process is still limited. The complexity of *in situ* bioremediation is due to simultaneous interactions between chemical, physical, and microbiological processes, and is compounded by the heterogeneous nature of many subsurface environments. Further, such heterogeneities vary both in type and scale from micro-scale (e.g., microbially-mediated processes) to macro-scale (e.g., advective transport in layers of varying hydraulic conductivity).

Groundwater transport modeling techniques have been in use for many years to quantitatively examine the subsurface transport of nonreactive contaminants. However, researchers have since recognized the important role of microorganisms in the

understanding of the ultimate subsurface fate of environmental pollutants. In particular, microbially-mediated reactions provide the only option for contaminant destruction in the subsurface. Accordingly, modeling studies undertaken more recently have highlighted this importance of incorporating microbial processes into conceptual and quantitative models of subsurface contaminant transport (Miralles-Wilhelm, et al., 1997).

Microorganisms are widely recognized as being present in all types of terrestrial, aquatic, and subterranean environments. Microbial growth in the subsurface and other environments is dependent upon the presence and quantity of various substrates and nutrients. Specifically, microorganisms require growth substrates, e.g., an electron donor and electron acceptor, as well as various nutrients including nitrogen, phosphorus, and sulfur (e.g., Odencrantz, 1992). Nevertheless, the presence of these constituents alone does not promote cellular growth, as the constituents must be available in aqueous phase, and at sufficient concentrations. The relative availability of the constituents to microorganisms is termed the bioavailability, and plays a key role in determining the success or failure of *in situ* technologies.

When the concentration of a nutrient (or nutrients) falls below a minimum value required to sustain growth, that nutrient (or nutrients) is said to become the limiting nutrient. For example, often nutrients, especially electron acceptors such as oxygen, nitrate and iron, will be depleted in contaminated environments. As a result, one goal of enhanced or engineered bioremediation is to add an abundance of the nutrients that have been determined to be a growth-limiting constituent. However, the addition of nutrients to the subsurface will only be successful if they are transported to the biologically active zone, or BAZ (Rittmann, et al., 1988). Thus, achieving this goal is complicated due to

the heterogeneities in the complex subsurface environment, which influences not only the contaminant location, but the delivery of nutrients as well.

Subsurface heterogeneity in naturally-occurring geologic media has been recognized as a hindrance in the understanding and modeling of the fate and transport of contaminants and other dissolved constituents (Freeze and Cherry, 1979). Indeed, the issue of heterogeneity was noted as impacting the successful application of *in situ* bioremediation early in the development of the field and there continues to be growing in interest with respect to this topic in the field of engineering. In particular, the influence of chemical and physical heterogeneities on the fate of subsurface pollutants, especially with respect to solute transport and/or biodegradation has been examined both in laboratory-scale experiments (e.g., Starr, et al. 1985; Szecody, et al., 1993) and mathematical modeling studies (e.g., Sudicky, et al., 1990; Quinodoz and Valocchi, 1993; Miralles-Wilhelm, et al., 1997; Oya and Valocchi, 1998). In addition, various researchers have examined the interrelationship between mass transfer processes, e.g., the bioavailability of the solute substrate to the microbial cells, and the resulting biotransformation of pollutants (e.g., Ghoshal, et al., 1996; Bosma, et al., 1997; Harms and Bosma, 1997; Ramaswami and Luthy, 1997a; Ramaswami and Luthy, 1997b). This project was focused on expanding upon the above research in an effort to better develop a quantitative understanding of the role of subsurface heterogeneities and interfacial processes with respect to *in situ* bioremediation.

2.0 SCOPE AND OBJECTIVES OF STUDY

The issue of physical and chemical heterogeneities encountered in subsurface environments and their impact on solute fate and transport has been an area of recent interest as was discussed in Chapter 1. In particular, the impact of such heterogeneities, and the resulting hydraulic and geochemical interfaces created by those heterogeneities, on the practice of *in situ* bioremediation is not well understood. The overall goal of the current research was, thus, to develop a fundamental quantitative understanding of the impact of physical, chemical, and biological heterogeneities, and the interfacial interactions resulting from these heterogeneities, on the biodegradation of subsurface contaminants. This goal was accomplished by the following two specific objectives:

1. To develop a quantitative framework comprised of a set of dimensionless parameters based on the relevant subsurface heterogeneities and interfaces, that will capture the effects of the competing physiochemical and biokinetic processes.
2. To conduct a series of systematic modeling experiments to determine the impacts of a wide range of scales and magnitudes of heterogeneities on *in situ* bioremediation, and to use the results to test the quantitative framework's utility for determining what, if any, engineered actions will augment the intrinsic *in situ* biodegradation.

Analysis of the quantitative framework entailed a sequential examination of the various mass-transfer rates and the biokinetics by way of comparison of several dimensionless parameters. The use of the dimensionless parameters (presented in Chapter 4) provides an appealing method for reducing the complexity of the interfacial

and biological kinetics and can be used to imply which given process within environmental system is rate-limiting (Ramaswami and Luthy, 1997a). Furthermore, these dimensionless parameters are defined in a manner such that readily available data or simple pilot-scale measurements that could be made in the field are used to help identify the rate limiting process and, thus, assist practitioners in their remedial alternative selection to enhance the limiting rate.

In the following chapter, Chapter 3, a review of the relevant background literature and an evaluation of contemporary research is completed. Chapter 4 provides the background theory associated with the governing equations for reactive subsurface transport. In addition Chapter 4 presents the derivation and use of dimensionless parameters, and describes the quantitative framework of dimensionless parameters that was used in this work to evaluate the complex interactions between the competing, scale-dependant physical/chemical interfacial processes and *in situ* biodegradation. In Chapter 5, the mathematical model selected to complete the numerical evaluation of the utility of the quantitative framework as a predictive tool is presented. The model is identified, verified through comparison to analytical and alternative numerical solutions, and the scenarios created for testing the quantitative framework are developed. Chapter 6 presents a summary and discussion of the numerical modeling results, and finally, in Chapter 7, the study's conclusions and recommendations for further work are presented.

3.0 BACKGROUND AND LITERATURE REVIEW

3.1 Introduction

This chapter presents the pertinent background information, including a review of the relevant contemporary literature, in support of this research. An understanding of the role of various types and scales of heterogeneities is crucial to this research. Thus, the first topics presented in this chapter include a review of the relevant scales of heterogeneities (e.g., microscopic, mesoscopic, and macroscopic), as well as the types of heterogeneities encountered in the subsurface (e.g., chemical, physical, and microbiological). Second, key background information is presented on the model contaminant, naphthalene, which was selected for this research, including it's sources, biodegradation, sorption, and bioavailability. Finally, this chapter also presents a summary of other modeling efforts that have focused, at least in part, on similar research topics.

3.2 Relevant Scales of Heterogeneities and Interfaces

Spatial heterogeneity in the subsurface can be defined as occurring at scales that range over several orders of magnitude. Specifically, the scales are generally described as microscopic (ranging in scale from 10^{-6} to 10^{-5} m), mesoscopic (ranging in scale from 10^{-5} to 10^{-2} m), and finally, macroscopic (ranging in scale from 10^{-2} to 10^{2} m). In this research, scenarios are developed that examine the microscopic and macroscopic levels of heterogeneity and, thus, these scales are further described in the following sections of this chapter.

Microscale variability occurs on an order of micrometers to millimeters. For example chemical and microbiological species exist at the scale of micrometers, whereas variability in geologic composition occurs at a scale of millimeters, e.g., at the physical scale of soil aggregates. In complex geologic conditions, macroscale heterogeneities range from the individual laminae scale (centimeters) to a site scale of entire geologic strata (meters) to a regional scale (kilometers). Importantly, the various physical and chemical heterogeneities that occur at each of these scales create, either directly or indirectly, interfaces, or boundaries between two phases, where there are strong contrasts in physical and chemical properties that exist over short distances (centimeters to meters) (Brockman and Murray, 1997). Specifically, the strong contrasts in physical and chemical properties at these interfaces control moisture flux, nutrient fluxes, and redox conditions, which, in turn, drive the distribution and activity of microbes in the subsurface (Brockman and Murray, 1997; McMahon and Chapelle, 1991). Further, it is evident that the hydraulic, physical, and geochemical properties for each zone or layer can determine microbial density and activity in that zone or layer (Brockman and Murray, 1997).

3.2.1 Microscale Heterogeneity

The research into the bioavailability of contaminants as microbial substrates has largely focused on pore-scale chemical heterogeneity resulting from interfacial phenomena produced by pore-scale physical heterogeneities of the porous media, especially dissolution at the non-aqueous phase liquid (NAPL)-aqueous phase water interface (e.g., Ramaswami and Luthy, 1997a and 1997b) and at sorption-desorption sites from soil particles (e.g., Brusseau, 1995) or sorption-desorption sites from biomass itself,

called biosorption (Stringfellow and Alvarez-Cohen, 1999). Thus, microscopic to pore-scale heterogeneities are exemplified by molecular level physical and chemical variations such as at the interface between aqueous phase constituents and a NAPL source, or at the interface between the aqueous phase and a solid phase. The interfacial transfer that occurs between such phases can be captured by a dissolution rate (e.g., for NAPL) or soil mass transfer rate (e.g., for solid phase) that can also result in local-scale heterogeneities when the rate is not uniform. Both of these transfer rates can have significant effects on the bioavailability and, thus, the biodegradation of contaminants.

Mass transfer effects on bioavailability and biodegradation have been studied by various investigators (e.g., Ramaswami and Luthy, 1997a and 1997b; Bosma et al., 1997; Harms and Bosma, 1997) in an effort to examine both the bulk mass transfer of contaminant to the microorganisms, as well as the intrinsic or actual microbially-mediated degradation of the contaminant. In certain cases, the actual biokinetics can limit the overall biotransformation rate. In these cases, it may be possible to reduce this limitation by removing a limiting factor (e.g., electron acceptor, or nutrient), or by improving environmental conditions (e.g., temperature or pH), and/or by increasing the amount of active biomass, such as by bioaugmentation (e.g., Rittmann et al., 1990; Smets et al., 1990). However, in reviewing bioremediation data, Bosma et al. (1997) noted that the intrinsic microbial activity (i.e., biokinetics) actually only limited bioremediation in a few cases; while in most cases, the full extent of biodegradation potential was dampened by mass-transfer limitations, e.g., delivery of the contaminant from sorbed-phase or non-aqueous liquid product phase to the aqueous (more readily degradable) phase. In this research the delivery of sorbed-phase contaminants is the focus.

3.2.1.1 Sorption Effects

Sorption (and desorption) processes at the solid phase-aqueous phase interface may determine the local physical and/or chemical conditions by effecting biomass distribution through sorption of microbial cells and/or by effecting aqueous concentrations through solute sorption (van Loosdrecht et al., 1990; Ghiorse and Wilson, 1988; Madsen and Ghiorse, 1993). Under certain conditions, the sorption sink can become very significant, such that a reduction of the aqueous phase solute available for biodegradation is witnessed as has been demonstrated in numerous studies (Miller and Alexander, 1991; Scow and Alexander, 1992; Mihelcic and Luthy, 1991; van Loosdrecht et al., 1990).

The sorption component is modeled using either equilibrium or nonequilibrium rate models (Weber et al., 1991; Toride, et. al, 1993). While equilibrium conditions are more commonly applied, nonequilibrium sorption conditions have been observed under field conditions, such as the well-studied Borden aquifer (e.g., Ball and Roberts, 1991; Brusseau and Rao, 1989) and have been modeled using various approaches including a pore diffusion-based model (e.g., Pedit and Miller, 1995).

As described in Chap. 4, this research employs a relatively straightforward approach for considering mass transfer kinetics between the soil and aqueous phases, utilizing a linear driving force and a lumped first order mass-transfer coefficient (adapted from van Genuchten and Wierenga, 1976). More complex non-linear or non-first order kinetics are beyond the scope of this research, but have been evaluated by others (e.g., Brusseau and Srivastava, 1997).

3.2.1.2 Microbiological Effects

The physical and chemical heterogeneity at the pore-scale, as described above can, in turn, cause microbiological heterogeneity to occur at a pore to pore scale. Specifically, microbial heterogeneity results from varied microbial physiology, or in some cases by the presence or absence of microbial populations all together. Such conditions area result of physical and chemical heterogeneities, and geologic and geochemical conditions (Brockman and Murray, 1997).

3.2.2 Macroscale Heterogeneity

Macroscopic heterogeneities are exhibited on a site or regional scale, and are exemplified by bulk transfer and hydraulic mixing of contaminants and other substrates in the subsurface, such as with the advection and dispersion of a dissolved contaminant plume into a pristine aquifer. In certain conditions, such as in a highly stratified lithology, macroscopic heterogeneity can be further defined at a laminal or stratum scale where the contact between subsurface media with different hydrogeologic properties creates an interface that can affect the mass transport of solutes and the availability of substrates, nutrients and electron acceptor to microbes. Such macroscopic laminal heterogeneities occur in the geologically complex subsurface environment as a result of the stratified nature of the deposits and the actions of geochemical processes over geologic time periods (Brockman and Murray, 1997).

3.2.2.1 Advection and Dispersion

Under this type of heterogeneity, biodegradation of the contaminant is dependant upon or limited by the rate of advection and dispersion of the contaminant from the

contaminated zone into the clean aquifer or from one layer into another of different hydraulic characteristics. Advection specifically refers to the movement of dissolved constituents with the bulk flow of groundwater (Freeze and Cherry, 1979). Obviously, this is an important process for the transport of dissolved substrates and the biodegradation of contaminants. Importantly, as described by Darcy's law, the bulk flow rate of groundwater is proportional to the hydraulic conductivity, K, of the formation. Therefore, heterogeneity in the magnitude of K in the formation has major effects on the movement of dissolved constituents, as discussed further below.

Various scales of heterogeneity also induce mechanical dispersion, or hydraulic mixing, of solutes dissolved in groundwater. Thus, hydrodynamic dispersion plays an important role in creating aqueous-phase chemical heterogeneities because diffusion and the heterogeneity- induced mechanical dispersion are the only mixing process for solutes in the deep subsurface. The resulting effect of dispersion on the rates of solute and nutrient transport and mixing in turn impacts the microbial activity and ultimately *in situ* bioremediation.

3.2.2.2 Hydraulic Conductivity and Stratified Layer Effects

With respect to dispersive mixing, vertical transverse dispersion is a particularly important process for creating zones of mixing (Sudicky et al., 1985). One situation in which vertical transverse dispersion is critical is when there are heterogeneities in hydraulic conductivity. For example, laminal-scale hydraulic layer interfaces can be particularly important because interlayer mass transfer of solutes can affect the rate of supply of limiting substrates, such as oxygen and nutrients near the interface of various layers, such as where a lense or bed of clay in a sand aquifer inhibits transverse

dispersion across its boundary, and thus affects the rate of biodegradation (e.g., Odencrantz, 1992). This interfacial process of hydraulic mixing at the interface between layers, e.g., the interface of the dissolved contaminant plume and the "clean" aquifer of another layer, is induced by variations in porous media which result in a heterogeneous layered hydraulic conductivity distribution. Indeed, laboratory (Szecsody et al., 1994) and modeling studies (Odencrantz, 1992; Wood et al., 1990) with two-dimensional (vertical), two-layer stratified systems, under dual substrate limitation, demonstrate increased microbial activity and biomass production near the two-layer interface where hydraulic mixing between waters carrying different substrates occurs due to dispersion. Further, field studies have also indicated that varying layers of hydraulic conductivity are an important factor controlling *in situ* biodegradation (Molz and Widdowson, 1988; Barker et al., 1987). Heterogeneity of the hydraulic conductivity also occurs on a "small scale" below the observational scale of most field investigations, such as in the Borden aquifer (e.g., Sudicky, 1986). Experimental (Murphy et al., 1997) and modeling (MacQuarrie and Sudicky, 1990a; Murphy et al., 1997) studies indicate that small-scale hydraulic conductivity heterogeneity with dual substrate limitation can create regions of increased solute mixing, which in turn result in enhanced microbial growth. Therefore, hydraulic conductivity heterogeneities have significant impacts on microbial activity and biomass production by creating hydraulic interfaces where mixing between waters carrying different substrates occurs.

A second case for which transverse dispersivity is critical is for oxygen transfer across the water table. Theoretical and field studies (Borden and Bedient,1986; Borden et al., 1986) indicate that vertical transverse dispersion can have a significant impact on

oxygen exchange and the contaminant decay rate; however, the weak vertical dispersion/diffusion process limits this impact to relatively shallow plumes, e.g., less than two meters below the water table (MacQuarrie and Sudicky, 1990b).

3.3 Naphthalene: Sources, Biodegradation, and Bioavailability

Naphthalene was selected as the specific model electron-donor contaminant substrate for this study because of its importance as a pollutant, and its biodegradability. In addition, although like other polycyclic aromatic hydrocarbons (PAHs) it has generally poor mobility in the environment (e.g., low solubility, high sorption, and low volatility), it has a sufficiently high water solubility to facilitate the laboratory experiments performed by other students as part of this project. Naphthalene is a PAH manufactured from petroleum refining and coal tar distillation processes (Vershueren, 2001). Its chemical formula is $C_{10}H_8$, consisting of two cyclic, planar aromatic carbon-hydrogen rings, as shown in Figure 3.1.

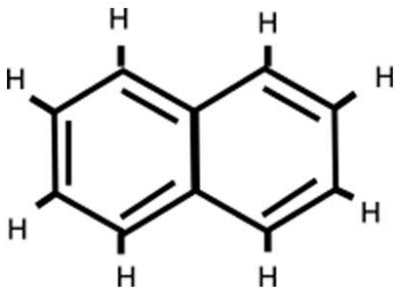

Figure 3.1. Chemical structure of Naphthalene.

Numerous products include naphthalene as a component, such as moth balls, solvents, lubricants, cleaners/degreasers, and petroleum products, e.g., gasoline, diesel,

and No. 2 fuel oil. The subsurface presence of naphthalene is, thus, often ubiquitous due to its presence in so many common products, especially in petroleum fuels, and the resulting accidental releases of these products (e.g., from leaking underground storage tanks). Naphthalene is also commonly found as a subsurface contaminant at former manufactured gas plants (MGP), and thus researchers (e.g., Ghosal, et al., 1996; Ramaswami and Luthy, 1997) have investigated the biodegradation of naphthalene derived from or in the presence of residual coal tar associated with the MGP sites.

Laboratory and field investigations have explored the biodegradation (both aerobic and anaerobic, e.g., denitrifying) as well as the sorption-desorption and bioavailability of naphthalene. Early research in which the microbially-mediated degradation of naphthalene was observed dates to the 1970's (e.g., Cerniglia and Gibson, 1977). Subsequent work expanded to include the investigation of the biodegradation of naphthalene in environmental microcosms (Heitkamp, et al., 1986) and later the evaluation of naphthalene degradation under varying aerobic and denitrifying conditions (Mihelcic and Luthy, 1988a, 1998b, 1991; Wilson, et al., 1997; Rockne and Strand, 2001: Durant, et al., 1997).

Using the method of McCarty (1975), Durant, et al. (1997) presented the stoichiometry of naphthalene biodegradation under aerobic and denitrifying conditions, respectively, as follows:

$$C_{10}H_8 + 5.83O_2 + 0.88NO_3^- + 0.88H^+ \Rightarrow 0.88C_5H_7O_2N + 5.6CO_2 + 1.34H_2O \qquad (3.1)$$

$$C_{10}H_8 + 5.66NO_3^- + 5.66H^+ \Rightarrow 0.86C_5H_7O_2N + 5.71CO_2 + 2.40H_2O \qquad (3.2)$$

In both cases, nitrate was assumed to be the nitrogen source. These equations served as the basis for the conceptual model of biodegradation utilized in this research, and were used as the stoichiometric basis for developing reaction parameters (e.g., yield coefficients), as discussed further in Chap. 5.

Several investigators have examined the impact of sorption on the bioavailability and biodegradation of naphthalene. Mihelcic and Luthy (1991) developed a model of a sequential solute (naphthalene) desorption-degradation process. It was experimentally observed that the naphthalene sorption-desorption process was reversible and rapid with respect to the subsequent rate of microbial degradation of the desorbed aqueous-phase naphthalene. Other researchers have further examined the sorption-desorption kinetics of naphthalene (e.g., Connaughton, et al., 1993). In addition, evidence of the sequential sorption-desorption-biodegradation process has subsequently been presented by others (e.g., Guerin and Boyd, 1997; Guerin and Boyd, 1992; Park, et al., 2002). Although much of the research has focused on biodegradation of the solute naphthalene, others have also examined the bioavailability and degradation of sorbed or non-desorbing naphthalene (Guerin and Boyd, 1997; Guerin and Boyd, 1992; Burgos, et al., 1999; Park et al., 2001). In general, this research has found the sorbed-phase naphthalene to be biodegradable, but at lesser rates and extents than for aqueous naphthalene. Guerin and Boyd (1992) found the bioavailability of sorbed-phase naphthalene to be highly variable with respect to different bacteria, and concluded that important organism-specific properties were responsible for the extent of sorbed naphthalene bioavailability. Accordingly, most modeling evaluations conservatively assume that only aqueous-phase naphthalene is bioavailable, in part to reduce the computational runtimes.

Other research has focused on the bioavailability of naphthalene in the presence of, or after dissolution from, a non-aqueous phase liquid, e.g., pure phase coal tar (e.g., Ghosal, et al., 1996; Ghosal and Luthy, 1996; Ramaswami and Luthy, 1997a and 1997b). In all cases, naphthalene was found to become bioavailable after its dissolution from the coal tar; however, the extent of the bioavailability and subsequent rate of biomineralization was dependant on the rate of mass transfer (dissolution) of the naphthalene from the coal tar non-aqueous phase liquid into the aqueous phase.

3.4 Reactive Transport Modeling

Various types of numerical computer models have been developed to investigate the fate and transport of groundwater contaminants. Typically, such models vary in several key aspects. For example, models can vary from one to three dimensions, with the latter being more sophisticated. In addition, models often differ in the ability to vary from steady-state to transient conditions. Also, the number and complexity of the modeled components can vary significantly, ranging form basic two substrate models (electron donor and electron acceptor) to complex models that can incorporate sequential decay of multiple species, or that can incorporate complexation reactions of integrated reduction-oxidation processes. Furthermore, the reactions that the solute(s) undergo(es) also can vary between models. Degradation can range from basic first-order decay, to more sophisticated biokinetics such as single or double Monod kinetics or biofilm kinetics. Sorption effects can also be implemented via varying means of describing water-soil partitioning, including linear, Freundlich, and Langmuir partitioning, and can also differ in regards to the kinetic treatment of sorption (and desorption) including equilibrium and non-equilibrium kinetics. Lastly, the techniques for solving the

numerical structure can vary, including Crank-Nicholson Finite-Difference, Galerkin Finite Element, Eulerian-Legrangian, Runge-Kutta, and Operator Splitting techniques. A discussion of the benefits and drawbacks of each of these types of models is beyond the scope of this research; however, compilations and comparisons of some of these aspects have been completed by others (e.g., Srivastava and Brusseau, 1996).

Several numerical models of the fate and transport of groundwater contaminants are readily available and/or have been used by numerous researchers. The Principle Direction finite element method developed by Frind (1982) served as the basis for several numerical codes, including PDPRIME, PDREACT, and FEREACT as summarized by Odencrantz (1992). This group of numerical codes, originating with PDPRIME, and modified through to FEREACT, have been well-documented in the literature (e.g., MacQuarrie and Sudicky, 1990a and 1990b; Oya and Valocchi, 1998; Odencrantz, 1992; and Tebes-Stevens, et al., 1998). Rifai et al. (1988) and Rifai and Bedient (1990) developed a two-dimensional code, BIOPLUME I/II that is commonly in use due to it's widespread availability from the US Environmental Protection Agency. A multi-species fate and transport model MT3D was developed by Zheng (1997) and later derived into a reactive multi-species model, RT3D (Clement, 1997). Lesser known, or non-commercially or publicly available models have also been developed by numerous researchers (e.g., Srivastava and Brusseau, 1996).

Importantly, there have been a number of numerical modeling efforts that have examined heterogeneous subsurface flow and complex biodegradation kinetics and which are, therefore, useful for comparison to the results of this work. This research was discussed above in Section 3.2, as part of the review of subsurface heterogeneities and

interfaces. However, these modeling efforts are reiterated here in terms of the relevant concepts examined, in order to set up the discussion in Chap. 6. Specifically, for the case of heterogeneous subsurface conditions, many modeling efforts have examined randomly heterogeneous hydraulic conductivity or velocity (e.g., Sudicky, et al., 1990; Yabusaki, et al., 1998; MacQuarrie and Sudicky, 1990a and 1990b; Srivastava and Brusseau, 1996; Quinodoz and Valocchi, 1993), or stratified heterogeneous conditions (e.g., Oya and Valocchi, 1998; Wood et al., 1994; Starr et al., 1985; Szecsody et al., 1994; Odencrantz, 1992). Further, the use of Monod-type kinetics in conjunction with heterogeneous transport has been examined by several investigators (e.g., MacQuarrie and Sudicky, 1990a and 1990b; and Odencrantz, 1992).

4.0 DEVELOPMENT OF QUANTITATIVE FRAMEWORK

This chapter presents the mathematical background and derivation of the equations developed to investigate the research problem. The governing equations for the problem are presented, and a system of dimensionless parameters and a quantitative framework for evaluating the equations are developed.

4.1 Governing Equations

The governing equation of reactive solute transport utilized for the research problem is the two-dimensional form of the oft-applied advection-dispersion-reaction (ADR) equation,

$$\frac{\partial S}{\partial t} = D_x \frac{\partial^2 S}{\partial x^2} + D_y \frac{\partial^2 S}{\partial y^2} - \frac{q_x}{nS_w}\frac{\partial S}{\partial x} \pm G_i \qquad (4.1)$$

where S is the aqueous-phase solute concentration [M L^{-3}], t is time [T]; D_x is the longitudinal hydrodynamic dispersion coefficient [L^2T^{-1}]; x is distance in the direction of flow [L]; y is distance in the direction vertically transverse to the direction of flow [L]; D_y is the transverse hydrodynamic dispersion coefficient [L^2T^{-1}]; q_X is the specific discharge [LT^{-1}]; n is soil porosity; S_W is the water saturation; and G_i is the source/sink term [$ML^{-3}\ T^{-1}$] where i denotes any number of source or sink equations, e.g., sorption, G_S, or biodegradation, G_B.

The partial differential terms on the right side of Eq. 4.1 represent longitudinal dispersion, transverse dispersion, and longitudinal advection, respectively. This research

assumes isotropic, homogeneous hydraulic conductivity with one-dimensional flow within each layer of the model; thus, there is no transverse advection term.

In the following paragraphs the processes of advection and dispersion are reviewed in more detail. In addition, two source/sink terms are developed to represent the reaction processes, G_i, that were utilized for the numerical experiments. These processes are aqueous-phase solute biodegradation, denoted G_B, and kinetic sorption between aqueous-phase solute and solid matrix, denoted G_S.

4.1.1 Advection

Advection is the bulk or macroscopic process by which solute is transported by the motion of flowing groundwater. In eq. 4.1 above, advection is described by the q_x/nS_w term. As mentioned above, the model is assumed to be homogenous and isotropic with respect to hydraulic conductivity in each layer, with only one direction of flow. Commonly, this principle direction of the flow is the x-direction. Because flow within each layer is characterized by steady-state conditions with saturated flow and constant porosity, the term q_x/nS_w can be replaced by v_x, or simply v when it is assumed that flow occurs only in the x-direction, which is the seepage or average pore velocity in the longitudinal direction. Seepage or average pore velocity can be defined from Darcy's Law as,

$$v = -\frac{K}{n}\frac{dh}{dl} \tag{4.2}$$

where K is the hydraulic conductivity [LT^{-1}], n is porosity as defined above, and dh/dl is the hydraulic gradient over the model region or domain [LL^{-1}] (Freeze and Cherry, 1979).

4.1.2 Dispersion

Dispersion is the process by which a solute spreads away from the path predicted or expected from advection or bulk movement alone. For two-dimensional isotropic systems, dispersion is limited to longitudinal dispersion in the direction of flow (the x-direction) and transverse dispersion perpendicular to the flow direction. From Eq. 4.1, above, the components for dispersion are,

$$\frac{\partial S}{\partial t} = D_x \frac{\partial^2 S}{\partial x^2} + D_z \frac{\partial^2 S}{\partial z^2} \tag{4.3}$$

where D_x and D_z are the longitudinal and transverse hydrodynamic dispersion coefficients [L^2T^{-1}], respectively. The hydrodynamic dispersion coefficients represent the combined effects of mechanical and molecular diffusion, and can be defined as follows:

$$D_i = \alpha_i v_i + D^* \tag{4.4}$$

where D_i represents the hydrodynamic dispersion coefficient in direction *i*, α_i is the dynamic dispersivity in direction *i* [L], and D* is the effective coefficient of molecular diffusion in the porous medium [L^2T^{-1}]. The dynamic dispersivity is a characteristic property of the porous medium, whereas the coefficient of molecular diffusion is a characteristic property of the solute (Freeze and Cherry, 1979). The partial differential terms on the right side of Eq. 4.3 are second order because dispersion is proportional to the concentration gradient.

4.1.3 Reactions

The following sub sections present the equations for the two kinetic reaction terms focused on in this research: sorption and biodegradation.

4.1.3.1 Kinetic Sorption

The first of the two reaction terms to be discussed is sorption. For this project it is assumed that only the electron donor solute is subject to sorption as has been done by others (e.g., Oya and Valocchi, 1997; McGuire, et al 2002). Therefore, only one equation representing sorption (for the electron donor) is required. For this research, a simple approach was applied for describing the mass-transfer kinetics between soil aggregates and the mobile water phase, with a linear driving force (Lapidus and Amundson, 1952; van Genutchen and Wierenga, 1976):

$$G_S = \frac{\partial S}{\partial t} = -k_m \left(S - \frac{\bar{S}}{K_d} \right) \tag{4.5}$$

where $\bar{S}$ is the solid-phase or sorbed electron donor concentration [MM^{-1}], k_m is the kinetic mass transfer coefficient [T^{-1}], and K_d is the linear partitioning coefficient [L^3M^{-1}]. The term $\bar{S} / K_d$ represents the aqueous concentration of solute that would be in equilibrium with the sorbed electron donor concentration. Thus, at equilibrium, the term in the parentheses is zero, and there is no change in concentration over time. At any other value, the term in the parentheses can be seen as an expression of the distance from equilibrium (Tebes-Stevens, et al, 1998), the magnitude of which is the driving force for sorption or desorption. A greater difference in the S and $\bar{S}/K_d$ values results in a "steeper" gradient. The magnitude of the kinetic mass transfer coefficient, k_m, term represents rate limitations due to the sorption processes such as availability of sorption sites. Note that the equation can be forced into equilibrium conditions if a relatively large

value of is k_m is used, e.g., on the order of 200 day^{-1} (Valocchi, et al. 1998) to 1000 day^{-1} (Tebes-Stevens, et al. 1998).

4.1.3.2 Double-Monod Biodegradation

As stated in Chapter 3, it is widely recognized that biologically-mediated metabolic reactions can reduce contaminant concentrations in subsurface environments. Three conceptual models have been used to describe biodegradation in the subsurface (Baveye and Valocchi, 1989): (1) the biofilm model, (2) the microcolony model, and (3) the strictly macroscopic model. Odencrantz (1992), performed a comparison of two of the three types, namely the biofilm and macroscopic models, and found that the two model solutions converged for the organic substrate plume and biomass distribution for realistic groundwater conditions. Thus, the use of either biofilm or Monod kinetics could be selected based on the needs in defining and solving the research problem. In the case where the goal is to model solute concentration, the added complexity of the biofilm (and microcolony) model(s) is probably not needed for the typical groundwater scenarios. Therefore, the macroscopic model was selected for this research.

In addition to the conceptual model, it is also necessary to select a model for the substrate utilization kinetics. The multiplicative Monod model has been applied by numerous authors (e.g., Borden and Bedient, 1986; MacQuarrie and Sudicky, 1990; MacQuarrie, et al., 1990; and Odencrantz, 1992) for modeling multiple substrate limited biodegradation in subsurface environments. Therefore, the multiplicative Monod model was applied in this research to incorporate dual substrate limiting biokinetics for modeling biological growth in the saturated geologic media. Use of a model that accounts for dual substrate limitation is critical for this research because it allows for the

investigation of the use of engineered efforts undertaken in order to enhance the rates of biodegradation reactions, as is the case where limiting nutrients or electron acceptors are supplied to the subsurface via various methods of injection.

Dual substrate limitation as applied to substrate utilization can be expressed by the multiplicative Monod model as follows:

$$G_B = \frac{\partial S}{\partial t} = -q_{\max} X \left(\frac{S}{K_S + S} \right) \left(\frac{A}{K_A + A} \right) \tag{4.6}$$

where q_{max} is the maximum specific substrate utilization rate [$M_{donor}M^{-1}_{cells}T^{-1}$]; X is total biomass concentration (pore volume basis, i.e. the total concentration of cells per liter of pore water) [$M_{cells}\ L^{-3}$]; S is electron donor substrate concentration (as previously defined) [$M\ L^{-3}$]; K_S is the donor half-maximum rate constant [$M\ L^{-3}$]; A is electron acceptor substrate concentration [$M\ L^{-3}$]; and K_A is the acceptor half-maximum rate constant [$M\ L^{-3}$]. The practical application of the multiplicative equation in analyzing rate-limited reactions is provided in a simple example. In an evaluation of the effect of limited donor or acceptor availability on biodegradation, mathematical analyses reveals that as either [A] or [S] become limited (i.e., approach very small values or zero), that portion of the equation will approach zero as well. Thus, through the multiplicative process, so too will the entire equation approach zero, and the overall equation, G_B.

4.1.4 Biomass

Biomass growth is proportional to substrate utilization described by the multiplicative Monod model of Eq. 4.6, given above, where the proportionality factor is Y, the true yield coefficient. In addition to biomass growth, loss or death of biomass

must also be taken into account, which is represented by a kinetic decay term. Therefore, the equation for biomass takes the form,

$$\frac{\partial X}{\partial t} = q_{\max} Y X \frac{S}{K_S + S} \frac{A}{K_A + A} - k_d X \tag{4.7}$$

where k_d is a biomass decay coefficient [T^{-1}].

4.1.5 Summary of Governing Equations

A reactive transport model that effectively describes a subsurface scenario must solve a system of linear or nonlinear equations. The number of equations in the system is dependant upon the number of individual components with the system. For a system with two aqueous substrates (electron donor and electron acceptor), and two immobile components (biomass and substrate), a system of four equations is required.

Rearranging the terms in Eq. 4.1 and substituting in the kinetic reaction terms of Eqs. 4.5 and 4.6 yields the following governing equation for the electron donor substrate:

$$\frac{\partial S}{\partial t} = D_x \frac{\partial^2 S}{\partial x^2} + D_z \frac{\partial^2 S}{\partial z^2} - v \frac{\partial S}{\partial x} - k_m \left(S - \frac{\bar{S}}{K_d} \right) - q_{\max} \gamma X \left(\frac{S}{K_S + S} \right) \left(\frac{A}{K_A + A} \right) \tag{4.8}$$

where γ is the stoichiometric yield coefficient, and all other terms are as previously defined. The governing equation for electron acceptor is comparable to Eq. 4.8, with the exception that the electron acceptor is considered nonsorbing, and thus the sorption term is deleted:

$$\frac{\partial A}{\partial t} = D_x \frac{\partial^2 A}{\partial x^2} + D_z \frac{\partial^2 A}{\partial z^2} - v \frac{\partial A}{\partial x} - q_{\max} \gamma X \left(\frac{S}{K_S + S} \right) \left(\frac{A}{K_A + A} \right) \tag{4.9}$$

where all other terms are as previously defined. The governing equations for biomass growth and solid-phase donor, respectively, are summarized below,

$$\frac{\partial X}{\partial t} = q_{\max} Y X \frac{S}{K_S + S} \frac{A}{K_A + A} - k_d X \tag{4.10}$$

$$\frac{\partial \bar{S}}{\partial t} = k_m \frac{\theta}{\rho_b} \left(S - \frac{\bar{S}}{K_d} \right) \tag{4.11}$$

where bulk density (ρ_b) and porosity (θ) have been added to present the sorbed phase ($\bar{S}$) on a mass per mass of aquifer solids basis. Thus, the numerical model utilized during this research had to solve a system of four equations based on Eqs. 4.8 through 4.11, above.

4.2 Dimensionless Parameters

One goal of this research is to develop a simple predictive tool that can be utilized to determine what enhancements or other engineering activities would be beneficial for accelerating bioremediation at a site. This is achieved by developing a means of evaluating the system of equations developed above that characterize the *in-situ* environment.

A group of dimensionless parameters was developed that can be used to quickly compare the rate of the various processes occurring, e.g., advection, dispersion, sorption, biodegradation or non-aqueous phase liquid dissolution. Once developed, a comparison of these dimensionless parameters can be used to predict which of the subject rates are the so-called rate-limiting process in the system. Use of dimensionless parameters for comparing complex interactions or rate-limiting processes in contaminated environments

has been previously documented in the literature (e.g., Seagren, et al. 1993, Brusseau, 1995, Ramaswami and Luthy, 1997, Oya and Valocchi, 1998, Brusseau, et al. 1999). Such parameters are developed by substituting non-dimensional units of time, mass, and length into the equations developed for the analysis. For this research, non-dimensional units were substituted into Eqs. 4.8 through 4.11. The non-dimensional units of time (t*) direction (x*, z*), and concentration (S*, A*, and X*) used in this research are summarized in Fig. 4.1, where L is the characteristic length (i.e. the length of the domain) [L], S_0 is the initial substrate concentration [ML^{-3}], $\bar{S}_0$ is the initial sorbed-phase concentration [MM^{-1}], A_0 is the initial acceptor concentration [ML^{-3}], and X_0 is the initial biomass concentration [MM^{-1}]. All initial concentration values reference the background or injected concentration for the cases where no background concentration of the species is present.

$$x^* = \frac{x}{L} \qquad z^* = \frac{z}{L} \qquad t^* = \frac{t}{L/v_x} \qquad S^* = \frac{S}{S_0}$$

$$\bar{S}^* = \frac{\bar{S}}{\bar{S}_0} \qquad A^* = \frac{A}{A_0} \qquad K_S{}^* = \frac{K_S}{S_0} \qquad K_A{}^* = \frac{K_A}{A_0} \qquad X^* = \frac{X}{X_0}$$

Figure 4.1. Dimensionless units (e.g., Oya and Valocchi, 1998)

Following substitution of the above non-dimensional units, Eq. 4.8 can be re-written as follows:

$$\frac{\partial S^*}{\partial t^*} = \frac{D_x}{L v_x}\frac{\partial^2 S^*}{\partial x^{*2}} + \frac{D_z}{L v_x}\frac{\partial^2 S^*}{\partial z^{*2}} - \frac{\partial S^*}{\partial x^*} - \frac{L k_m}{v_x}\left(S^* - \bar{S}^*\right) - \frac{q_{\max} X_o L}{S_o v_x} X^* \left(\frac{S^*}{K_S{}^* + S^*}\right)\left(\frac{A^*}{K_A{}^* + A^*}\right) \tag{4.12}$$

Although not shown here, a similar dimensionless equation can be derived for the electron acceptor, biomass, or solid phase starting from Eqs. 4.9 through 4.11; however, for this research, the dimensionless parameter framework focuses on the removal of electron donor from the system, and thus only Eq. 4.12 is shown. Each of the terms in Eq. 4.12 (advection, diffusion, reactions) has an associated dimensionless group of constants that represents the relative rate of change for that term as compared to advection. For example, the rate of change for transverse dispersion relative to advection can be observed by inspection of the term D_z / Lv_x. Further, additional relative rate terms can be constructed by comparing the various dimensionless relative rate terms from Eq. 4.12 to each other. For example, comparison of the term that represents the relative rate of biodegradation to advection ($q_{\max} X_o L / S_o v_x$) to the term D_z / Lv_x, can by rearranging of the terms, result in a parameter $q_{\max} X_o L^2 / S_o D_z$, which can be used to compare the relative rate of biodegradation to the transverse dispersion. By convention, the dimensionless parameters used herein are written only in terms of the electron donor, as derived from Eq. 4.12 as described above, although similar comparisons can be made for the system of dimensionless parameters for electron acceptor. It is not as common to complete this as the electron acceptor is typically modeled as non-sorbing and non-degrading, and thus the suite of dimensionless parameters becomes limited in nature.

For this research, dimensionless numbers were derived from the dimensionless parameters evaluated from Eq. 4.12, and are presented in Fig. 4.2 (note that the z in the

transverse hydrodynamic dispersion coefficient D_z has been replaced with a T to more effectively depict the transverse nature of the term):

$$Pe_T = \text{Transverse Peclet Number} = \left(\frac{advection\ \ rate}{transverse\ \ dispersion\ \ rate}\right) = \frac{v_x L}{D_T}$$

$$St_2 = \text{Stanton Number 2} = \left(\frac{soil\ \ mass\ \ transfer\ \ rate}{advection\ \ rate}\right) = \frac{Lk_m}{v_x}$$

$$Da_2 = \text{Damköhler Number 2} = \left(\frac{biodegradation\ \ rate}{advection\ \ rate}\right) = \frac{q_m X_o L}{v_x S_o}$$

$$Da_5 = \text{Damköhler Number 5} = \left(\frac{biodegradation\ \ rate}{soil\ \ mass\ \ transfer\ \ rate}\right) = \frac{Da_2}{St_2} = \frac{q_m X_o}{S_o k_m}$$

$$Da_6 = \text{Damköhler Number 6} = \left(\frac{biodegradation\ \ rate}{transverse\ \ dispersion\ \ rate}\right) = Da_2 \times Pe_T = \frac{q_m X_o L^2}{S_o D_T}$$

$$Sh_2' = \text{Modified Sherwood Number 2} = \left(\frac{soil\ \ mass\ \ transfer\ \ rate}{transverse\ \ dispersion\ \ rate}\right) = St_2 \times Pe_T = \frac{L^2 k_m}{D_T}$$

Figure 4.2. Definition of dimensionless numbers and parameters.

4.3 Dimensionless Parameter Framework

Using the dimensionless parameters presented in Section 4.2, a framework was developed to quantitatively identify the rate-limiting process (after Ramaswami and Luthy, 1997). The framework, depicted in Fig. 4.3, presents a flowchart that can be used to identify the rate-limiting process. The first three steps of the flowchart are used to identify the limiting mass-transfer rate (e.g., advection or dispersion and soil mass transfer or sorption). The fourth step compares the limiting mass transfer process with

the biodegradation rate to determine the overall rate limiting process for the system. This type of approach is viable as long as the dimensionless parameters are significantly smaller or larger then unity, beyond which the results may not be conclusive (Ramaswami and Luthy, 1997). In practice, the dimensionless parameters are recommended to be less than 0.2 for cases where the value is to be less than unity, and 5 for cases where the value is to be greater than unity (Ramaswami and Luthy, 1997).

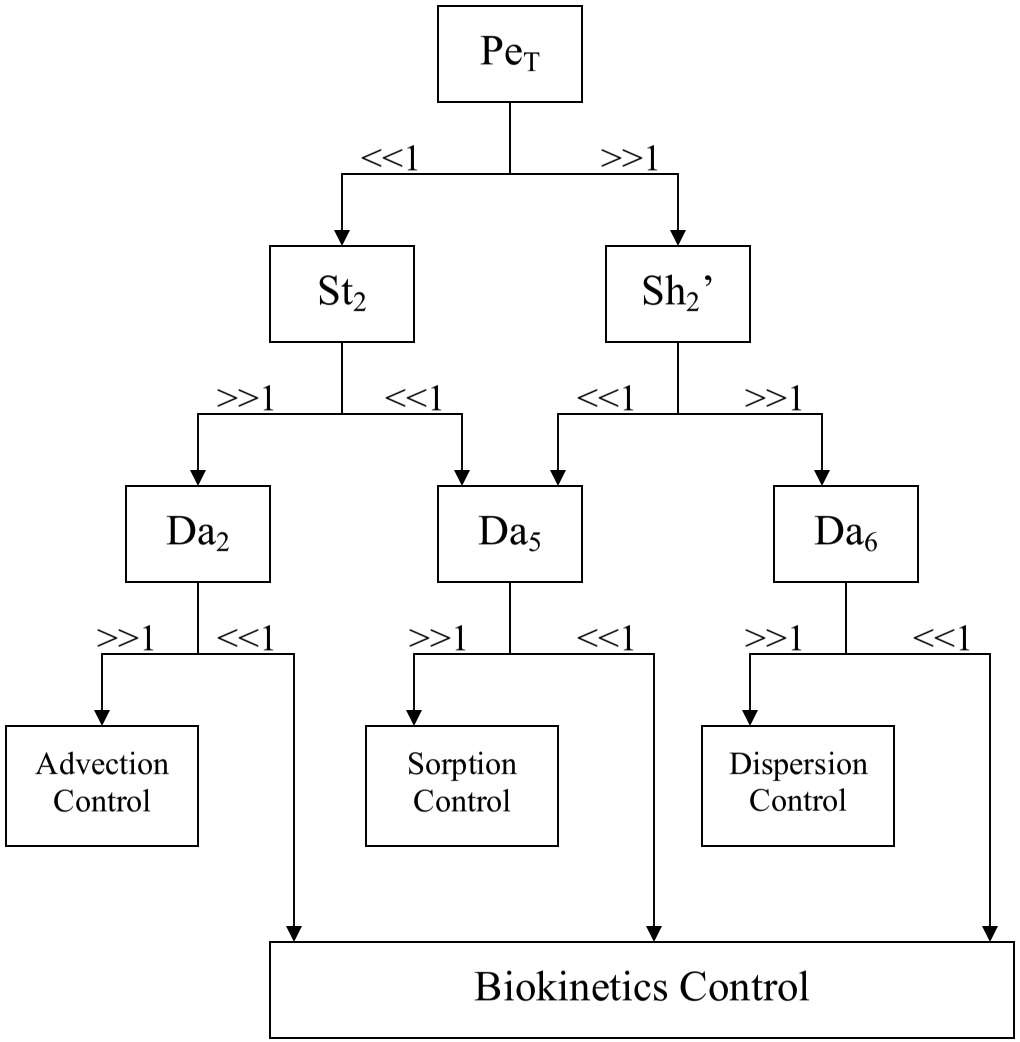

Figure 4.2. Quantitative framework development. (adapted from Ramaswami and Luthy, 1997)

4.4 Analysis of Framework Experimental Scenarios

The following section introduces the baseline experiments (scenarios) that were used to analyze the utility of the dimensionless parameter framework developed in Section 4.3. The baseline scenarios were designed to provide a useful evaluation of the framework. In addition, as is discussed further in Chapter 5, simulated engineering enhancements were made to the baseline scenarios to further test the predictive capabilities of the framework. Specifically, the quantitative framework was used to predict the rate-limiting process and guide selection of an appropriate remedy to alleviate that limitation and enhance the biodegradation rate.

4.4.1 Baseline Simulations

The baseline simulation scenarios were developed such that numerical modeling and laboratory-scale experimental conditions could be evaluated. This research focuses on the use of numerical simulations to evaluate two baseline conditions. These baseline simulations are termed experiments #1(a) and #3, following the terminology developed in conjunction with ongoing laboratory experiments being performed by Ms. Xin Song, a Ph.D. candidate in the Department of Civil and Environmental Engineering, University of Maryland, College Park. In each of these scenarios, the conditions were selected such that the overall biotransformation rate is limited by a single interfacial mass-transfer process (advection, sorption, or dispersion) or biokinetics.

First, in Experiment #1(a), a two-layered porous media was developed such that macro-scale transverse dispersion controls. This was established by selecting values of the hydraulic conductivity and seepage velocity so that transverse dispersion from the

fast-conductivity layer to the slow-conductivity layer was the rate-limiting process. This experiment was performed under conditions to promote relatively fast biokinetics and rapid sorption/desorption to prevent either of these from becoming the limiting process. In this scenario, a slug of electron donor is present in an otherwise pristine system (e.g., the leading edge of a migrating plume) and observations are made as to the effects of advection on the biodegradation.

Second, in Experiment #3, the porous media and sorption characteristics remain the same as in #1(a), but the biological parameters were altered so that slower biokinetics prevailed as the overall rate limiting process. Similar to #1(a), a "plume front" of an input slug was observed; however, this time under varying biokinetics. Additionally, the plume was not in the form of an existing "slug" under initial conditions, but rather the plume was injected over the early timeframe of the model run and observations were made once the injection was stopped.

5.0 NUMERICAL MODELING

In the previous chapter, a quantitative framework and a system of equations required to solve the problem task were developed. This chapter describes the process used in this study to develop a numerical model and code to solve the system of equations, and ultimately evaluate the quantitative framework.

5.1 Evaluation of Numerical Codes

Numerous academic and commercial multidimensional reactive transport models exist for the mathematical analysis of subsurface flow. Such models generally vary with respect to several key features, namely the ease of use and alteration (e.g., FORTRAN or C++ based codes), the availability of user-friendly interface (e.g., Microsoft WINDOWS®-based graphical user interfaces, or GUIs), and the output formats (ASCII text and/or data files). The objective of the numerical code selection process in this study was to utilize an existing modeling program and to only modify the code as necessary to evaluate the quantitative framework and analyze the scenarios introduced in Chapter 4.

The numerical codes selected for evaluation had to meet the criteria needed to model the system of governing equations. Specifically, the codes needed to include multi-species reactive transport of the aqueous components, include key interactions with immobile system components (e.g., contaminant associated with the solid-phase and attached biomass), and be capable of capturing multiple kinetic reactions (e.g., biokinetics, and the kinetics of sorption) coupled together in one time step. Numerous codes are available allowing the user to model either the kinetics of sorption or biodegradation; however, a review of publicly-available products that could directly

model both kinetic components simultaneously limited the options significantly. The resulting evaluation was completed for two models that appeared to meet the requirements of the study: FEREACT, a model with built-in capabilities of modeling both types of kinetics, and RT3D (*R*eactive *T*ransport in *3*-*D*imensions), a flexible modular-based program without the internal or pre-packaged ability to model both kinetics, but with a means that allows for the inclusion of relatively straightforward user-defined kinetic modules.

5.1.1 PDREACT/FEREACT

FEREACT, a finite element multi-species reactive transport model for one and two dimensional steady-state groundwater flow conditions was developed by Dr. Albert Valocchi and co-workers at the University of Illinois at Urbana-Champaign. FEREACT was based upon two previous numerical codes PDREACT and PDPLUS also developed by Valocchi and co-workers, and has, thus, undergone significant testing and verification (e.g., Tebes-Stevens et al., 1998). The significant change between FEREACT and its predecessors is the manner and method used to solve the kinetic and transport equations (Valocchi et al., 1998).

FEREACT was initially chosen for use in this study primarily because it is a FORTRAN program that is easily executed utilizing a UNIX mainframe, its stated ease of use, and its modular reaction structure allowing for a wide variety of reactive scenarios, as well as the inclusion of user-defined and generic kinetic reactions. Thus, the use of FEREACT required no underlying code alterations. Valocchi et al. (1998) and Tebes-Stevens et al. (1998) provide a summary of the operation of FEREACT.

FEREACT was developed primarily to examine the coupled effects of two-dimensional steady-state flow, equilibrium aqueous speciation and kinetically-controlled interphase reactions. Based upon a model assumption of steady-state flow under saturated conditions, the governing equation for the aqueous components in FEREACT is,

$$\frac{\partial C_j}{\partial t} + L\left(C_j\right) = R_j \qquad j = 1..N_C \tag{5.1}$$

where C is the aqueous component concentration; $L(C_j)$ is the advection-dispersion operator; R_j is the reaction source/sink terms; and N_c is the number of aqueous components, j.

For one-dimensional saturated flow through hydraulically homogeneous and isotropic media, with homogeneous anisotropic dispersion within each aquifer layer, the advection-dispersion operator can be written as,

$$L(C) = \frac{\partial}{\partial x}\left(v_x C - D_x \frac{\partial C}{\partial x}\right) + \frac{\partial}{\partial y}\left(D_y \frac{\partial C}{\partial y}\right) \tag{5.2}$$

where all parameters are as previously defined in Chapter 4. For the case of two aqueous substrates, e.g., an electron donor and electron acceptor, N_c equals two, and Eq. 5.1 can be written for each component as follows:

$$\begin{aligned} \frac{\partial C_S}{\partial t} + L(C_S) &= R_S \\ \frac{\partial C_A}{\partial t} + L(C_A) &= R_A \end{aligned} \tag{5.3}$$

where S denotes the electron donor substrate and A denotes the electron acceptor substrate, as has been described in Chapter 4.

Equation 5.3 is a system of non-linear partial differential equations that are coupled to one another by means of the kinetically-controlled reaction source/sink terms R. In addition to the aqueous components, the immobile components, i.e., biomass and sorbed substrates, can mathematically be described by a mass balance equation similar to Eqs. 5.1 and 5.2, with the exception that no advection-dispersion operator is incorporated:

$$\frac{\partial m_k}{\partial t} = R_k \qquad k=1..N_m \tag{5.4}$$

where m is the immobile component concentration, R_k is the reaction source/sink terms, and N_m is the number of immobile components. Equation 5.4 may be rewritten to describe the specific immobile constituents of interest, e.g., the biomass and sorbed electron donor (not shown). For the purposes of these simulations, the electron acceptor is considered to be nonsorbing. This assumption has been used by others (e.g., Oya and Valocchi, 1997 and 1998) and was previously discussed in Chapter 4.

Equations 5.3 and 5.4 are nonlinear partial differential equations coupled together by the rate terms. To efficiently solve this system, FEREACT utilizes an iterative approach for incorporating the geochemical and microbial reaction processes into the differential equation governing the solute transport. This approach requires that the reaction terms are first decoupled from the transport terms. The sequential iterative approach (SIA) utilizes two-steps during each iteration to solve the decoupled equations by first estimating the reaction source/sink term from a trial solution, and then applying that solution as a constant reaction term in solving the mass balance terms of Eqs. 5.2 and 5.4. The iterations are continued until the convergence criteria are met. The trial solution from each iteration then becomes the basis for the estimated reaction rate term for the next iteration. Each nonlinear expression is linearized by being approximated by a

truncated first-order Taylor's series, which results in a set of N_c linear partial differential equations and N_m ordinary differential equations that are decoupled and can be solved independently at each segment of the finite element grid.

5.1.2 RT3D

The second modeling program evaluated for use in this research was the Reactive Transport in 3-Dimensions code (RT3D) which is a finite difference model code similar in nature to FEREACT (finite element) that solves the coupled partial differential equations for reactive transport of multiple mobile and immobile species. However, unlike FEREACT, RT3D was created to operate in a three-dimensional saturated groundwater system domain. RT3D was developed by T. Prabhakar Clement and co-workers at Battelle Pacific Northwest National Laboratory in Richland, Washington, as an enhancement to the basic multi-species version of the U.S. Environmental Protection Agency transport code, MT3D (Zheng, 1990). At the outset of this project and code evaluation, the current version of RT3D was version 1.0, which uses the advection and dispersion solvers from the DOD_1.5 (1997) version of MT3D (Clement, 1997). The reaction program RT3D has been described in the literature and compared against both analytical and numerical solutions (e.g., Clement et al., 1997a and 1997b). It has been successfully used in modeling a wide ranging variety of scenarios, such as solving for a system of reactive transport equations under sequential aerobic and anaerobic conditions (Lu, et al., 1999), and evaluating the natural attenuation of chlorinated solvents at a field site (Clement, et al., 2000). A detailed evaluation of the reaction kinetics used in RT3D, including Monod-type biodegradation, was completed by Sun et al (1998). The appeal of the RT3D code is its unique implicit reaction solver that makes the code sufficiently

flexible for simulating various types of chemical and microbial reaction kinetics using both built-in reaction modules, and user-defined modules.

As with FEREACT, a basic model assumption of steady-state flow under saturated conditions leads to a series of governing equations for the aqueous and immobile components in RT3D, respectively, as is shown below:

$$\frac{\partial C_k}{\partial t} = \frac{\partial}{\partial x_i}\left(D_{ij} \frac{\partial C_k}{\partial x_j} \right) - \frac{\partial}{\partial x_i}(\upsilon_i C_k) + \frac{q_s}{\theta} C_{s_k} + r_c \quad \text{(k = 1,2,…m)} \tag{5.5}$$

$$\frac{\partial \tilde{C}_{im}}{\partial t} = \tilde{r}_c \quad \text{(im = 1,2,…(n-m)} \tag{5.6}$$

where *n* is the total number of species; *m* is the total number of aqueous species; *im* is the total number of immobile species; x_i and x_j are the distance in the direction of x_i and x_j, respectively [L]; t is time [T]; C_k is the aqueous phase concentration of the k^{th} species [ML^{-3}]; C_{im} is the solid phase concentration of the im^{th} species [MM^{-1}]; D_{ij} is the hydrodynamic dispersion coefficient [L^2T^{-1}]; v_i is the average pore water velocity [LT^{-1}]; q_s is the volumetric flux of water per unit volume of aquifer representing source and sinks of groundwater [T^{-1}]; C_{sk} is the concentration of species k in the source/sink [ML^{-3}]; r_c represents the reaction rate of sources and sinks [$ML^{-3}T^{-1}$]; $\tilde{r}_c$ represents the reaction rate of the solid phase [MM-1T-1]; and θ is porosity (adapted from Clement, 1997). These equations are consistent with the background presented for FEREACT, namely Eq. 5.1 when it has been rewritten to include the operator function of Eq. 5.2.

Similar to MT3D, the reactive code RT3D only computes the chemical fate of the modeled species and requires the U.S. Geological Survey-developed groundwater flow code MODFLOW (McDonald and Harbaugh, 1988) for computing spatial and temporal

variations in the groundwater head distribution (Clement, 1997). Thus, saturated groundwater flow velocities are calculated from the hydraulic-head values that are computed by solving a three-dimensional groundwater flow model. The flow equations used are taken from Zheng (1990):

$$S_S \frac{\partial h}{\partial t} = \frac{\partial}{\partial x_i}\left(K_{ii} \frac{\partial h}{\partial x_i} \right) + q_s \tag{5.7}$$

$$v_i = -\frac{K_{ii}}{\theta}\left(\frac{\partial h}{\partial x_i} \right) \tag{5.8}$$

where h is the hydraulic head [L], S_s is the specific storage coefficient [L^{-1}], and K_{ii} are the principal components of the hydraulic conductivity tensor [LT^{-1}] in any of *i* directions (Clement, 1997). Equations 5.7 and 5.8 can be rewritten as a single partial differential equation that can be solved numerically irrespective of the type of reactions included within Eqs. 5.5 and 5.6. This means that a numerical simulation in which only minor variations are made between steps can be completed quite efficiently if the flow portion of the model is to stay the same – and therefore the flow component of the model actually need not be re-run each time.

The RT3D code was developed to solve the multi-species reactive transport equations for aqueous species in the form of Eq. 5.5, and immobile species in the form of Eq. 5.6. While the FEREACT code uses the SIA approach, RT3D utilizes the operator-splitting (OS) numerical strategy. This allows the program to solve any number of coupled transport equations as long as they conform to the format of Eqs. 5.5 and 5.6 (Clement, 1997). The solution algorithm initially solves the advection, dispersion and

source-sink mixing steps independently for all mobile components for the transport time step *dt*. Specifically, after solving the transport for a single time step, *dt*, the coupled reaction equations (aqueous and immobile source/sink) are solved implicitly by using a differential equation solver. The solver automatically computes the time-step sizes required to precisely integrate the reaction equations (Clement, 1997). The system of numerical equations: advection (Eq. 5.9), dispersion (5.10), source/sink mixing (Eq. 5.11), and aqueous reaction, where r represents any number of reactions (Eq. 5.12) that comprise the solution at each time step are as follows:

$$\frac{\partial C}{\partial t} = -\frac{\partial (v_i C)}{\partial x_i} \tag{5.9}$$

$$\frac{\partial C}{\partial t} = \frac{\partial}{\partial x_i}\left(D_{ij} \frac{\partial C}{\partial x_j} \right) \tag{5.10}$$

$$\frac{\partial C}{\partial t} = \frac{q_s}{\theta} C_s \tag{5.11}$$

$$\frac{\partial C}{\partial t} = r \tag{5.12}$$

where the term *r* represents any number or type of reaction equations.

Once the aqueous terms are solved, the aqueous and immobile terms are coupled and solved for the particular time step. Figure 5.1 depicts a general flow-chart for the solution technique of OS as applied in RT3D.

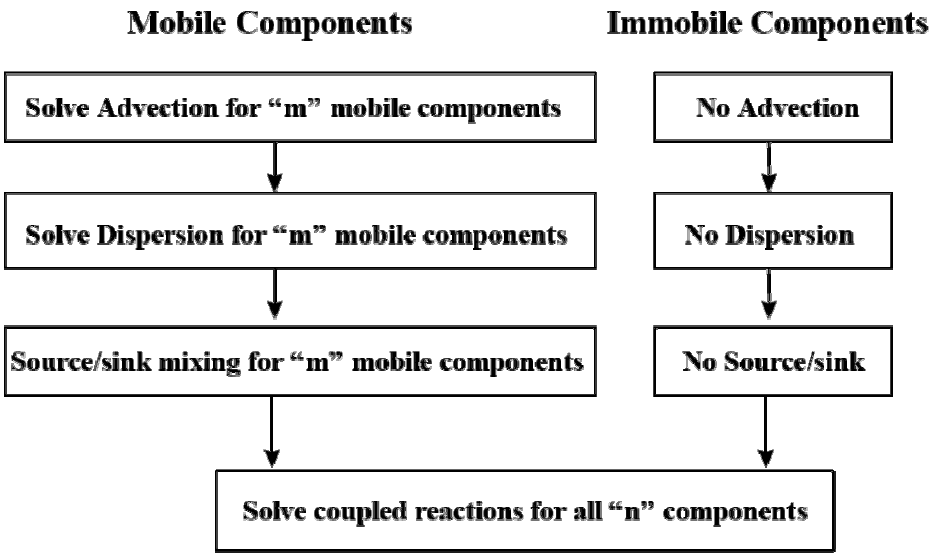

Figure 5.1. Flow chart depicting the solution strategy of Operator Splitting technique in RT3D (after Clement, 1997).

The programs MODFLOW and RT3D are stand alone FORTRAN-based programs that can be operated using WINDOWS®-based executable files and input files generated using a basic text editor. Due to the popularity of these types of models, WINDOWS®-based GUI have been developed to assist users in the set-up, operation, and analysis of model scenarios. For this research, the program obtained that bundled together MODLFOW and RT3D in the GUI format was Visual MODFLOW (VMOD) created by Waterloo Hydrogeologic, Inc., of Waterloo, Ontario. The VMOD program allows the user to develop a model by using simple GUI-based menus and pull-down features to input the model data. Execution of the model is completed within the VMOD environment, and output can be viewed within the package as well, or exported for other purposes.

5.2 Selection of Numerical Code

As stated above, FEREACT was originally selected as the numerical modeling program for this research project. During early implementation, several factors arose which eventually led to the selection of an alternative modeling program. First, FEREACT and its predecessors, PDPLUS and PDREACT were written for use within a UNIX mainframe. Our early observations indicated that the runtimes associated with relying on the University mainframe system were prohibitive in nature; often the system would "time-out" before the model had completed the scenario. Thus, an alternate model that was WINDOWS®-based and could be run on a personal computer was attractive for long runtimes. Secondly, and more importantly, the FEREACT code is best suited for simple one-dimensional and two-dimensional systems of coupled equations where equilibrium conditions are present. During our evaluation, it became obvious that operating under nonequilibrium, rate-limiting mass transfer conditions greatly increased the runtime compared to modeling sorption under linear equilibrium conditions (thus, no additional kinetic reaction). For these reasons, the VMOD program, incorporating MODFLOW and RT3D, was ultimately selected for performing the numerical experiments required for this research.

5.3 Development of the UMD RT3D Module

In the previous chapter, the system of governing equations (Eqs. 4.8, 4.9, 4.10, and 4.11) for the research problem was presented. These equations are partial differential equations (PDEs) that require time sequential integration over the model domain to arrive at a closed form solution. As indicated above, while FEREACT required no alterations to the code to operate as intended, the use of RT3D required the development of a user-

defined module to be used in the VMOD environment. To accomplish this modification of RT3D a series of ordinary differential equations was developed from the partial differential governing equations of Chapter 4, and from modifications to existing components of the RT3D pre-defined model packages, which were then combined into one user-defined reaction module. Using the notation of RT3D, this series of equations can be written as follows:

$$\frac{d[D]}{dt} = -\mu_m \frac{\rho_b X_s}{\theta}\left(\frac{[D]}{K_D + [D]}\right)\left(\frac{[A]}{K_A + [A]}\right) - \frac{\rho_b}{\theta} K_m \left(K_d \times [D]^n - D_s\right) \tag{5.13}$$

$$\frac{d[A]}{dt} = -\mu_m Y_{A/D} \frac{\rho_b X_s}{\theta}\left(\frac{[D]}{K_D + [D]}\right)\left(\frac{[A]}{K_A + [A]}\right) \tag{5.14}$$

$$\frac{dX_S}{dt} = \mu_m Y_{X/D} X_s \left(\frac{[D]}{K_D + [D]}\right)\left(\frac{[A]}{K_A + [A]}\right) - k_d X_S \tag{5.15}$$

$$\frac{dD_s}{dt} = K_m \left(K_d \times [D]^n - D_s\right) \tag{5.16}$$

where [D] is electron donor aqueous concentration, replacing the term *S*, used in previous sections (ML^{-3}); μ_m is the specific substrate utilization rate (T^{-1}) (Note that normally in the environmental engineering literature, this term is symbolized by q_{max} or k as in earlier sections); X_s is the solid-phase biomass concentration (MM^{-1}); K_D is the donor substrate half-saturation coefficient (ML^{-3}); [A] is electron acceptor aqueous concentration (ML^{-3}); K_A is the acceptor substrate half-saturation coefficient (ML^{-3}); K_m is the kinetic mass-

transfer coefficient (T^{-1}); D_s is the solid phase donor concentration (MM^{-1}); K_d is the linear partitioning coefficient (L^3M^{-1}); $Y_{A/D}$ is the stoichiometric ratio of acceptor consumed to donor consumed; $Y_{X/D}$ is the stoichiometric yield of biomass produced to donor consumed; n is the Freundlich exponent; and k_d is the biomass decay coefficient (T^{-1}). It should be noted that in these sets of equations, the Freundlich exponent was included for potential future application, but for the numerical scenarios completed as part of this research, the exponent was assigned a constant value of 1.0. Eqs. 5.13 through 5.16 are equations representing electron donor, electron acceptor, biomass, and sorbed-phase donor change with time that are analogous to Eqs. 4.8 through 4.11, respectively. Because the RT3D code utilizes the OS technique, the advection and dispersion terms of Eqs. 4.8 and 4.9 for electron donor and acceptor, respectively, have been eliminated. Another notable difference includes the use of biomass as the solid phase concentration requiring use of conversion terms (bulk density and porosity) to convert to a mass per unit pore volume basis.

Equations 5.13 through 5.16 were written into a dynamically linked library (DLL) file in accordance with the procedures for developing a user-defined RT3D reaction module (Clement, 1997), the text of which is included as Appendix I. Using the DLL format, a FORTRAN subroutine for the user-defined reaction package was compiled as a stand-alone DLL using Microsoft Fortran Powerstation. Because of the complexity associated with the use of RT3D within the VMOD environment, the process of compiling the new RT3D DLL module had to be completed by the technical developers of VMOD to ensure compatibility of the FORTRAN versions. Therefore, the module with the desired equations was prepared with the assistance of Dr. Sergui Chmakov, of

Waterloo Hydrogeologic, Inc. Once compiled, the new module, *rxns.dll* was simply copied into the same operating folder as the VMOD and RT3D executable files (*.exe) such that the DLL module could be called once in the VMOD environment. With the user-defined DLL in place, input of the model operating parameters and species details was completed as would be for any of the pre-defined RT3D modules. This new RT3D DLL module is referenced herein as the UMD module. The operation of VMOD and the RT3D component within VMOD is described by Waterloo Hydrogeologic, Inc. (2000). For this project, VMOD version 2.8.2.52, compiled December 2000 was used.

5.4 Numerical Modeling Settings

As presented above, the reactive transport model RT3D was selected for use in this research. This section presents a brief summary of the numerical modeling input structure and techniques that were used during the completion of the model verification (Section 5.5) and experimental analyses (Section 5.6).

The individual model parameters were selected from several sources. First, values were chosen from related research literature (e.g., Odencrantz, 1992). This allowed in some cases for relatively straight forward comparison to previously published results, e.g., the verification processes detailed below. Second, values were selected from literature sources determined to represent similar model, laboratory, or field conditions, e.g., the selection of hydrogeologic parameters. Efforts were made to ensure that the selected variables and parameters made "real-world" sense in terms of technical feasibility beyond the scope of the numerical modeling.

In order to minimize certain numerical or mathematical effects that can skew results, the well-known Peclet and Courant criteria were calculated and applied to the

selection of numerical parameters (Frind, 1982). The Peclet and Courant Number constraints provide the necessary conditions for the finite element mesh design and the selection of time steps in transport modeling. The Peclet Number constraint requires that the spatial discretization of the flow regime is not larger than twice the dispersion potential of the porous medium. The Peclet Number is defined as $v_x dx / D_x$, dx is the longitudinal node spacing [L], and v_x and D_x are as defined above. It is generally stated that values of the Peclet Number should be less than 2 for a model run to ensure that numerical dispersion and oscillation are minimized (Odencrantz, 1992).

The Courant Number constraint requires that the distance traveled by advection during one time step is not larger than one spatial increment (i.e., one element). The Courant Number is defined as $v_x dt / dx$, dt is the length of each sequential time step [T], and v_x and dx are as defined above. Similar to the Peclet Number, a value of the Courant Number can be calculated for each model trial. In practice, numerical effects are minimized when the Courant Number is less than 1.

As stated above, the reactive transport model RT3D was used for the numerical simulations with the aid of the GUI VMOD. Scenario parameters were input into VMOD using the Input, Setup, and Run menus as described in the VMOD user's manual (Waterloo Hydrogeologic, Inc., 2000). Once the data were input into the GUI interactive menus, the model trial was prepared to run. All model runs as part of this research were completed in the same manner to ensure consistency. For this research, the MODFLOW 96 version loaded into the VMOD program was used. The Advection Method used was the Upstream Finite Difference Method with an Implicit GCG Solver with Jacobi

Preconditioners. These criteria were selected to further minimize numerical effects while providing accurate results (Waterloo Hydrogeologic, Inc., 2000).

5.5 Model Verification

Prior to conducting the modeling experiments detailed in Section 5.4, below, verification simulations were completed. The verification process was conducted for several reasons. First, simulations were completed to become familiar with the VMOD program operation. Second, while VMOD has been available commercially for several years, confirmation of its accurate operation was required, as represented by the analytical verification. Third, verification of the operation of the new UMD revised code was necessary. The latter was accomplished by comparing its output to numerical simulations produced using the unaltered RT3D modules.

Verification was conducted using a two-dimensional solute transport scenario after Odencrantz (1991) and MacQuarrie et al. (1990). One analytical verification and two numerical verification simulations were completed. For each scenario, the model domain was the same while the transport and reaction parameters were varied based on the type of scenario being modeled. Figure 5.2 depicts the model grid used for the verification process. The following sections present the procedures and results of the verification process.

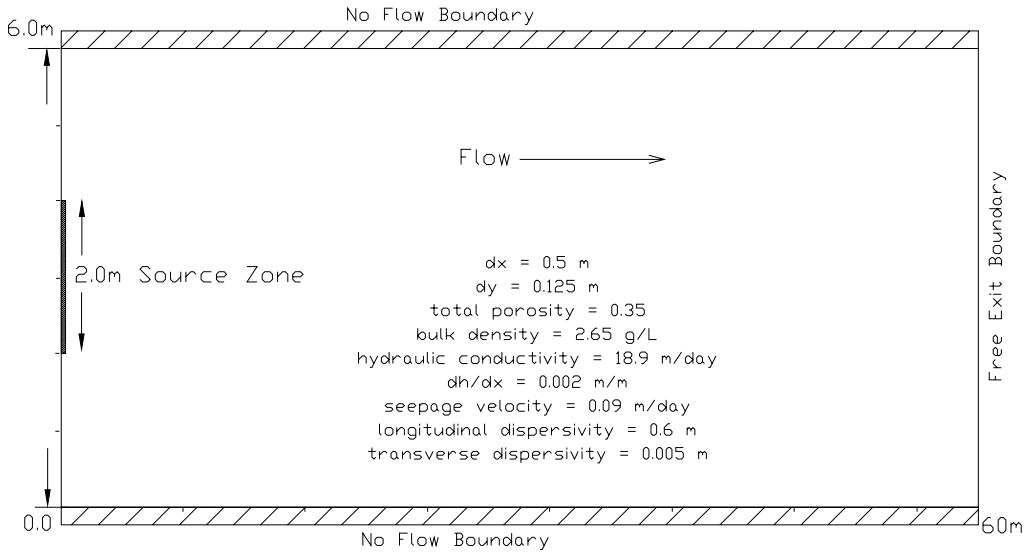

Figure 5.2. Model domain and input parameters for first order decay scenario.

5.5.1 Boundary and Initial Conditions

The first step in completing the verification process was to derive an analytical solution to the governing equations and to identify the initial and boundary conditions needed to reach a closed-form analytical solution. In presenting the background information on the initial and boundary conditions, it is convenient to present these conditions for a simple non-steady-state, one-dimensional problem. In this case, one initial condition and two boundary conditions are required.

The general initial condition for the solute concentration in the domain is:

$$C(x,0) = f(x) \quad (t = 0) \tag{5.17}$$

where the function f(x) may take on several forms, including the specific case where f(x) is a constant value. For this model verification, a constant value is assumed and Eq. 5.17 becomes:

$$C(x,0) = C_i \tag{5.18}$$

Thus, for a domain that is initially pristine, i.e., free of all contaminant solute i, $C_i = 0$.

At x = 0, there are two main types of inlet boundary conditions. The so-called first-type inlet-boundary condition has the form:

$$C(0,t) = g(x) \quad (x = 0) \tag{5.19}$$

where g(x) is a constant value for all time t. For this case, the value g(x) is assumed equal to 0 or C_o, written as:

$$C(0,t) = \begin{cases} C_o & 0<t<t_o \\ 0 & t>t_o \end{cases} \tag{5.20}$$

The second common inlet-boundary condition is the so-called flux-type boundary condition where

$$\left(-D_x \frac{\partial c}{\partial x} + vC\right)\Big|_{x=0} = \begin{cases} vC_o & 0<t<t_o \\ 0 & t>t_o \end{cases} \tag{5.21}$$

The flux-type inlet boundary condition, also called a third-type condition, is so-called due to its incorporation of a variable flux of solute across the boundary rather than a constant value C_o for all time t. Both inlet boundary condition types were evaluated as part of the verification.

The outlet or lower-boundary condition can also take different forms just as with the inlet-boundary condition. In numerical modeling a commonly applied outlet boundary condition is a second-type boundary condition assuming an infinite domain. In this case the domain outlet becomes a free-exit boundary where:

$$\frac{\partial C}{\partial x}(\infty, t) = 0 \tag{5.22}$$

Equation 5.22 essentially states that the solution to the ADR solute transport equation must converge to a solution (0) within the system domain.

5.5.2 Two-Dimensional Analytical Verification

The governing equation for two-dimensional solute transport with first-order equilibrium sorption, isotropic advection, longitudinal and transverse dispersion, and first-order decay is,

$$R\frac{\partial C}{\partial t} = D_x \frac{\partial^2 C}{\partial x^2} + D_z \frac{\partial^2 C}{\partial z^2} - v_x \frac{\partial C}{\partial x} - \lambda C \qquad (5.23)$$

where C is the aqueous-phase solute concentration [M L^{-3}], t is time [T]; D_X is the longitudinal hydrodynamic dispersion coefficient [L^2T^{-1}]; x is distance in the direction of flow [L]; v_X is the seepage velocity [LT^{-1}]; D_Z is the transverse hydrodynamic dispersion coefficient [L^2T^{-1}]; z is distance in the direction vertically transverse to the direction of flow [L]; R is the retardation coefficient; and λ is a first-order decay coefficient [T^{-1}]. The initial and boundary conditions developed above for a one-dimensional domain can similarly be applied to this two-dimensional case. Specifically, the initial domain condition is expressed by Eq. 5.18, the inlet-boundary is the first-type boundary condition of Eq. 5.20, and a free-exit boundary is applied as expressed by Eq. 5.22. In addition, the two-dimensional case requires two more boundary conditions, for the top and bottom of the two dimensional domain (vertical or y-direction). In both cases, the second-type boundaries are applied where $\frac{dC}{dy} = 0$, indicating a no-flow boundary. Figure 5.2, above depicts the two-dimensional domain and boundary conditions adapted from Odencrantz (1992) and MacQuarrie, et al., (1990).

A closed-form analytical solution to the governing ADR (5.23) with the selected initial and boundary conditions for the relative solute concentration at any point in space or time takes the following form for a two-dimensional domain (Domenico and Schwartz, 1990):

$$\frac{C(x,y,0,t)}{C_o} = \left(\frac{1}{4}\right)\exp\left\{\left(\frac{x}{2\alpha_x}\right)\left[1-\left(1+\frac{4\lambda\alpha_x}{v}\right)^{1/2}\right]\right\} erfc\left[\frac{x-vt\left(1+4\lambda\alpha_x/v\right)^{1/2}}{2\left(\alpha_x vt\right)^{1/2}}\right] \left\{erf\left[\frac{y+Y/2}{2\left(\alpha_y x\right)^{1/2}}\right] - erf\left[\frac{y-Y/2}{2\left(\alpha_y x\right)^{1/2}}\right]\right\} \tag{5.24}$$

Although Eq. 5.24 is shown for the case of a two-dimensional domain, the solution can be readily adapted to three-dimensional conditions by incorporating a second bracketed error function term, similar to the y term above. Naturally, for two-dimensional conditions, z = 0 throughout the domain.

Along the centerline of the plume, where both y = 0 and z = 0, Eq. 5.24 can be rewritten as follows:

$$\frac{C(x,0,0,t)}{C_o} = \left(\frac{1}{2}\right)\exp\left\{\left(\frac{x}{2\alpha_x}\right)\left[1-\left(1+\frac{4\lambda\alpha_x}{v}\right)^{1/2}\right]\right\} erfc\left[\frac{x-vt\left(1+4\lambda\alpha_x/v\right)^{1/2}}{2\left(\alpha_x vt\right)^{1/2}}\right] \left\{erf\left[\frac{Y}{4\left(\alpha_y x\right)^{1/2}}\right]\right\} \tag{5.25}$$

This analytical solution was written into a Microsoft Excel® (2000 version) spreadsheet for ease of computation and used to compile the data in a form that could be presented graphically and easily compared to the numerical model solution. For the analytical verification of the VMOD suite, MT3D was selected to complete the numerical simulation. As discussed previously, MT3D is the basic multi-species transport model

that serves as the basis of the RT3D program, and therefore warrants verification in addition to subsequent evaluations for RT3D as well.

The input parameters for the analytical model verification are summarized in Table 5.1. These data were applied in both the analytical spreadsheet calculations using Eq. 5.25, and as the input data for the numerical simulation using MT3D. The calculations of the analytical verification data, in spreadsheet format, are included in Appendix II.

Table 5.1. Input parameters for analytical verification - first order decay.

Parameter	**Value**	**Units**
Seepage velocity	0.09	m/hr
Longitudinal dispersivity	0.6	m
Transverse dispersivity	0.005	m
Decay – first order	0.007	day^{-1}
Porosity	0.35	unitless
Soil bulk density	2,650	g/l
Soil partition coefficient	$1.32x10^{-4}$	l/g

Longitudinal profiles at 10, 40, 120, and 280 days were created from the analytical solution, using the parameters in Table 5.1 and Eq. 5.25, and were plotted against those from the numerical solution of VMOD and MT3D. A comparison between the analytical and numerical solutions is presented in Figure 5.3. Clearly, the numerical solution compares very well to the analytical solution in all cases, confirming an accurate solution using VMOD and MT3D.

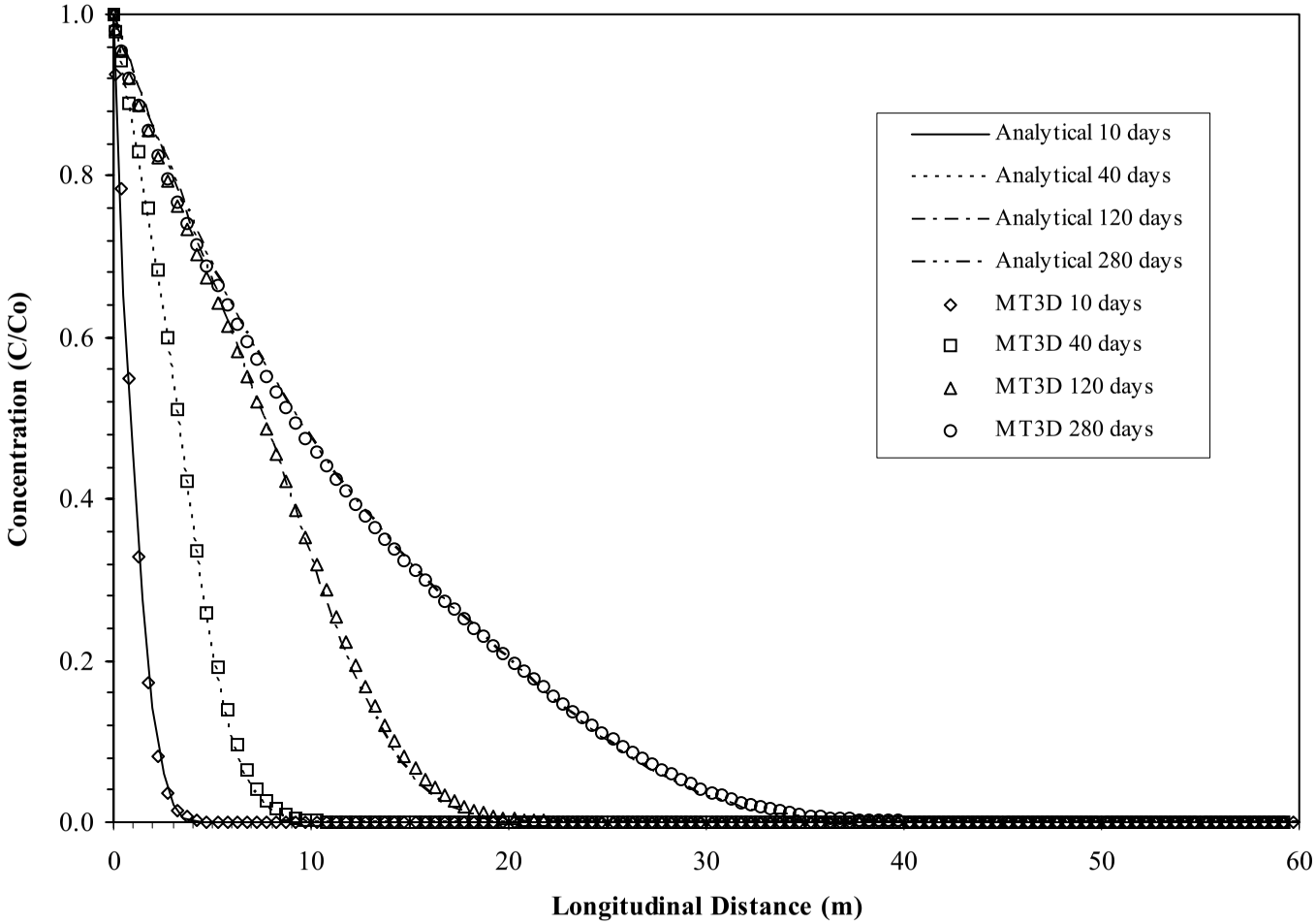

Figure 5.3. Comparison of analytical to numerical model: first order decay scenario.

5.5.3 Two-Dimensional Numerical Verification

With the successful comparison of VMOD and MT3D to a closed-form analytical solution, the next procedure was to perform verification simulations of the new UMD module by comparing it to the unaltered built-in RT3D modules. Two numerical verification simulations were completed. The first simulation was completed using a kinetic sorption reaction with no biodegradation, and the second simulation was completed using a double Monod biodegradation reaction with no sorption. For each scenario, the UMD module was compared against the unaltered RT3D with the appropriate reaction module (e.g., kinetic sorption or double Monod biodegradation) selected from the VMOD transport reaction selection menu (Waterloo Hydrogeologic, Inc., 2000). Comparison plots were generated to present solute concentration along the centerline of the plume in the longitudinal direction.

5.5.3.1 Kinetic Sorption Verification

The domain used for the verification of the sorption component of the UMD module was the same as that of the analytical verification described above (e.g., Fig. 5.2). The sorption verification was completed by first running VMOD using only the built-in rate-limited kinetic sorption module of RT3D. The next step was to model the scenario using the UMD module with rate-limited kinetic sorption. In order to compare the sorption modules with no external influences, the solute biodegradation and biomass growth equations of the UMD module effectively had to be effectively "turned off". To accomplish this, the reaction parameter q_{max} (see Eqs. 5.13 through 5.15) was minimized. This allowed the biodegradation and biomass growth to become negligible. However, a

value of $q_{max} = 0$ cannot be entered into VMOD. Instead, to turn off the biodegradation and growth equations, a minimal value had to be entered, such as 10^{-25} or a value similar in magnitude, to make those reaction terms much smaller than the scale of the other reaction sinks. The relevant input parameters for the sorption verification are presented in Table 5.2.

Table 5.2. Input parameters for kinetic sorption verification.

Parameter	**Value**	**Units**
Seepage velocity	1.65	m/day
Longitudinal dispersivity	0.6	m
Transverse dispersivity	0.005	m
Soil bulk density	2,650	mg/l
Porosity	0.35	unitless
Mass transfer coefficient, K_m	100	day^{-1}
Soil partition coefficient, K_d	$2.642x10^{-4}$	l/mg

The results of the comparison of the RT3D sorption module and the UMD module with biodegradation and biomass growth minimized are illustrated in Fig. 5.4. Inspection of Fig. 5.4 reveals the comparison to be quite favorable, indicating that the rate-limited sorption term as implemented in the UMD module functions appropriately.

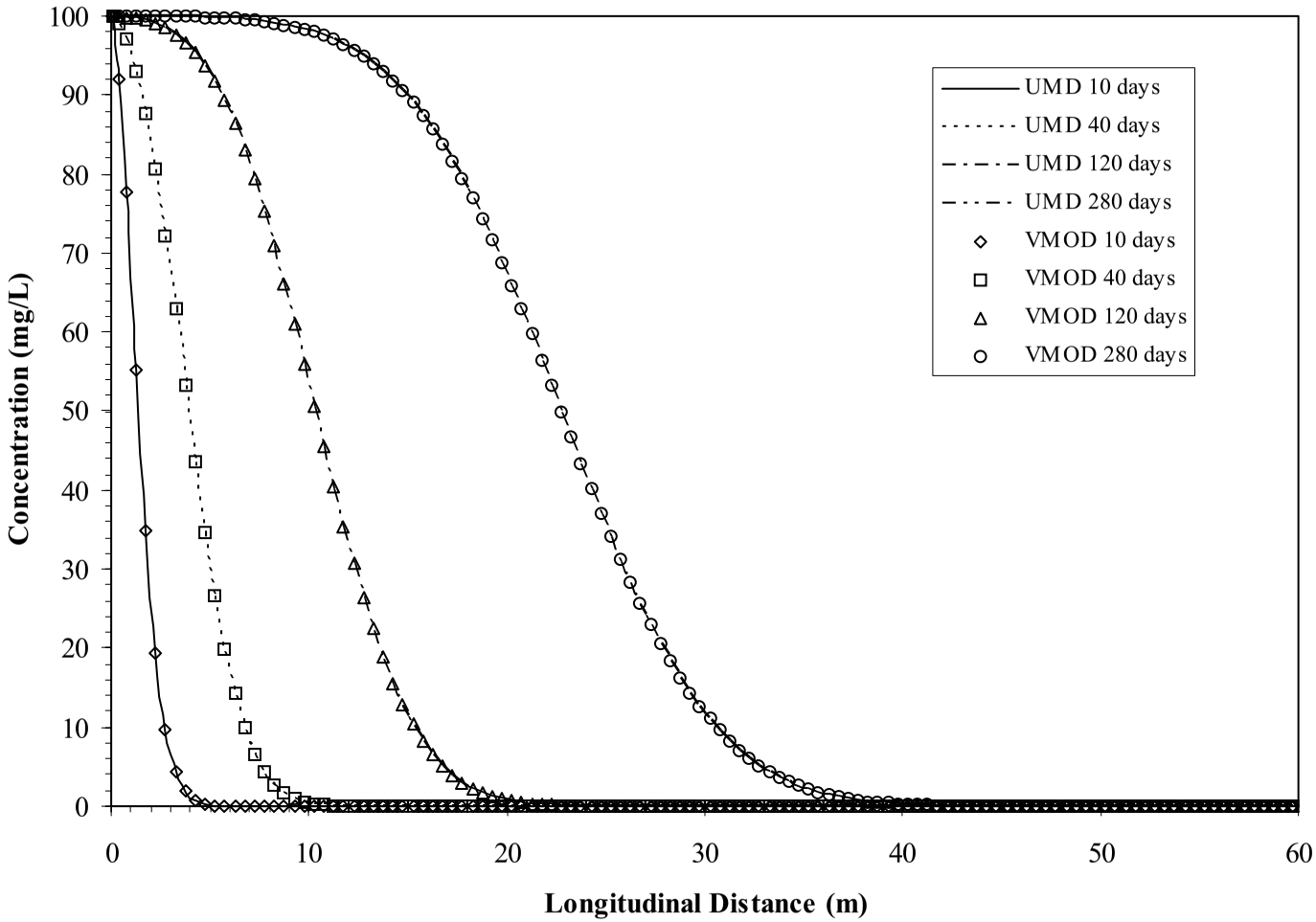

Figure 5.4. Comparison of UMD to VMOD numerical models: sorption-only scenario.

5.5.3.2 Double Monod Biodegradation Verification

Comparison of the biodegradation component of the UMD module to the built-in RT3D equivalent was completed in a similar manner to that described above for sorption. In this case, the sorption parameters (e.g., the kinetic partitioning coefficient, K_d) were minimized to make the sorption reaction sink insignificant and to isolate the biodegradation components. The relevant input parameters for the biodegradation verification are presented in Table 5.3.

Table 5.3. Input parameters for biodegradation (dual Monod) verification.

Parameter	**Value**	**Units**
Seepage velocity	1.65	m/day
Longitudinal Dispersivity	0.6	m
Transverse dispersivity	0.005	m
Soil bulk density	2,650	mg/l
Porosity	0.35	unitless
Mass transfer coefficient, K_m	~0.0	day^{-1}
Soil partition coefficient, K_d	~0.0	l/mg
Half-saturation constant, Donor, K_S	$2.89x10^{-6}$	mg/l
Half-saturation constant, Acceptor, K_A	$1.46x10^{-1}$	mg/l
Specific utilization rate, q_{max}	.238	day^{-1}

The results of the biodegradation comparison are illustrated in Fig.5.5. As with the sorption comparison of Fig. 5.4, the comparison is very favorable, indicating that the biodegradation and biomass growth reaction terms as implemented in the UMD module provide accurate results.

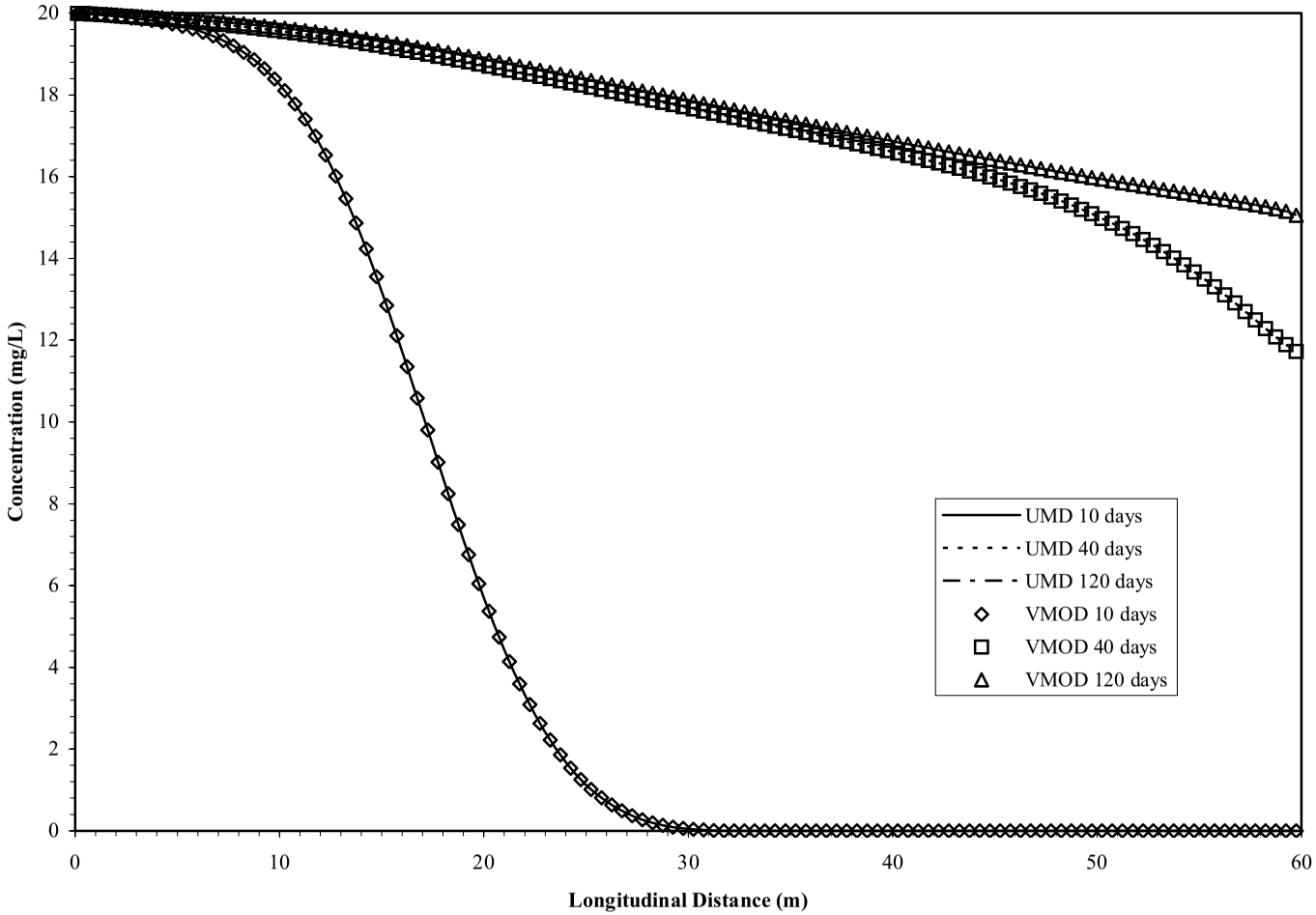

Figure 5.5. Comparison of UMD to VMOD numerical models: biodegradation only (dual Monod) scenario.

5.6 Baseline Experiments

The following subsection provides the details of the simulations carried out to evaluate the quantitative framework developed in Chapter 4. In Section 4.4.1, the baseline scenarios were briefly introduced. For the numerical modeling portion of this research, a conceptual model was developed that would be consistent with the sand tank reactor developed and utilized by Ms. Xin Song as part of her Ph.D. research. The resulting conceptual model for the sand tank domain is depicted below in Fig. 5.6

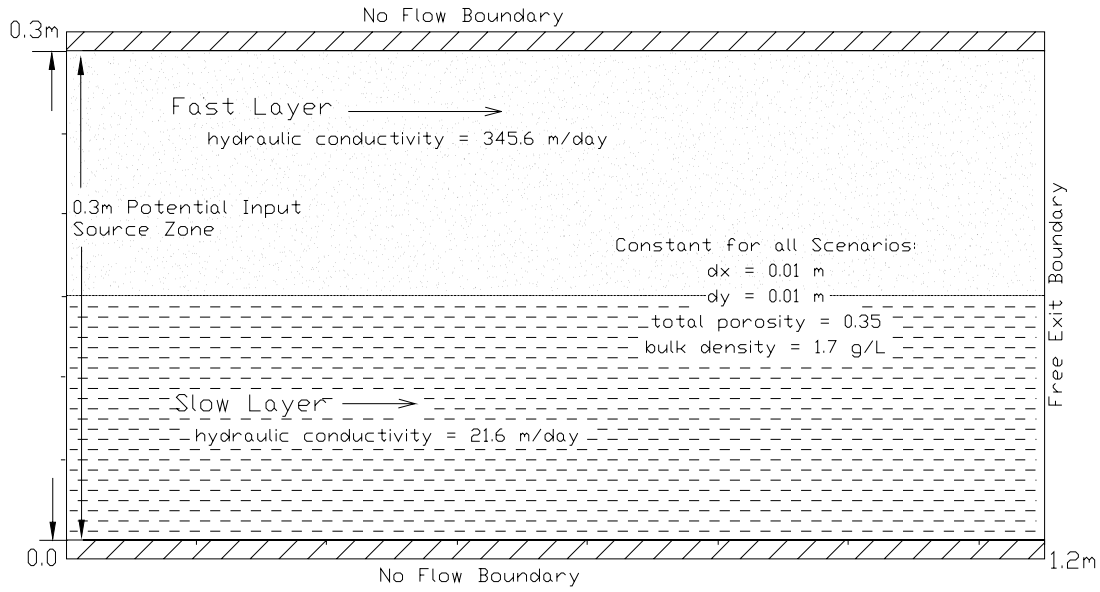

Figure 5.6. Conceptual model domain for numerical scenarios.

Use of this basic two-dimensional domain allows for relatively complex modeling experiments while still producing meaningful output to demonstrate that the quantitative framework can be used *a priori* to predict the overall rate-limiting phenomena. For the purposes of the RT3D modeling, a corresponding two-dimensional model was set-up and

a unit thickness was chosen (e.g., a thickness of 0.1 m with just one column/row) to eliminate any advection or dispersion into the third dimension.

Importantly, bench-scale experimentation can be performed in a bench scale system representing this conceptual model domain by constructing a bi-layered system of silica sands with varied properties (e.g., diameter, sorption capacity, etc.). Further, this domain suits the needs for the quantitative evaluation by allowing for a straightforward numerical and experimental manipulation of several key conditions. First, the processes of advection and dispersion are evaluated by implementation of macro-scale heterogeneities represented by varied vertical stratification, with a different hydraulic conductivity in each layer. Second, pore-scale (meso-scale) interfacial processes can be evaluated by varying sorption/desorption conditions. Note that while in the numerical model changing the sorptive properties associated with each layers is straightforward, in the laboratory is more complicated. Nevertheless, the sorptive properties can be altered by appropriately selecting or modifying the porous media. Finally, the micro-scale (biodegradation) conditions can be evaluated by varying the numerical parameters (Monod), or by changing the biomass culture or the type or concentration of the input electron acceptor in the bench-scale model.

The numerical experiments presented here were broken down into two Phases of operation. Phase One experimentation represented natural conditions (baseline) for each of the test scenarios. This phase represents intrinsic *in situ* biodegradation, where any number of factors can influence the environment and result in a rate-limiting process. The specific background conditions that were modeled for each test scenario are described further below. Phase Two experimentation represented enhancements to the

baseline conditions to develop an understanding of what engineered treatments can be employed to overcome the rate-limiting process.

In the remaining sections of this chapter, the Phase One baseline experiments and Phase Two enhancements are presented in detail. Additionally, the input data for each model run is presented, and the types of output data generated are discussed. A summary of the numerical scenarios, including the baseline limiting rate, dimensionless parameter evaluation for the baseline scenario, and the predicted appropriate and alternative enhancements for each scenario is presented in Table 5.4.

For each of the numerical scenarios, a basic model domain was established. The dimensions of the domain, grid sizing, and basic domain parameters (e.g., porosity and soil bulk density) did not vary throughout the scenarios. To the extent possible, the basic domain parameters were selected to be consistent with the bench-scale laboratory sand tank investigation being evaluated by Ms. Xin Song. For each scenario described in the sections below, a table with the relevant parameters specific to that scenario is included. Detailed spreadsheet tables with all scenario input parameters are also included in Appendix III.

Table 5.4. Summary of the numerical modeling scenarios to demonstrate the quantitative framework.

Experiment	Experimental Setup	Limiting Rate	Dimensionless Parameters	Possible Stimulants	Predicted Dominant Stimulant	Desired Goal from Stimulant
1 (a)	2-layer porous media Macro-scale transverse dispersion = rate-limiting process Aerobic; Fast Kinetics Weak Sorption	Macro-scale mixing controls	Pet >> 1 Sh2' >> 1 Da6 >> 1	Increase flushing to increase mixing Add surfactant to increase desorption Increase biokinetics	Increase flushing to increase mixing	Increased flushing causes increased dispersion and mixing of substrates between layers
3	2-layer porous media Biokinetics = rate-limiting process Low Acceptor Weak Sorption	Biokinetics controls	Pet >> 1 Sh2' >> 1 Da6 << 1	Increase flushing to increase mixing Add surfactant to increase desorption Increase biokinetics	Increase biokinetics, e.g. by bioaugmentation or stimulation of biomass; or by converting from anaerobic to aerobic conditions	Increased biodegradation due to improved biokinetics

5.6.1 Scenario 1(a)

This first test scenario was characterized as having relatively fast biokinetics and low sorption (Table 5.4). Here, the macro-scale mixing between the two layers is of interest, and the macro-scale transverse dispersion between the fast and slow layers is predicted to be the rate-limiting process. As shown in Table 5.4, this condition was accomplished by setting the model input parameters such that the dimensionless parameters have the following values: $Pe_T >> 1$, $Sh'_2 >> 1$, and $Da_6 >> 1$. The quantitative framework (Fig. 4.2) is presented again as Fig. 5.7, here highlighting the relevant dimensionless parameters and framework pathway for predicting the rate-limiting process this scenario. The resulting expectation for this scenario is that the biodegradation rate will be limited by the transverse dispersion into the slow layer, and, thus, biodegradation will occur primarily at the interface between the two layers.

The relevant input parameters for Scenario 1(a), including the actual values of the dimensionless parameters for this scenario are summarized in Table 5.5 and the model domain established for scenario #1(a) is presented in Fig 5.8.

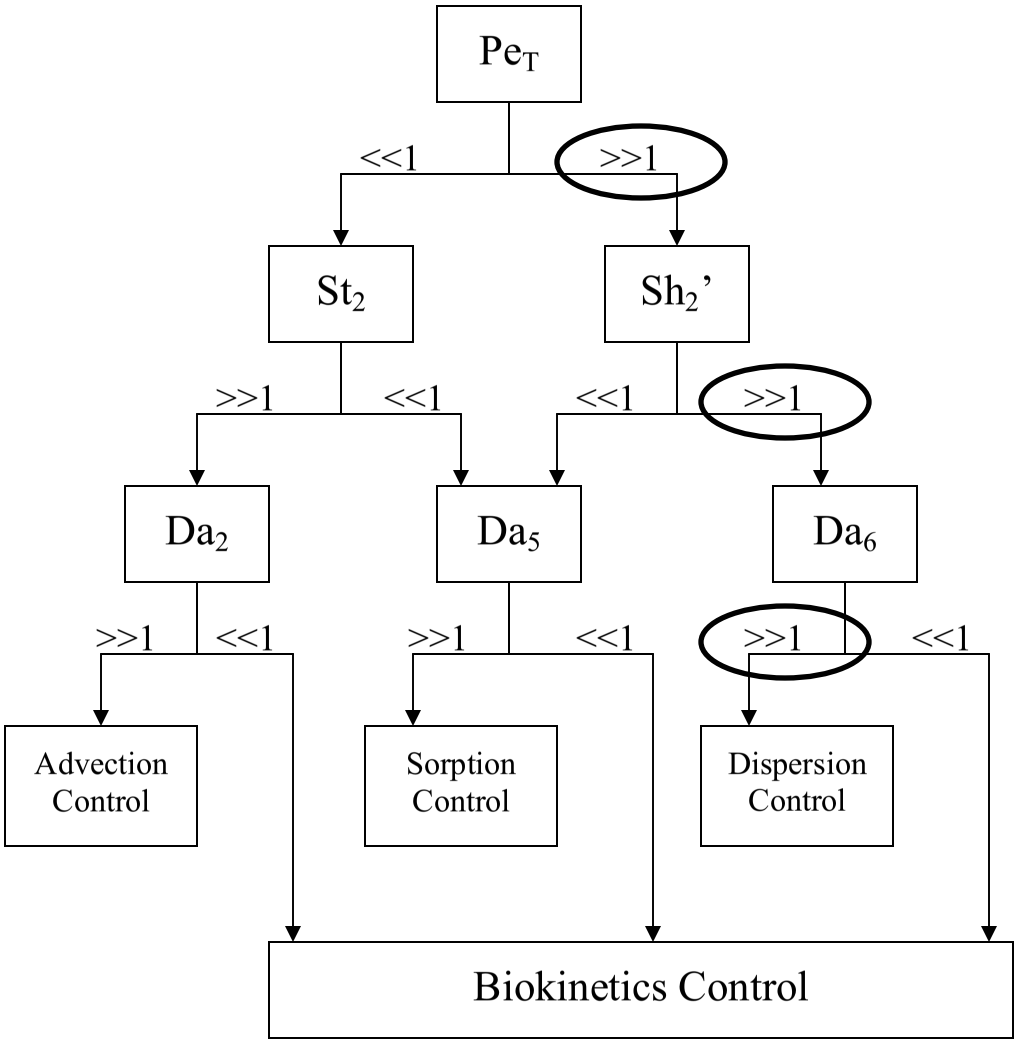

Figure 5.7. Quantitative framework highlighting Scenario 1(a) conditions.

Table 5.5. Scenario 1(a) baseline input parameters.

Parameter	**Value**	**Units**
Seepage velocity, fast layer	0.165	m/day
Seepage velocity, slow layer	0.010	m/day
Longitudinal Dispersivity, fast layer	0.003	m
Transverse dispersivity, fast layer	0.0015	m
Longitudinal Dispersivity, slow layer	0.001	m
Transverse dispersivity, slow layer	0.0005	m
Soil bulk density	1,700	mg/l
Porosity	0.35	unitless
Mass transfer coefficient	0.02	day^{-1}
Soil partition coefficient	$8.23x10^{-8}$	l/mg
Half-saturation constant, Donor	0.654	mg/l
Half-saturation constant, Acceptor	.146	mg/l
Specific utilization rate	0.0238	day^{-1}
Transverse Peclet No. (Pe_T), fast layer	748	dimensionless
Modified Sherwood No.2 (Sh_2'), fast layer	109	dimensionless
Damkohler No. 6 (Da_6), fast layer	3	dimensionless
Transverse Peclet No. (Pe_T), slow layer	557	dimensionless
Modified Sherwood No.2 (Sh_2'), slow layer	1301	dimensionless
Damkohler No. 6 (Da_6), slow layer	31	dimensionless

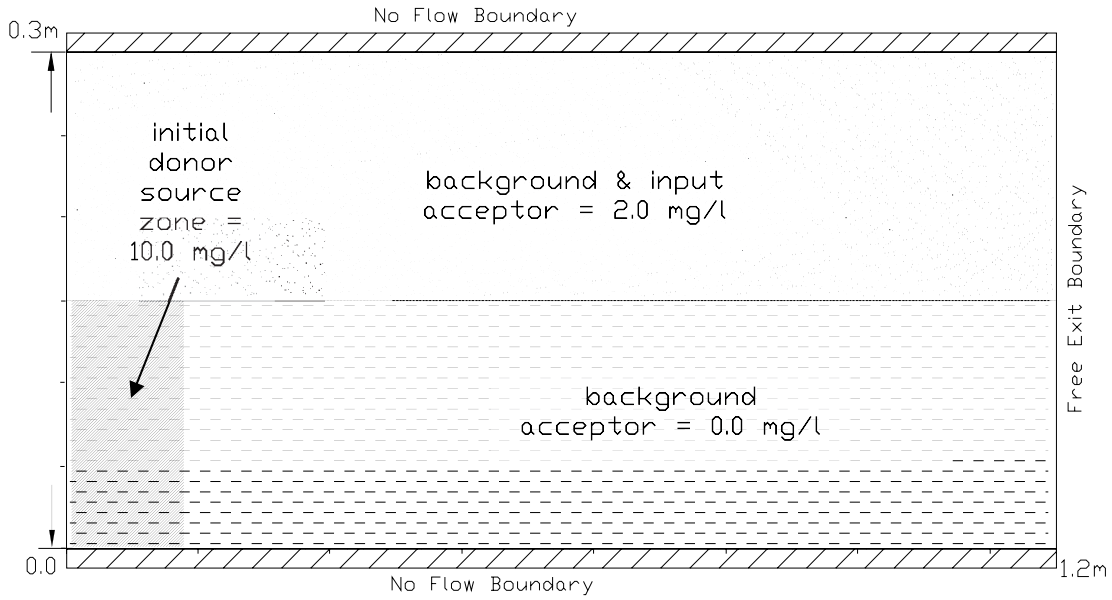

Figure 5.8. Input conditions for Scenario 1(a).

As illustrated, the baseline conditions for Scenario 1(a) were established such that the underlying lower conductivity layer was uncontaminated, except for a 0.1 m by 0.15 m area of the layer adjacent to the upgradient inlet boundary where aqueous electron donor is present at a concentration of 10.0 mg/l. For this layer it is assumed that the background electron-acceptor concentration is 0 mg/l. In the upper higher conductivity layer, electron acceptor has migrated throughout at a background concentration of 2.0 mg/l, due to the greater advection and dispersion in the higher conductivity material. For example, maybe the electron acceptor has not migrated into this area if it is a co-contaminant like nitrate. Alternatively, the acceptor (e.g. oxygen) in the lower layer may have already been depleted due to the previous presence of other donor contaminant(s). This scenario can be envisioned in practical terms as simulating an aquifer with a lens of lower permeability material where contamination is present. At the start of the model

run, 2.0 mg/l of acceptor is continuously injected across the inlet boundary of the upper layer under a seepage velocity of 0.165 m/day. These conditions for the baseline condition were specifically selected to allow observation of the mixing of the electron donor or acceptor substrates at the interface between the two layers of varying hydraulic conductivity.

5.6.2 Scenario 3

Under Scenario 3, the porous media and sorptive input conditions were similar to Scenario 1(a). However, for this experiment, the biokinetics were selected to be the rate-limiting process. Thus, the expectation was that the slower biokinetics limit the overall biotransformation rate. As summarized in Table 5.4, these conditions were accomplished by setting the model input parameters such that the dimensionless parameters have the following values: $Pe_T >> 1$, $Sh'_2 >> 1$, and $Da_6 << 1$. The quantitative framework (Fig. 4.2) is presented again as Fig. 5.9, here highlighting the relevant dimensionless parameters and framework pathway for predicting the rate-limiting process this scenario.

The baseline input parameters for Scenario 3, including the actual values of the dimensionless parameters for this scenario are summarized in Table 5.6 and the model domain established for scenario #3 is presented in Fig 5.10.

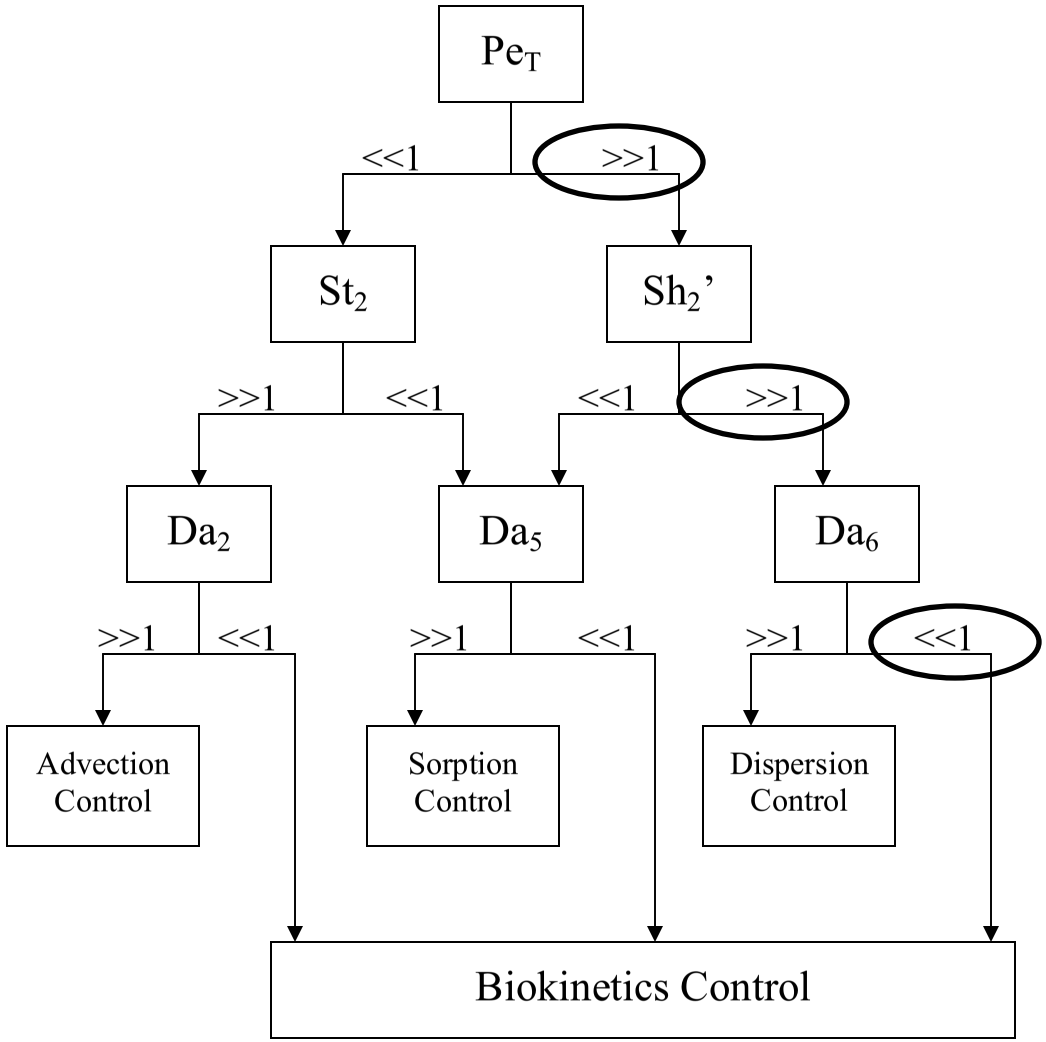

Figure 5.9. Quantitative framework highlighting Scenario 3 conditions.

Table 5.6. Scenario 3 baseline input parameters.

Parameter	**Value**	**Units**
Seepage velocity, fast layer	0.165	m/day
Seepage velocity, slow layer	0.010	m/day
Longitudinal Dispersivity, fast layer	0.003	m
Transverse dispersivity, fast layer	0.001	m
Longitudinal Dispersivity, slow layer	0.0003	m
Transverse dispersivity, slow layer	0.0001	m
Soil bulk density	1,700	mg/l
Porosity	0.35	unitless
Mass transfer coefficient	0.01	day^{-1}
Soil partition coefficient	$8.23x10^{-8}$	l/mg
Half-saturation constant, Donor	0.654	mg/l
Half-saturation constant, Acceptor	.146	mg/l
Specific utilization rate	0.000238	day^{-1}
Transverse Peclet No. (Pe_T), fast layer	2975	dimensionless
Modified Sherwood No.2 (Sh_2'), fast layer	217	dimensionless
Damkohler No. 6 (Da_6), fast layer	0.12	dimensionless
Transverse Peclet No. (Pe_T), slow layer	685	dimensionless
Modified Sherwood No.2 (Sh_2'), slow layer	799	dimensionless
Damkohler No. 6 (Da_6), slow layer	.44	dimensionless

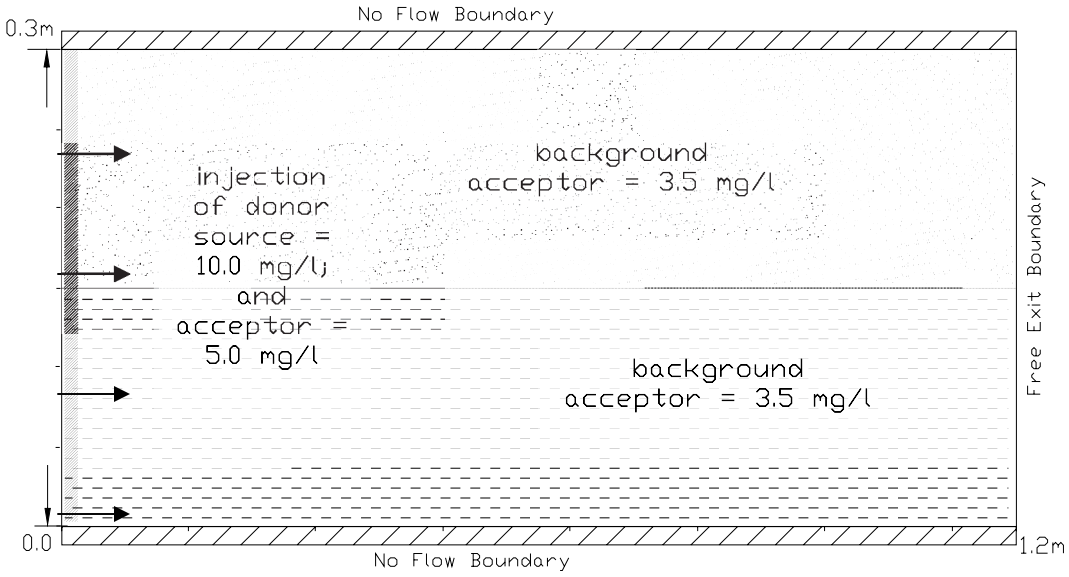

Figure 5.10. Input conditions for Scenario 3.

The input conditions for this scenario, as illustrated in Fig. 5.10, have important deifferences from those of Scenario 1(a). Under the Scenario 3 baseline conditions, the domain is "pristine" or uncontaminated, with a background concentration of 3.5 mg/l electron acceptor present. At the start of the model run, an electron donor source is injected at a concentration of 10.0 mg/l for one day. In addition, a continuous acceptor concentration of 5.0 mg/l is injection from start to the end of the model run. In this test scenario, the biokinetics are limited for some reason, e.g., the indigenous biomass is at a low concentration, or the microbes present have slow biodegradation kinetics for the particular contaminant present. This model scenario can be described as simulating a field site where an otherwise pristine aquifer (in this case both layers of the aquifer are "clean") is impacted by a slug release from some contaminant source. For example, perhaps the source is identified and prevented from further release after the first day, and thus, the source is effectively "shut-off" after one day. Observations for the baseline

Scenario 3 consisted of examining the migrating contaminant plume after the source was controlled after day one.

5.7 Enhancements to Baseline Experiments

This section presents the details of the conditions for the Phase Two experiments that were completed to represent select engineered enhancements to each of the baseline scenarios presented above. Each subsection describes the engineered perturbations that were implemented and their desired effect to stimulate the intrinsic conditions of the baseline experiments. The varied input parameters and resulting effect on the dimensionless parameters of the quantitative framework of Chapter 4 is also discussed.

5.7.1 Scenario 1(a) - Enhanced

As presented above, Scenario 1(a) was set up to represent a condition where the transverse dispersion between the lower (and slower) contaminated layer and upper (and faster) oxygenated layer is the factor limiting the biodegradation rate. Therefore the engineered perturbation predicted to be appropriate for this scenario was aimed at increasing the rate of transverse mixing between the two layers to stimulate growth. Numerically, this could be accomplished simply by increasing the value for the transverse dispersivity (α_T) or the hydrodynamic dispersion coefficient (D_T); however, in laboratory or field settings, changing either of these parameters alone is not feasible. Therefore, a more plausible means of increasing the transverse dispersion and, thus, the mixing between the two zones, is through an increase in the rate of advection, because the dispersion is in part a function of the seepage velocity (mechanical dispersion).

To accomplish the predicted appropriate enhancement of increased flushing, the advection rate was increased from 0.165 m/day to 0.987 m/day in the fast layer, and from 0.010 m/day to 0.062 m/day in the slow layer, which represents an approximately six fold increase. All other input hydrogeologic and reaction parameters remained the same. As a result, the coefficient of dispersion (transverse) increases in the fast layer from a baseline value of 5.11×10^{-4} m^2/day to 2.98×10^{-3} m^2/day in the enhanced case. Similarly, in the slow layer, transverse dispersion increases from 2.73×10^{-5} m^2/day to 7.87×10^{-5} m^2/day in the baseline and enhanced cases, respectively. These changes should provide enhanced transverse mixing of the two substrates across the interface of the two conductivity zones. The effect of this on the dimensionless parameters is a decrease in the value of Da_6 from 3 and 31 in the fast and slow layers for the baseline condition, respectively, to 0.5 and 14.3 in the fast and slow layers for the enhanced condition, respectively. A review of Fig. 5.7 indicates that this decrease in Da_6 should reduce the degree to which the overall biotransformation rate is limited by dispersion. Changes to all of the relevant dimensionless parameters are summarized in Table 5.7:

Table 5.7. Scenario 1(a): comparison of baseline and enhanced dimensionless parameters.

Parameter	**Baseline Value**	**Enhanced Value**	**Units**
Pe_T - fast layer	748	791	dimensionless
Sh_2' - fast layer	109	19.2	dimensionless
Da_6 - fast layer	3	0.5	dimensionless
Pe_T - slow layer	557	1547	dimensionless
Sh_2' - slow layer	1301	602	dimensionless
Da_6 - slow layer	31	14.3	dimensionless

As discussed above, alternative enhancements were also examined to more conclusively demonstrate that the quantitative framework can indeed be used to select the appropriate enhancement. Therefore, in addition to the use of flushing described above, enhancements to reduce mass transfer and biokinetics limitations were also completed. Specifically, a model run was completed where the sorption/desorption mass transfer coefficient, K_m, was increased to 1.0 day^{-1}, from 0.02 day^{-1} in the baseline condition. Additionally, a model run was completed where the specific utilization rate, q_{max}, was increased to 0.238 day^{-1}, from 0.0238 day^{-1} under the baseline condition. Caution was taken with regard to the increases in the relative rates detailed here such that the magnitude of the changes of the individual values as well as the dimensionless parameters, in the alternative enhancements were of the same order of magnitude as the predicted appropriate enhancement, while also maintaining values that were scientifically rationale (e.g., they could be demonstrated in the laboratory or a field site).

5.7.2 Scenario 3 - Enhanced

As discussed above, the Scenario 3 baseline condition represents a site where the biokinetics are the rate-limiting process. In a process similar to that for Scenario 1(a), the predicted appropriate enhancement is modeled under the same hydrogeologic and input conditions as the baseline case, and further, two additional alternative enhancements are analyzed.

Theoretically, the predicted enhancement to the baseline condition entails some means of stimulating the natural biomass such that the biodegradation rate is increased. In the field, this could be accomplished by several methods, including the addition of

biomass, or by increasing the specific utilization rate, e.g., via nutrient amendment, or by altering conditions from an anaerobic to aerobic setting. For the predicted enhancement, the latter was used. Specifically, it was assumed that by altering conditions from nitrate-reducing biotransformation to strictly aerobic conditions, an increase in the specific utilization rate could be achieved. Therefore, under the enhanced case, q_{max} was increased from 0.000238 day^{-1} to 0.238 day^{-1}. This increase in q_{max}, resulted in an increase in Da_6, the dimensionless parameter of concern, from 0.12 under the baseline condition to over 118 in the fast layer, and from 0.44 to over 392 in the slow layer. These changes indicate that biokinetics were no longer limiting (e.g., where the value of Da_6 was <<1 in the baseline case prior to enhancement) as can be seen in Fig. 5.9. Changes to the relevant dimensionless parameters are summarized in Table 5.8:

Table 5.7. Scenario 3: comparison of baseline and enhanced dimensionless parameters.

Parameter	**Baseline Value**	**Enhanced Value**	**Units**
Pe_T - fast layer	2975	2975	dimensionless
Sh_2' - fast layer	217	217	dimensionless
Da_6 - fast layer	0.12	119	dimensionless
Pe_T - slow layer	685	615	dimensionless
Sh_2' - slow layer	799	799	dimensionless
Da_6 - slow layer	0.44	393	dimensionless

Similar to Scenario 1(a), alternative enhancements were also compared to the enhancement predicted to be appropriate. Specifically, a model run was completed where the mass transfer coefficient was increased to 1.0 day^{-1}, from 0.01 day^{-1} in the baseline

condition. Additionally, another model run was completed where the advection rate was increased six-fold in an effort to increase the transverse mixing between substrates.

5.8 Model Output

The following chapter presents the results of modeling experiments discussed above. The first section defines the two types (quantitative and qualitative) of output created to analyze and compare the data results, while the remaining sections provide the results of each of the baseline experiments.

5.8.1 Output Methods

Output results of numerical modeling for solute transport typically take the form of a dataset consisting of x, y, and z coordinates, or the location of the node within the domain, and the value (e.g., species concentration) at that location. Such data files are often quite lengthy, especially when employing a fine grid mesh size, or when the area of the domain is large. Therefore, it is convenient to develop a means of capturing the data in a format that is easily interpreted for comparison between different time steps and between different species at one point in time.

The two types of techniques used for visualizing output data in this work are quantitative (e.g., calculation of total mass in a system), and qualitative (e.g., contour plots). The process of developing the output formats is described below.

5.8.1.1 Qualitative Output Methods

Qualitative output, in the form of contour plots provides for visual inspection and subjective comparison of model results between different time steps of the same species, or between different species during the same time step. Within the VMOD environment,

any number of time steps can be selected for which output data is generated. For each selected output step, the x, y, and z location, as well as the species value (concentration) is captured into a data file. While VMOD provides an output menu where contour plots can be viewed, a more robust form of contour plot was desired. To accomplish this, the output files were generated for the given time periods, and manipulated using Surfer®, Version 6.0, developed by Golden Software, Inc.

The first step in creating a contour plot within Surfer® is to "grid" the contour plot framework. This consists of importing the model grid spacing and dimensions into Surfer®. Shan and Stephens (1994) provide a recommended application of the gridding process to minimize the introduction of numerical errors as a result of an inaccurate grid development. Their recommended application ensures that the actual grid spacing from the numerical model is imported into Surfer® and used for the subsequent contour development.

With the grid accurately defined, the contour plot is then generated by interpolating spatial distribution using the dataset of known points. A common method of contouring, and the method used here, is kriging. Kriging is a geostatistical approach that relies on the actual spatial correlation and structure of data rather than by weighting the data to some constant value - e.g., weighted to the power of the inverted difference between two points under the inverse distance method of contouring (Anderson and Woessner, 1992). Originally developed for the mining industry to map ore deposits, kriging has developed into a technique utilized throughout the statistical realm and environmental applications (Anderson and Woessner, 1992) as well as other fields where data distribution is sought, such as the health industry and disease tracking (Krivoruchko

and Gotway, 2004). A subset of kriging known as ordinary kriging (OK) is a rigorous method that unlike other methods, optimizes the spatial prediction of an unsampled location by completing the spatial correlation of the unsampled location from local known points without needing to consider the actual fixed location of the known points. Rather, the interpolation of the unsampled locations is completed by focusing on the spatial correlation or distance to the sampled or known points. Once the contoured data file is generated, a two or three-dimensional plot can be developed. Through the kriging variogram, a usefeul tool is generated, known as the kriging variance. This variance of the distribution can be viewed at each estimation point to provide a measure of the uncertainty associated with the estimated value at the unsampled location. Using Surfer®, and the methods above for grid development and contouring through ordinary kriging, two-dimensional contour plots at the relevant time steps for each of the species, aqueous and solid phase electron donor, electron acceptor, and biomass were produced. Contour intervals for each species were held constant to the extent possible to accurately compare between contour plots for the time steps of interest. For each contour plot, the illustration is presented with the longitudinal distance (0.0 to 1.2 m) along the x-axis and the transverse distance (0.0 to 0.3 m) in a perpendicular direction along the z-axis. An example of a contour plot is depicted in Fig. 5.11

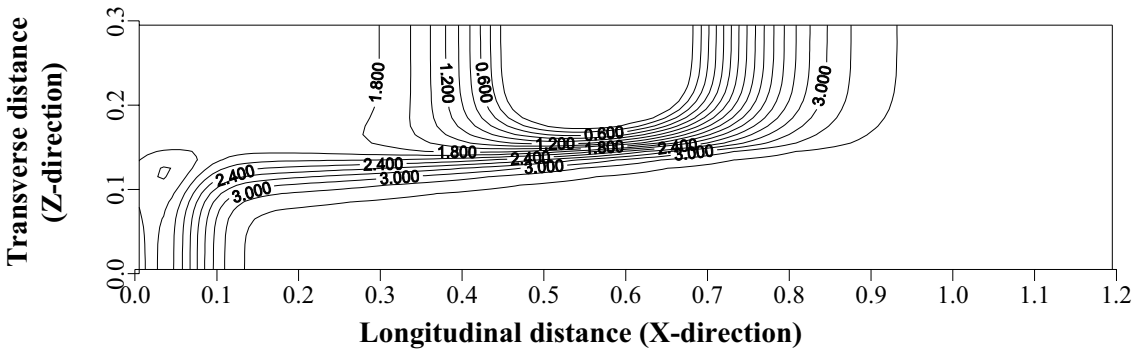

Figure 5.11. Example contour plot of electron acceptor concentration in domain. Contour interval is 0.2 mg/l.

5.8.1.2 Quantitative Output Methods

Quantitative output provides a measured or calculated result in the form of a specific value. It is useful here to apply quantitative techniques to calculate a species mass balance on the system. The mass balance is found by computing the total mass of each species as each given time step where output is generated. This calculation was carried out for a couple of reasons. First, a mass balance for all species at each time step can be compared to the same mass balance calculated at different sequential time steps. This provides an indication of whether or not mass in conserved in the system during the numerical analysis, or whether "breakthrough" has occurred or a loss at the downgradient end of the domain is observed. Second, a mass balance can be used to quickly compare the relationship between species or phases of one species at various time steps as the model progresses (e.g., confirming that an increase in the solid-phase concentration due to sorption is coupled with a decrease in aqueous-phase concentration).

Calculation of the species mass or mass balance can be completed in several ways. First, the species mass can be computed at each time step within the operation of a numerical code by mathematical calculation of input, output, and residual mass. When this routine is not included or easily extrapolated from a numerical code, a second means

of calculating mass balance is to compute mass using a contour plot and area calculation (e.g., Mravik et al, 2003). From basic integral calculus, the Riemann Sum is a calculation of the area under some function *f*(x). If a contour plot was generated from output data, and the shape of the contour could be described as a differential function *f*(x), then integration of the area under the curve of the contour can be approximated by dividing the area under the contour curve into appropriately sized rectangles to cover the area and the summing the area of those rectangles. This process can be achieved using a numerical code.

For the subject research, a more simplified means of calculating total mass was desired, namely due to the number of scenarios completed and the need to quickly view output results without the need for further numerical computation. To accomplish this, a method modified from the Riemann Sum was developed. The output files generated by VMOD provide the x, y, and z positions and concentration at each node of the domain. Rather than contour the data and attempt to describe the resulting contour intervals with some function *f*(x), a simplified approach was used where the area around each node with a concentration value was calculated. Fig. 5.12 depicts a portion of the model domain with a detail of a node. As an example, with a grid spacing of 0.01 m by 0.01 m, the first node closest to the origin is located at 0.005 m (x direction) and 0.005 m (y direction) with the node centered in the 0.01 m by 0.01 m square. The mass of the aqueous species at this location is given by Eq. 5.26

$$\underset{mass(mg)}{aqueous \quad species} = Concentration(mg/L) \times Area(m^2) \times Thickness(m) \times porosity \qquad (5.26)$$

Similar calculations can be made at each node and summed over the entire domain. This was accomplished by importing the output dataset into a Microsoft Excel® worksheet. The column of concentration data was multiplied by a column of areas (0.001 m^2), unit thickness (1 m), porosity (0.35), and 1000 (unit conversion for liters to cubic meters) with the result tabulated in another column. The resulting column was then summed for the entire domain providing the total mass of the species at the given time step. Similarly, the total species mass for sorbed constituents can be calculated. In this case, the porosity term is replaced with the bulk density. This calculation is given by Eq. 5.27

$$\begin{matrix} solid \quad species \\ mass(mg) \end{matrix} = Concentration(mg/kg) \times Area(m^2) \times Thickness(m) \times bulk \quad density \quad (5.27)$$

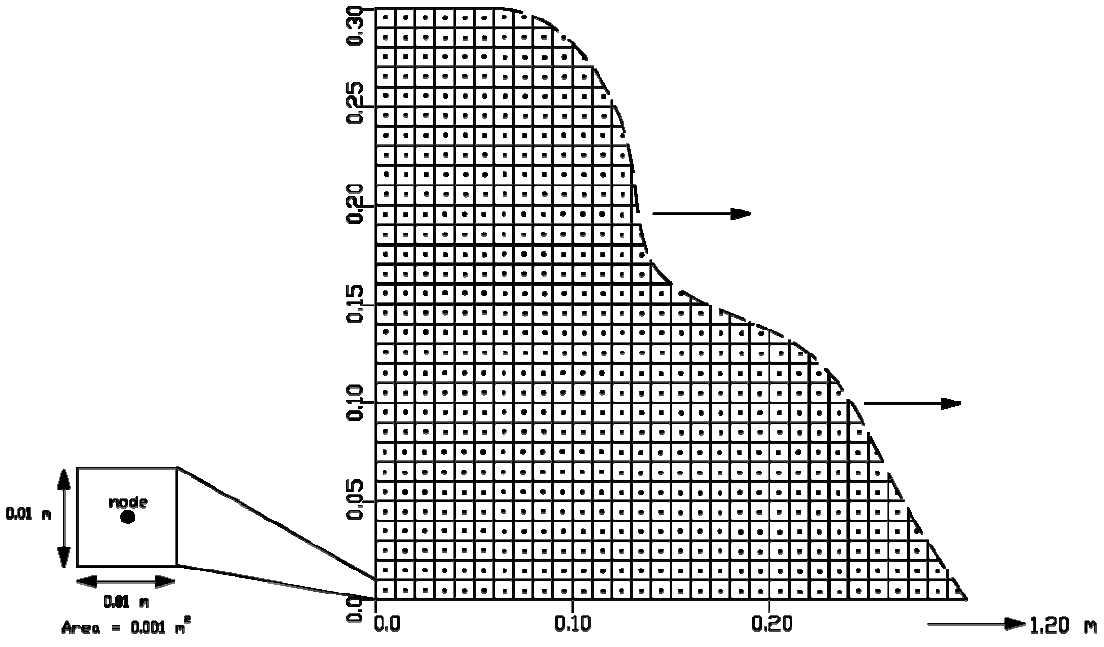

Figure 5.12. Detail of domain grid with method of area calculation around nodes.

6.0 RESULTS AND DISCUSSION

This chapter presents the results of the Phase One baseline scenario numerical simulations as well as those of the Phase Two enhanced scenario numerical simulations. In each of the following sections, one of the two evaluated scenarios is presented. First, a qualitative evaluation of the results for the baseline conditions (depicted graphically using contour plots) is presented, followed by the results of the predicted appropriate enhancement to the baseline conditions (also with the results depicted using contour plots). Next, a quantitative comparison between the baseline conditions and the conditions with the predicted appropriate enhancement is provided by using calculations of total mass in the system to quantify the effect of the enhancement. Finally, a quantitative comparison is made between the effects of the predicted appropriate enhancement and two alternative enhancements, also by using calculations of total mass in the system. The two scenarios evaluated here are presented sequentially, starting with Scenario 1(a) (section 6.1) followed by Scenario 3 (section 6.2).

6.1 Scenario 1(a)

6.1.1 Baseline Simulation Results

As described in detail in Chapter 5, the baseline Scenario 1(a) is a representation of a field site where a contaminant source is present in a low conductivity layer (e.g., a layer of a lower permeability matrix or a clay stringer in a stratified sand aquifer) in which oxygen has been depleted, or is present at very small concentrations. This layer is overlain by a higher conductivity layer where contamination is not present, but where there is a higher concentration of oxygen present, e.g., due to diffusion from the capillary

zone, and/or advection from an upgradient uncontaminated zone. This is an important scenario, as previous studies indicate that layers of varying hydraulic conductivity are an important factor affecting *in situ* biodegradation with contaminants predominantly persisting in low hydraulic conductivity layers (e.g., Murphy, et al., 1992; Szecsody, et al., 1994; Wood, et al., 1994; Yang, et al., 1994).

The baseline numerical simulation for Scenario 1(a) was run for 10 days using the VMOD/RT3D model. As presented in Fig. 5.7, above, the inputs consist of a finite source of aqueous naphthalene in the slower layer (10 mg/l source in a 0.1 m long by 0.15 m vertical area) with a background and constant influent injection concentration of 2.0 mg/l oxygen for the upper layer alone. The finite source of aqueous naphthalene can be seen as representing the leading edge of a plume migrating into an otherwise uncontaminated zone of the lower conductivity layer. Based on the quantitative framework outlined in Chapter 4.0, the rate-limiting process in this scenario is the rate of transverse dispersion, which is predicted to manifest itself primarily in the form of a limited degree of transverse mixing between the electron donor naphthalene and the electron acceptor oxygen present in the lower and upper layers, respectively (Odencrantz, 1992).

Contour plots for aqueous naphthalene, oxygen, biomass, and sorbed naphthalene are presented in Fig. 6.1 through Fig. 6.4, respectively, at 1, 3, 6, and 10 days during the model run. As can be seen in Fig. 6.1, the extent of longitudinal migration of the aqueous contaminant plume is marginal, with a longitudinal migration from the original source length of 0.1 m to approximately 0.25 m, where a concentration front of 1 mg/l is

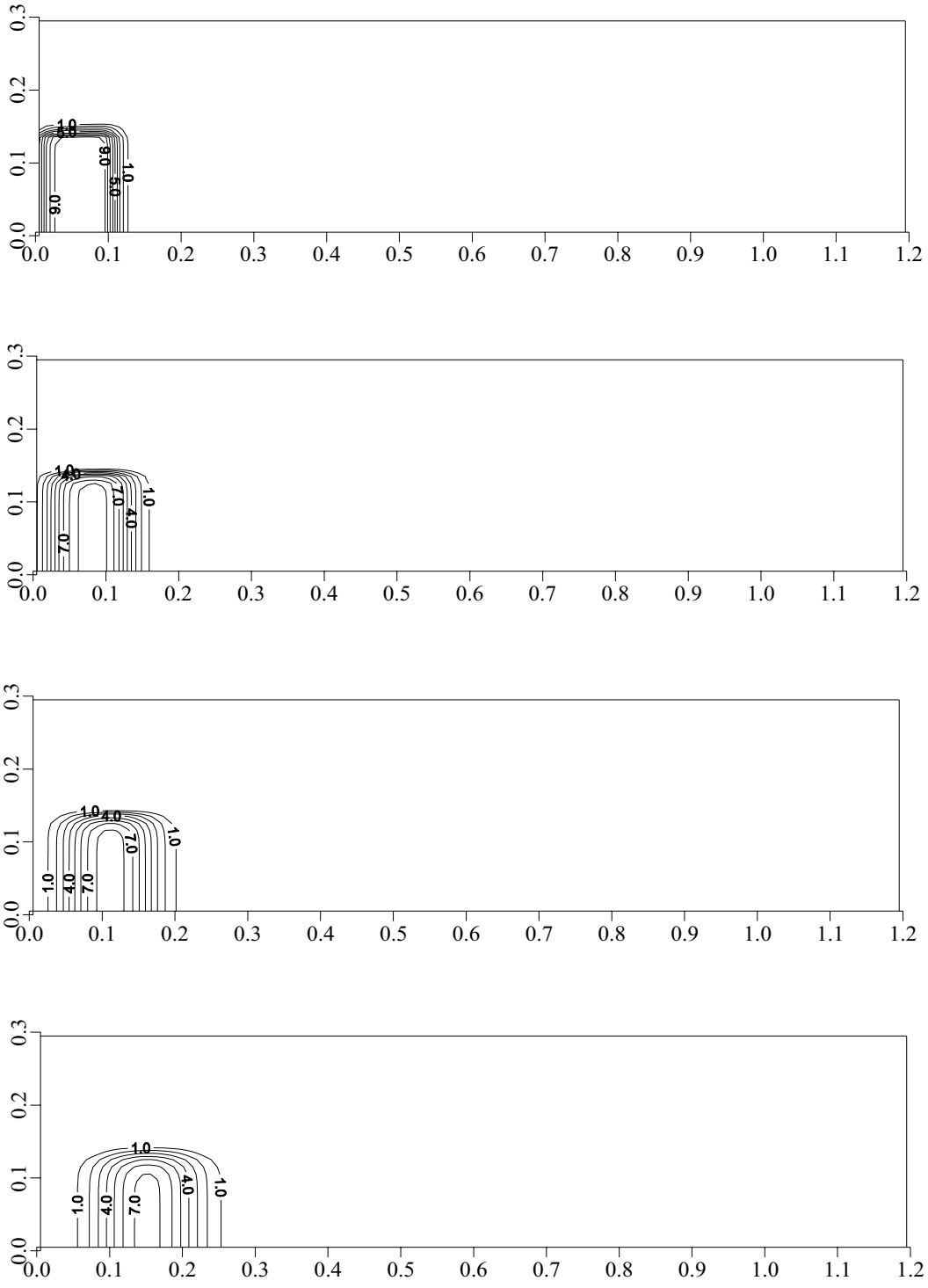

Figure 6.1. Scenario #1(a): Contour plots of naphthalene (aq.) at 1, 3, 6, and 10 days. Contour interval is 1.0 mg/l.

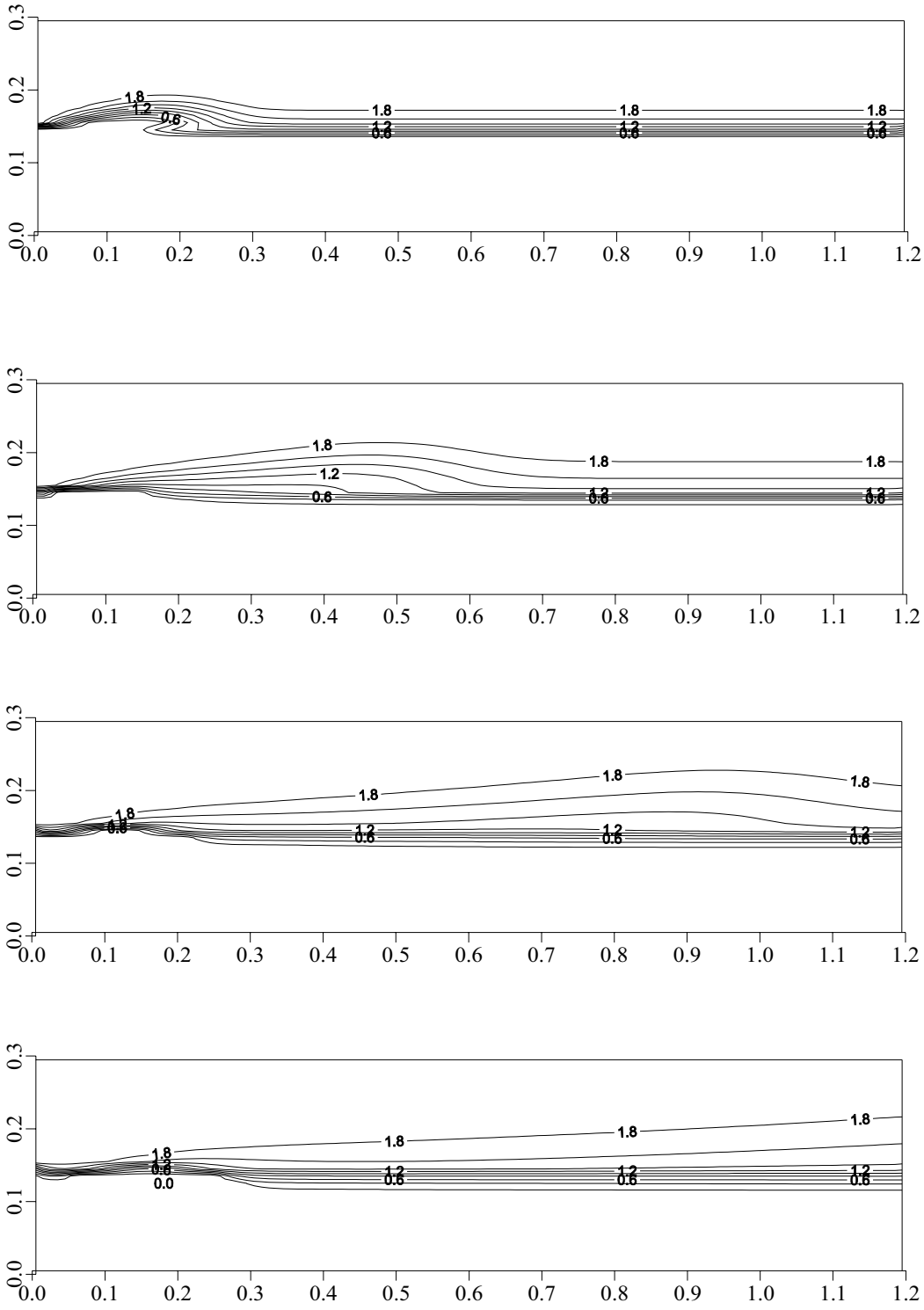

Figure 6.2. Scenario #1(a): Contour plots of oxygen at 1, 3, 6, and 10 days. Contour interval is 0.2 mg/l.

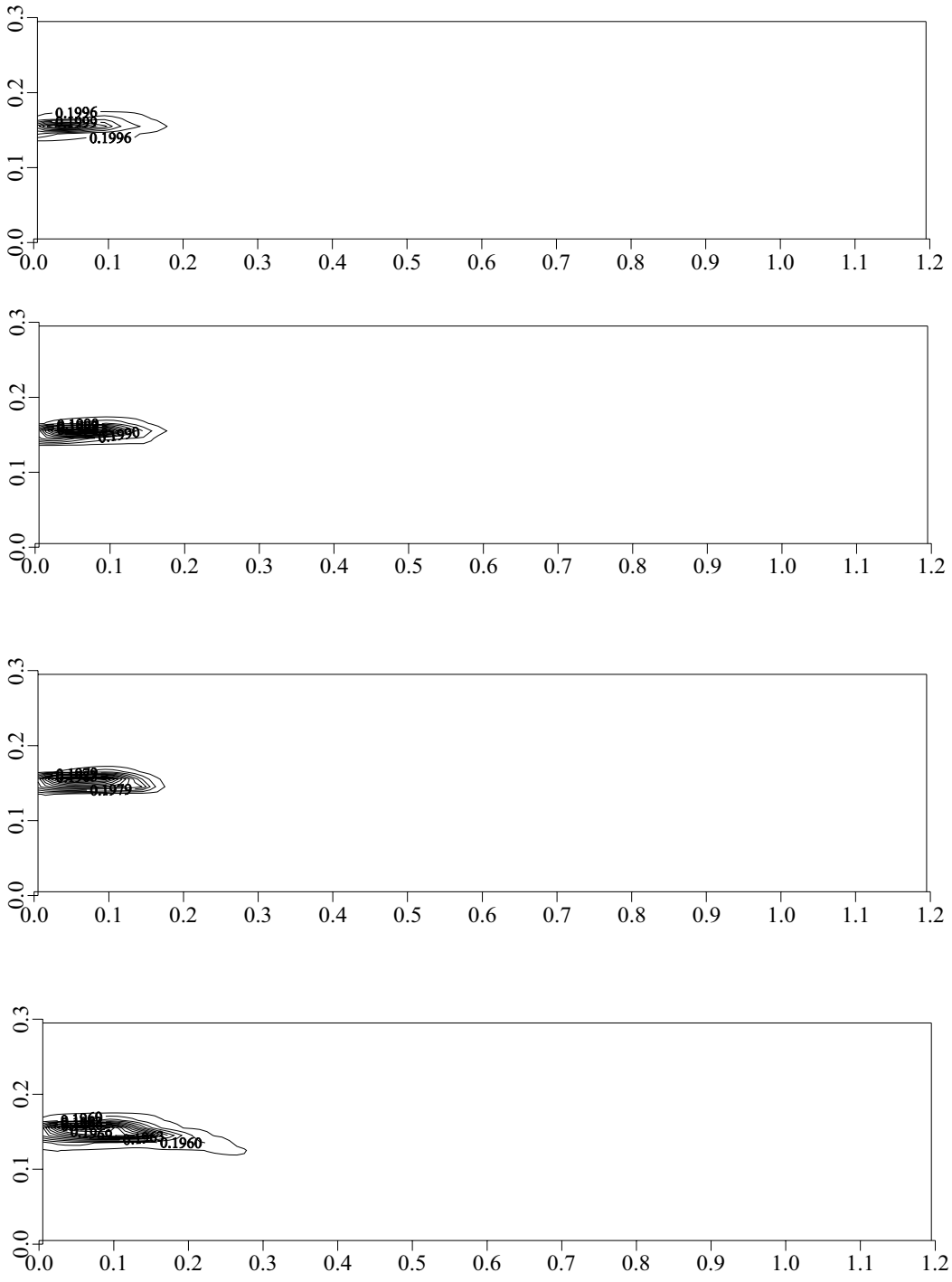

Figure 6.3. Scenario #1(a): Contour plots of biomass at 1, 3, 6, and 10 days. Contour interval is $1x10^{-4}$ mg/kg.

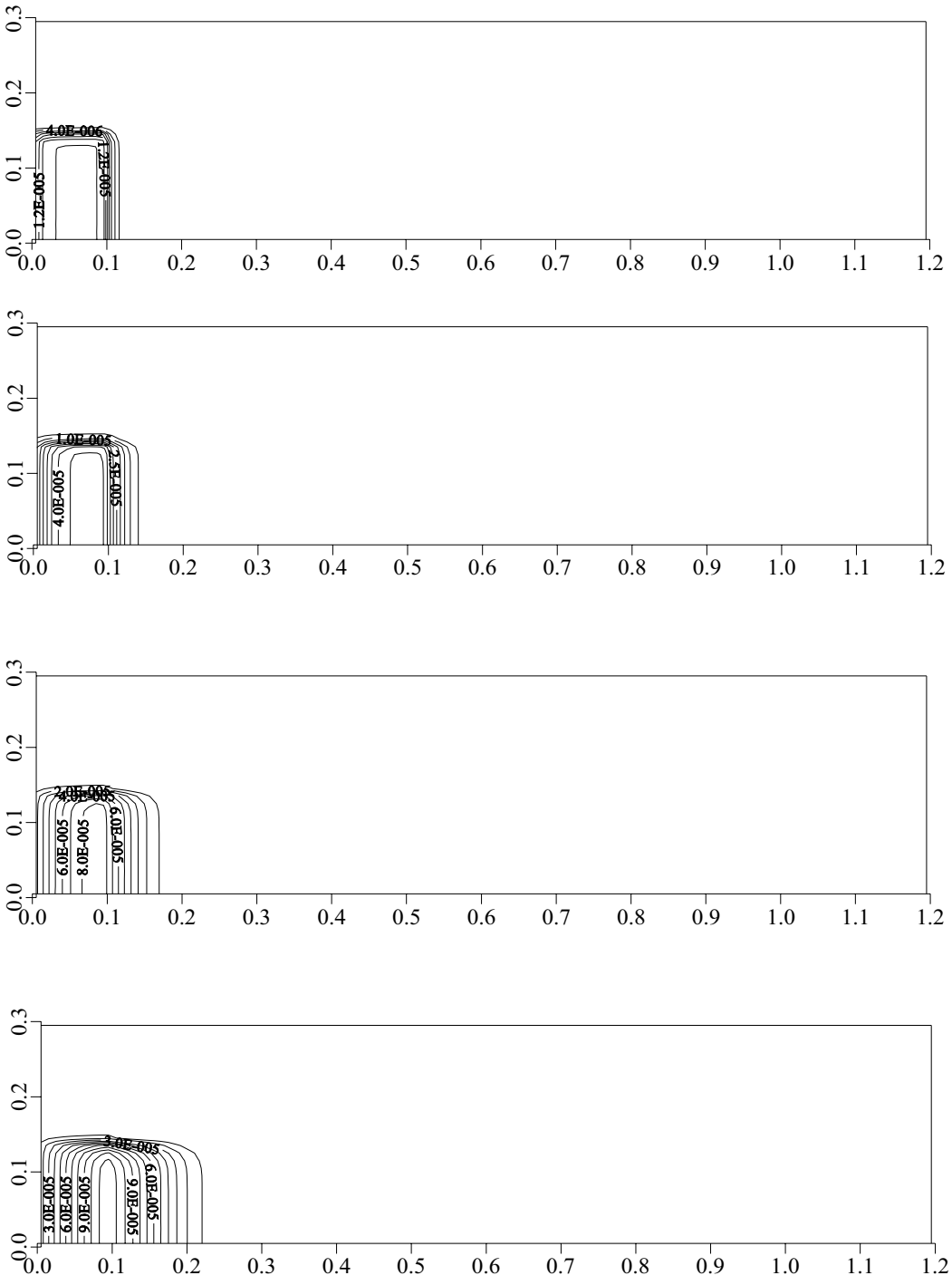

Figure 6.4. Scenario #1(a): Contour plots of naphthalene (sorbed) at 1, 3, 6, and 10 days. Contour interval is $2x10^{-6}$ mg/kg for 1 day, $5x10^{-6}$ mg/kg for 3 days, and $1x10^{-5}$ mg/kg for 6 and 10 days.

observed after 10 days. Vertically, the contaminant source is initially highly concentrated along the interface with the upper fast layer, with the concentration subsequently decreasing to some extent after ten days; however, the center of the contaminant plume still reveals a concentration of greater than 7 mg/l.

In Fig. 6.2, the oxygen (electron acceptor) profile is depicted. As can be seen from these panels, a concentration gradient develops along the interface of the two layers, where the initial oxygen concentration decreases from 2 mg/l in the upper layer, to 0 mg/l in the lower slow layer. The concentration gradient occurs mostly in the upper layer where a traveling wave of reduced oxygen concentration develops as a result of degradation at the source end of the domain. This traveling wave is identifiable by the mounding appearance of the 1.8 mg/l contour moving across the domain. A comparable, but lagging, traveling wave of reduced oxygen concentration resulting from biodegradation at the source zone is also observed in the slow layer. In addition to lagging individually, the vertical extent of this wave is smaller than in the fast layer, because the vertical extent of the oxygen diffusion and dispersion into the lower layer is minimal. These differences between the fast and slow layers can be explained quantitatively by reviewing Eq. 4.4, and the definition of dispersion: the longitudinal migration in the slow layer is limited by the reduced seepage velocity which is a direct a function of the media properties (i.e., the smaller hydraulic conductivity); and the reduced vertical dispersion into the slow layer is also a function of the slow layer media properties (i.e., the small vertical transverse dispersivity) and the reduced seepage velocity.

The biomass concentrations in the domain are presented in Fig. 6.3. Because the contaminant source zone is limited to the initial 0.1 m of the slow layer, an overall reduction in domain-wide biomass concentration (initially 0.2 mg/kg) is evident due to the general lack of electron donor substrate (naphthalene) in much of the domain and the biological decay (decay coefficient = 0.00208 day^{-1}); however, a biomass "finger" does develop along the interface between the two layers, coincident with the location of the lower layer contaminant source zone. The biomass concentration is still decreasing in this "finger" over each time step, although the degree of reduction is not as great as that for the surrounding areas. This phenomenon occurred because there is at least a minimal amount of electron donor contaminant available so as to reduce the rate of biomass decay as compared to that seen elsewhere in the domain. In general, the longitudinal extent of the biomass "finger" correlates to the longitudinal extent of the naphthalene plume. This phenomenon has been observed experimentally in similar systems. For example, Szecsody et al. (1994) performed a laboratory study of the transport and biodegradation of quinoline in a two-dimensional horizontally-stratified porous media under dual substrate limitation. They found that the interlayer mass transfer resulted in the arrival of substrate and oxygen 10's to 100's of hours sooner in the lower conductivity layer near the interface compared to other locations "deeper" within the lower conductivity layer where substrates arrived only via advection from the influent source. Early arrival of substrates near the interface resulted in biodegradation of quinoline for a longer period than within the layers, yielding increased growth in a 1-3 cm thick zone.

Finally, in Figure 6.4, the sorbed naphthalene data are depicted. In this series of panels, the distribution of sorbed phase is seen to correlate with the presence of the

aqueous phase naphthalene, as expected. The mass transfer kinetics and partition coefficients of this scenario were selected such that the system can be characterized as having an overall weak sorption sink. Therefore, the extent of sorption is minimal. As a result, after 10 days, in the center of the aqueous plume, where there is a maximum concentration of 7.0 mg/l, the corresponding sorbed concentration was only approximately $1x10^{-4}$ mg/kg.

6.1.2 Enhanced Simulation Results - Flushing

As presented in Chapter 5, the selected engineered perturbation for this scenario was aimed at increasing the rate of transverse mixing between the two layers to alleviate the overall rate-limiting process of transverse dispersion and, thereby, stimulate growth and increase contaminant degradation. This perturbation was accomplished numerically by increasing the rate of advection (i.e., the seepage velocity) and, therefore, the amount of vertical transverse mechanical dispersion (defined as α_T times v_x). In the field, the comparable engineered enhancement that is simulated here is the use of flushing (e.g., by installing vacuum or pumping wells) to increase the groundwater flow. Note that the effect of increased advection would not occur if the dispersion coefficient was diffusion controlled, in which case the degree of mixing would be independent of the magnitude of the advection rate (MacQuarrie and Sudicky, 1990)

Like the baseline numerical simulation, the enhanced simulation for Scenario 1(a) was run for 10 days using the VMOD/RT3D model. Thus, the input, as before, consisted of a finite source of aqueous naphthalene in the slower layer (10 mg/l source in a 0.1 m by 0.15 m area) with a background and influent injection concentration of 2 mg/l oxygen into the upper layer only. Contour plots for aqueous naphthalene, oxygen, biomass, and

sorbed naphthalene are presented in Fig. 6.5 through Fig. 6.8, respectively, at 1, 3, 6, and 10 days during the enhanced model run.

As can be seen in Fig. 6.5, the extent of longitudinal migration of the aqueous contaminant plume is substantial in each time step compared to the baseline case, with an ultimate longitudinal migration of the plume center from the original source location to approximately 0.7 m after 10 days, at which point the concentration in the center of the plume was approximately 3.5 mg/l. The plume front is also more dispersed compared to the baseline case, as expected with the increase in mechanical dispersion. For example, the concentration front of 1 mg/l is now observed at greater than 0.8 m after 10 days, compared to 0.25 m for the baseline case. Vertically, the contaminant source is initially highly concentrated along the interface with the upper fast layer, as was seen with the baseline condition; however, after 10 days, compared to the baseline case, there is a greater degree of vertical dispersion and resulting loss due to biodegradation, as expected.

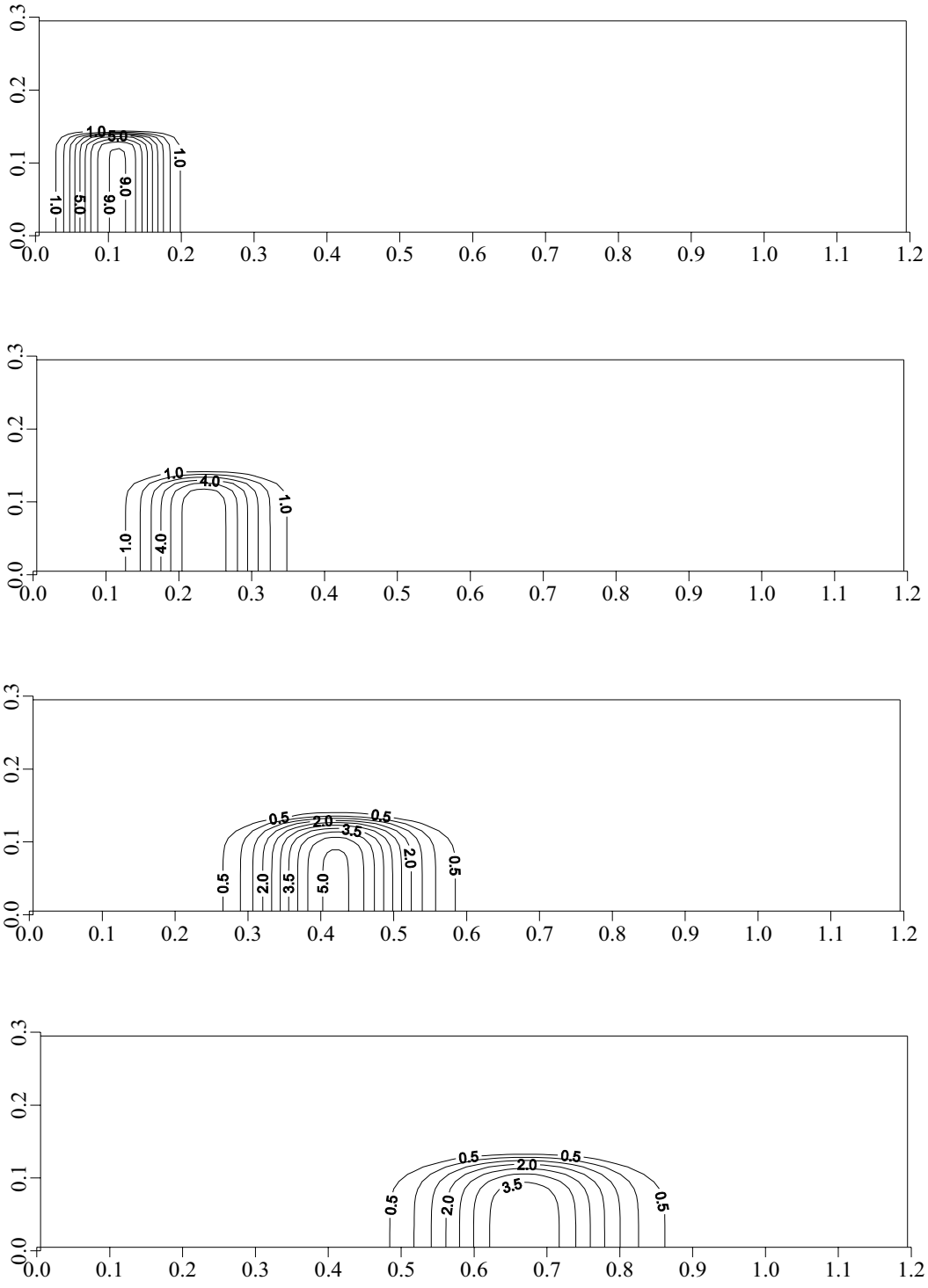

Figure 6.5. Scenario #1(a) (enhanced): Contour plots of naphthalene (aq.) at 1, 3, 6, and 10 days. Contour interval is 1.0 mg/l for 1 and 3 days, and 0.5 mg/l for 6 and 10 days.

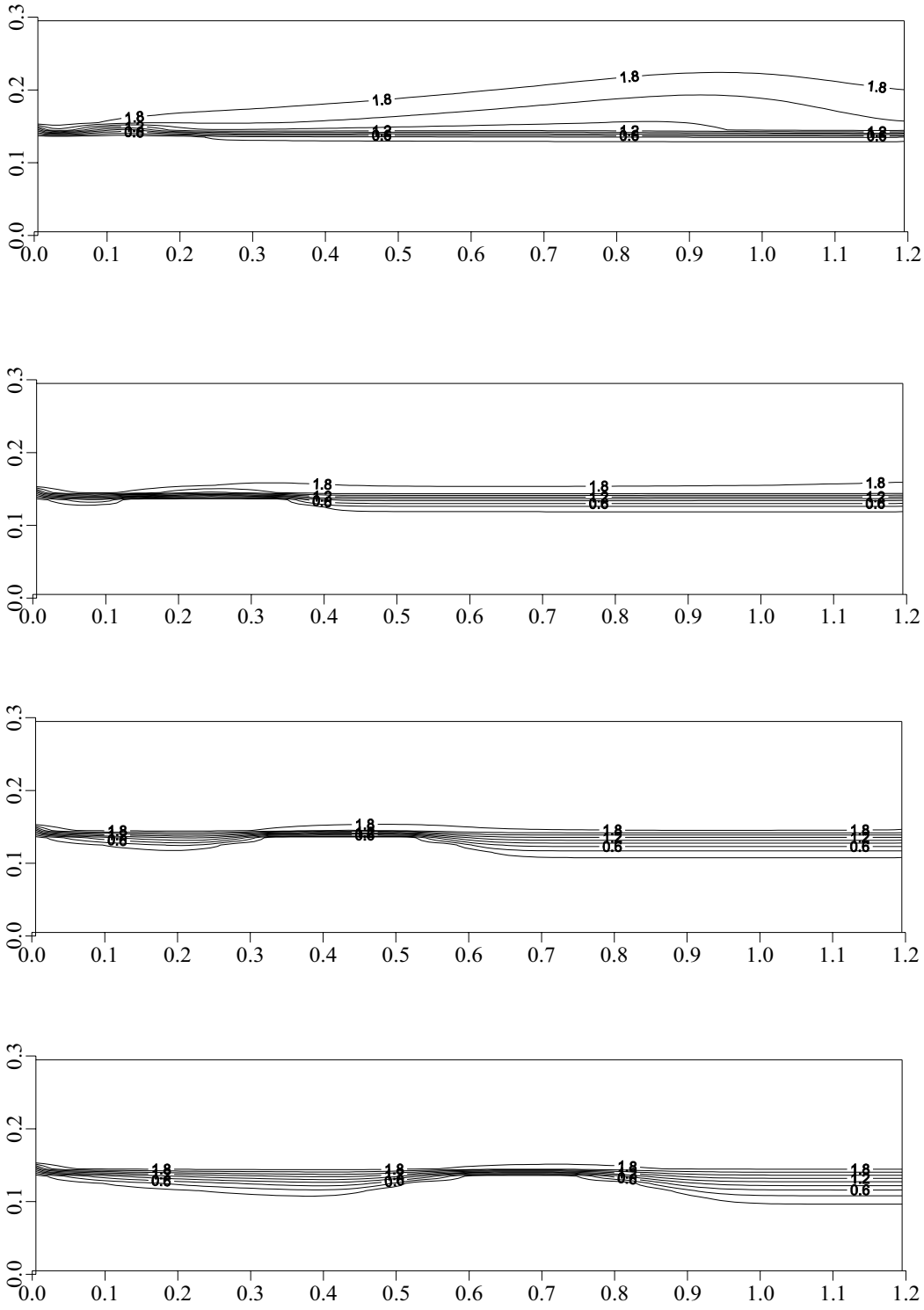

Figure 6.6. Scenario #1(a) (enhanced): Contour plots of oxygen at 1, 3, 6, and 10 days. Contour interval is 0.2 mg/l.

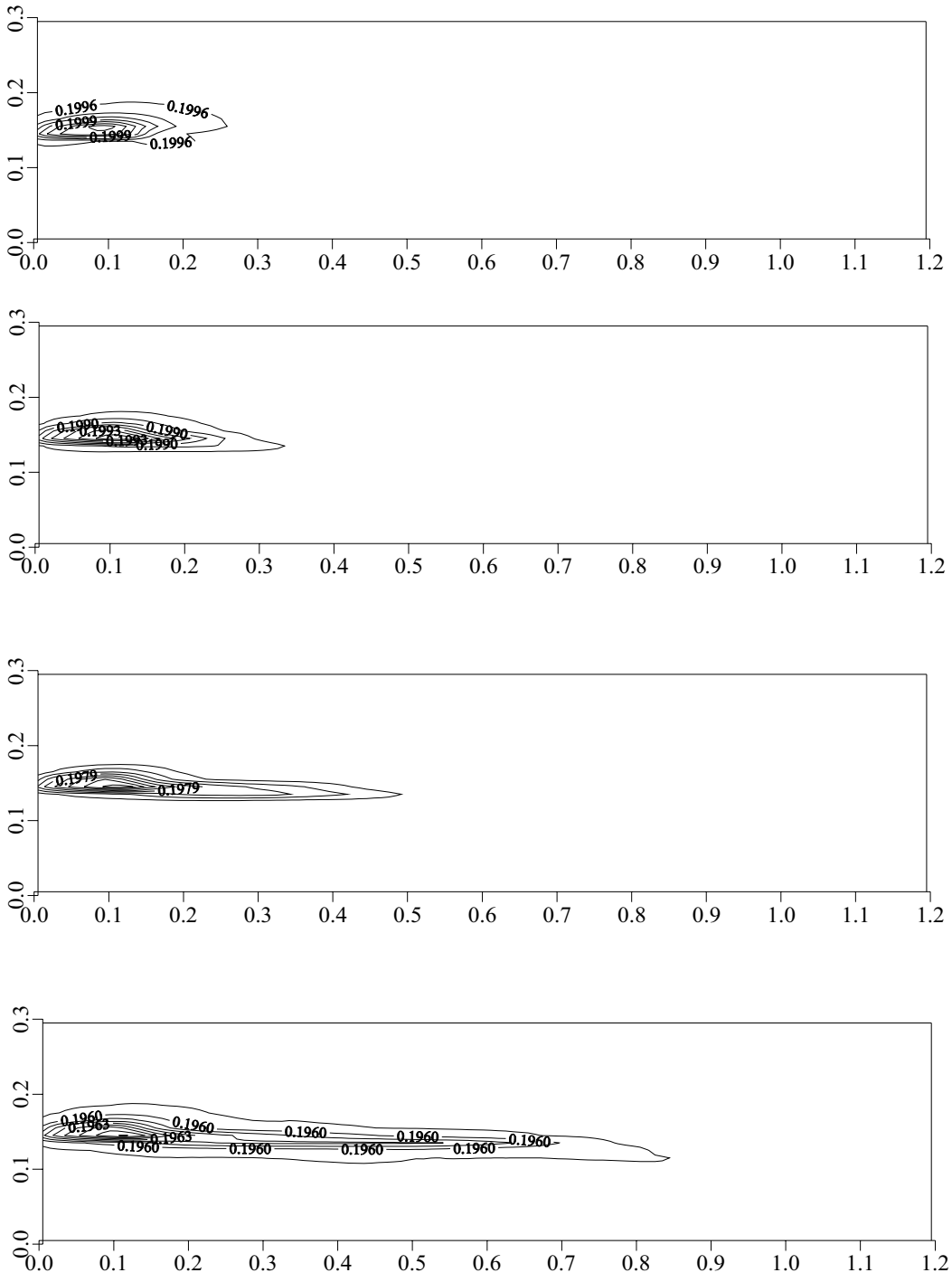

Figure 6.7. Scenario #1(a) (enhanced): Contour plots of biomass at 1, 3, 6, and 10 days. Contour interval is $1x10^{-4}$ mg/kg.

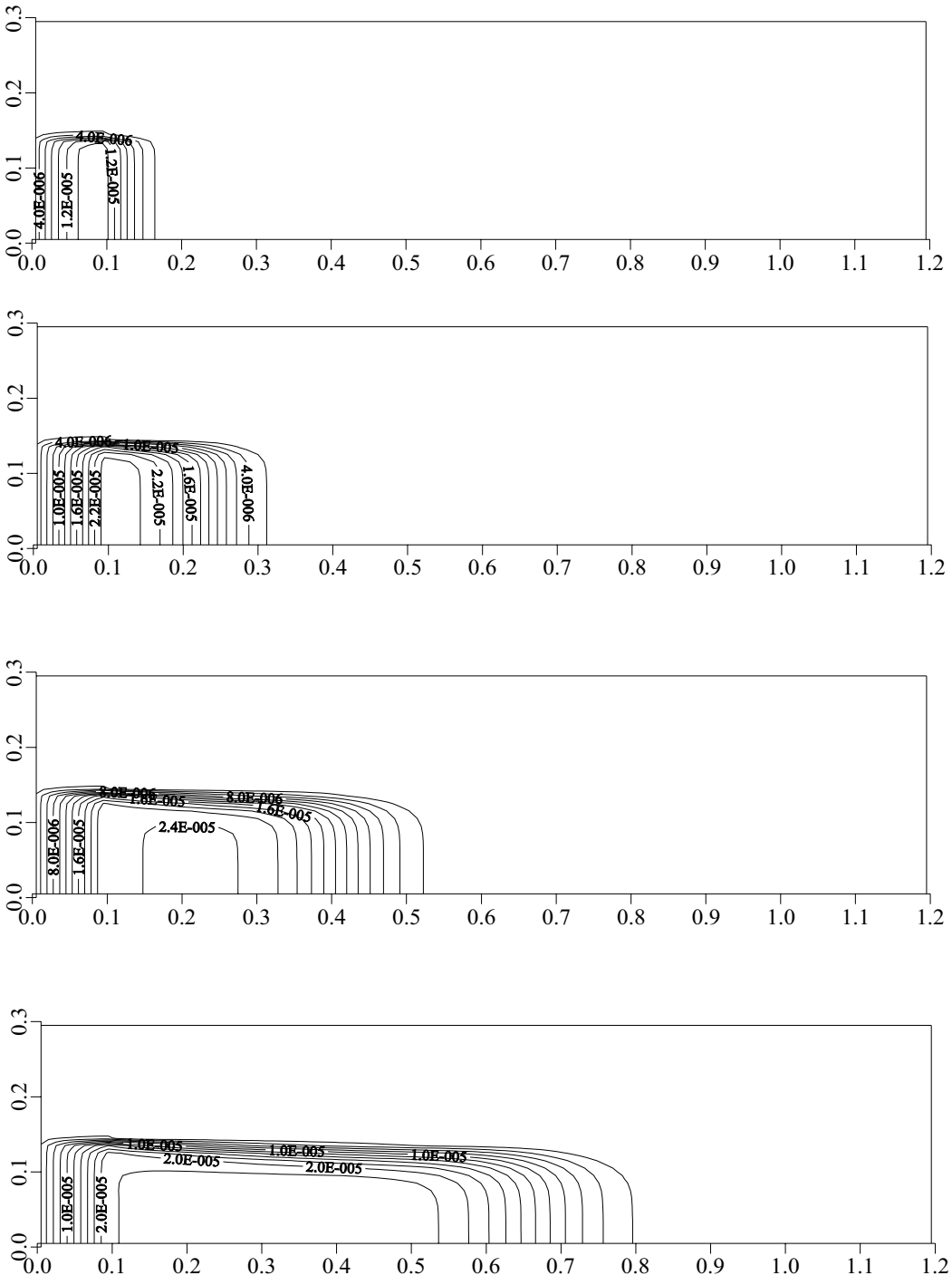

Figure 6.8. Scenario #1(a) (enhanced): Contour plots of naphthalene (sorbed) at 1, 3, 6, and 10 days. Contour interval is 2×10^{-6} mg/kg.

In Fig. 6.6, the oxygen (electron acceptor) profile is presented for the enhanced case. As can be seen from these panels, a concentration gradient similar to that seen in the baseline case (Fig. 6.2) develops along the interface of the two layers; however, due to the increased advection, oxygen in the upper layer is replenished more quickly than for the baseline case. As a result, the concentration gradient more rapidly becomes uniform in the upper layer, because the traveling wave of reduced concentration, or mounding appearance of the 1.8 mg/l contour, travels across the domain significantly faster than in the baseline condition. This replenishment of oxygen across the upper layer results in an increased transverse dispersion of oxygen into the lower layer. Stated in other terms, the result is a greater and more consistent depth of penetration of oxygen into the lower layer. This result, as seen by others (e.g., Odencrantz, 1992) results in a greater zone of mixing of the two substrates.

The biomass concentration profiles are presented in Fig. 6.7. Similar to the baseline condition, an overall reduction in domain-wide biomass concentration from the initial concentration of 0.20 mg/kg is evident, again, due to biomass decay (where the decay coefficient = 0.00208 day^{-1}) and the fact that the contaminant electron donor is only present in a small area of the domain. However, the biomass "finger" that developed in the baseline condition, also develops here along the interface between the two layers in the location of the lower layer contaminant source zone. Further, the longitudinal and vertical extent of the biomass "finger" is much greater for the enhanced case. Although the magnitude of the biomass concentration is still overall decreasing in this "finger" over each time step, compared to the baseline condition, there is an overall increase in the area within each contour interval, and a resulting greater extent of the

biomass “finger” along the interface. These observations are a direct result of the greater zone of mixing between the electron donor and electron acceptor substrates discussed above. Other modeling (Odencrantz, 1992; Wood, et al., 1994; Yang, et al., 1994) and laboratory (Szecsody et al., 1994) studies with two-dimensional (vertical) stratified systems, under dual substrate limitation, have also demonstrated increased microbial activity and biomass production near the two-layer interface where hydraulic mixing between waters carrying different substrates occurs due to dispersion. Although the accumulation of biomass in these mixing regions can have a positive effect on contaminant degradation, it could also lead to localized plugging of a subsurface formation, creating additional permeability heterogeneity and significantly reduced groundwater flow and transport (Sturman et al., 1995).

In Fig. 6.8, the sorbed naphthalene data are illustrated. Similar to the baseline conditions, the distribution of the sorbed phase is correlated with the location of the aqueous phase naphthalene plume, with a longitudinally extended solid phase distribution along the domain length. Because the scenario was set up with relatively weak sorption parameters, and the plots of aqueous phase naphthalene under the enhanced conditions (Fig. 6.5) indicate greater decreases in the aqueous concentrations over time as compared to the baseline conditions, it was expected that the concentration of sorbed phase naphthalene throughout the lower layer would also decrease as compared to the baseline conditions. This effect is observed, albeit not dramatically, via inspection of the contour plots alone; however, the effect is illustrated more clearly by an examination of the total sorbed mass in the system over time, which is discussed in the next section.

6.1.3 Mass Calculations for Scenario 1(a)

As discussed in Chapter 5, the contour plots illustrated in Figs. 6.1 through 6.8 provide a means of qualitatively comparing the results of the baseline scenario to the enhanced conditions; however, it is also important to perform a quantitative analysis with which to examine the contaminant mass removal for the baseline and enhanced cases in light of the quantitative framework. Therefore, using the methods described in subsection 5.8.1.2, graphs of total mass in the system over the runtime (10 days) were generated for the constituents of concern (i.e., aqueous donor, aqueous acceptor, biomass, and sorbed donor). For the initial mass in the system, the calculation was made from the initial domain concentration and region as appropriate for each constituent (e.g., for aqueous donor, the calculation was made using the 10 mg/l concentration in the 0.1 m by 0.15 m source zone of the lower layer). Such calculations were made for both scenario trials (baseline and enhanced) within Microsoft Excel® so that the data could be compared on the same series of graphs. For each series of graphs, the baseline condition data are plotted using black-filled symbols for each data point, while the enhanced condition symbols are plotted using symbols with an open center.

The total mass of aqueous naphthalene in the system is presented as a function of time in Fig. 6.9. These data clearly show an overall greater decrease in the total mass for the enhanced condition, with greater advection, and therefore, increased dispersion. For example, the total mass at time 10 days in the baseline condition is approximately 4.1 mg, whereas the total mass at the same time with the enhanced condition is approximately 3.6 mg. However, it is important to note that although the naphthalene plume degrades at a more rapid rate with increased advection, it does travel further in a given time frame then

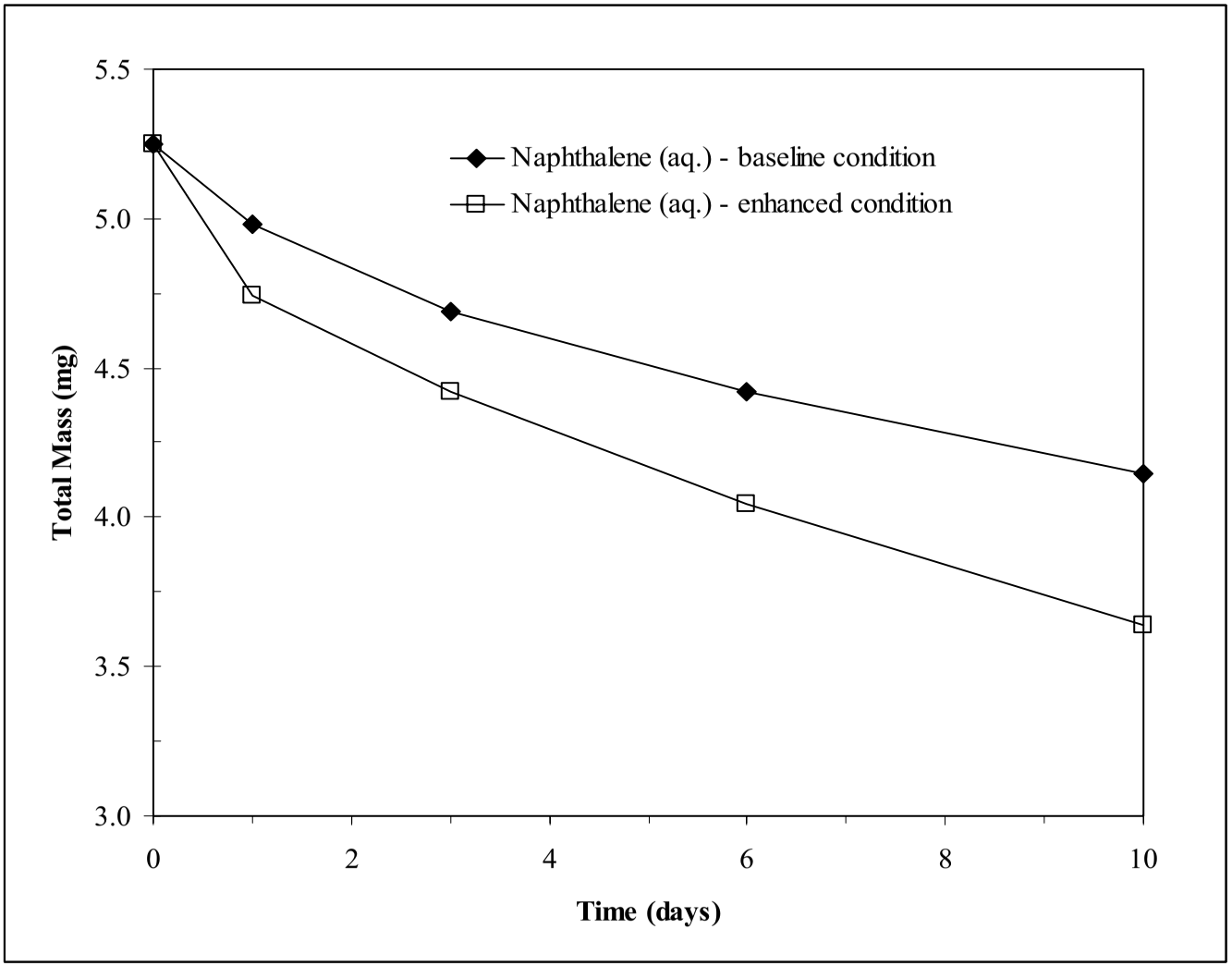

Figure 6.9. Scenario #1(a): Total mass versus time, naphthalene (aq.).

the plume does with the baseline conditions (e.g., compare Figs. 6.1 and 6.5), as discussed above. Thus, if the plume location is more important in a given situation than the time needed for substantial mass loss (e.g., due to proximity to a receptor of concern), then a rapidly migrating contaminant plume may be of greater concern, despite the fact that the mass loss is occurring more rapidly (MacQuarrie and Sudicky, 1990). In addition to looking at the total mass removal, it is also instructive to examine the rate of mass change, which was calculated from the slope of the total mass plot (change in mass divided by change in time). The resulting total rates of change for the two conditions are shown in Table 6.1.

Table 6.1. Scenario 1(a): comparison of removal rates for aqueous naphthalene as a function of time.

Day	Baseline Rate (mg/day)	Enhanced Rate (mg/day)
0-1	0.269	0.510
1-3	0.146	0.161
3-6	0.089	0.125
6-10	0.069	0.102

As can be seen in Table 6.1, the initial removal rate of naphthalene is significantly greater in the enhanced condition early in the model run (day 0 to 1). This can be explained by the initial proximity of the electron donor substrate to the electron acceptor along the interface and the resulting increased transverse mixing between the two in the enhanced case, and is consistent with the results seen by others (e.g., MacQuarrie and Sudicky, 1990; Odencrantz, 1992). As the time series progresses, the zone of mixing is broadened across the interface; however, the concentration gradients are reduced with time, and therefore, the difference in the mass removal rates becomes less over time.

The rate of change for the electron donor can also be explained by a review of the total mass data for the electron acceptor oxygen (Fig. 6.10). These data indicate that the total mass of oxygen initially decreases for both conditions, as the electron acceptor is used up by the biomass in the source zone. However, for the enhanced condition, the oxygen mass in the system quickly rebounds due to the constant injection of the "clean" groundwater in the fast layer at the higher advection rate, whereas for the baseline condition, the initial drop is more significant. Although the time required for the oxygen mass to rebound is slower for the baseline condition due to the slower advection (input) rate the rebound does occur, nevertheless. As a result, the difference in the rates of removal of donor mass becomes less dramatic over time, as discussed above. Interestingly, after day 1, the total mass of electron acceptor is less in the baseline condition than for the enhanced, which is in contrast to the observations of Odencrantz (1992) who found for a similar domain that increased transverse dispersion resulted in a greater decrease of electron acceptor mass. However, these contrasting observations can be explained by the differences between this study and that of Odencrantz (1992). One, Odencrantz (1992) changed transverse dispersion by simply changing the magnitude of the dispersivity, whereas, in this study, dispersion was changed by increasing advection. Although Odencrantz's (1992) approach was easier to implement and evaluate, the approach used in this study is a more realistic simulation of how dispersion can be increased in the field. Two, there is a difference between the input domain of this study and that of Odencrantz (1992), where there was a background concentration of electron donor present throughout the entire domain. Odencrantz's (1992) conditions led to increased electron acceptor usage compared to that with the "slug" plume of donor in the

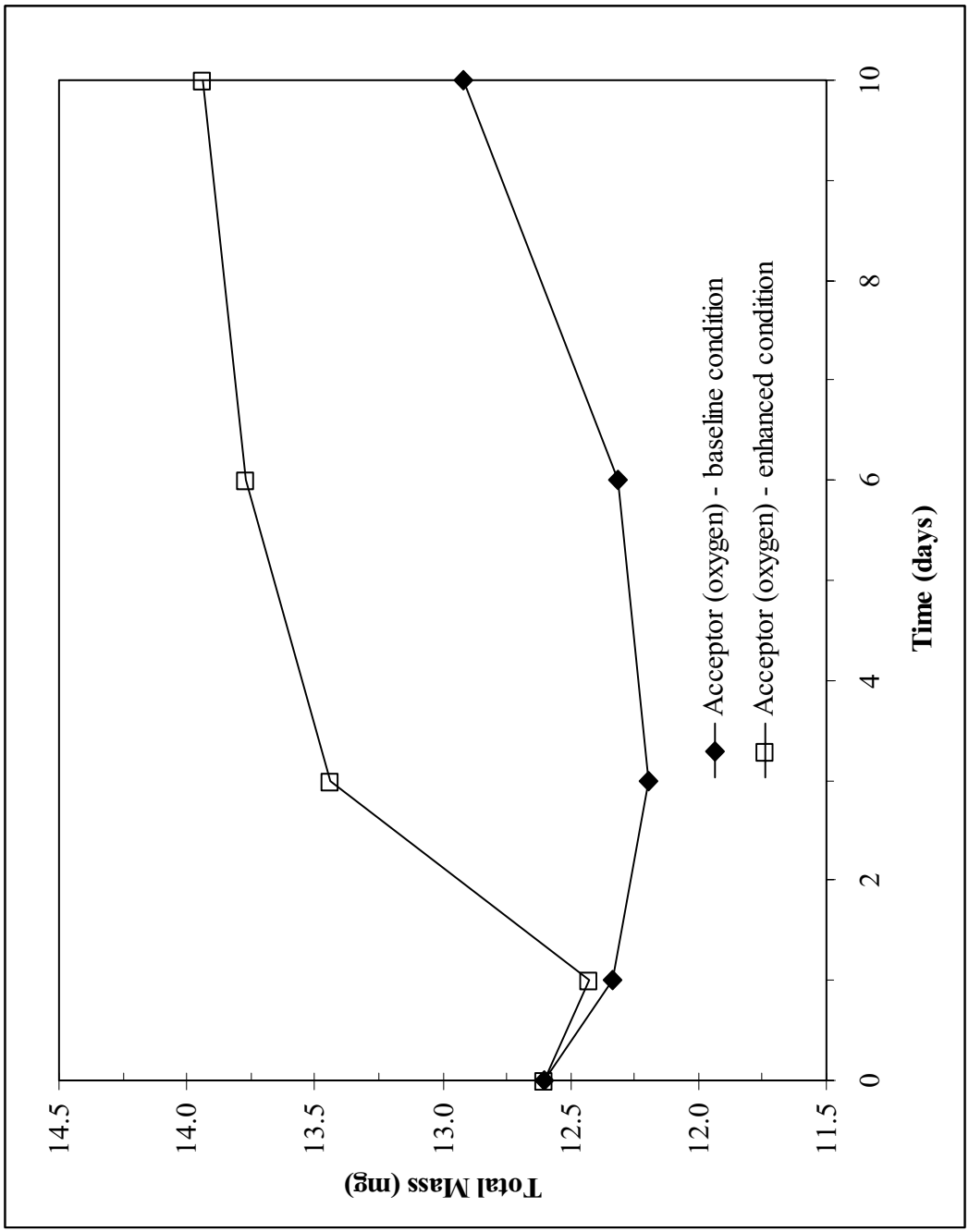

Figure 6.10. Scenario #1(a): Total mass versus time, electron acceptor.

current study. However, Odencrantz's (1992) use of a background concentration throughout the entire domain led to the mass loss of the donor out of the domain due to advection, a condition that was avoided in this study by only presenting the contaminant source in the slower layer. This method better captures the interfacial nature of the mixing between the electron donor and acceptor as the two input zones are kept separate with a sharp interface between the two.

Figures 6.11 and 6.12 present the comparison of total mass of biomass and sorbed naphthalene, respectively. Based on Fig. 6.11, a comparison of the total mass of biomass illustrates that there is no perceptible difference in the biomass for the two conditions. As was discussed above, the total mass of biomass in the system was expected to decrease over time due to the use of the input biomass decay constant (0.00208 day^{-1}) and the fact that the input donor was limited to just a small corner of the domain. While trials could have been completed without the biomass decay factor, this is not reflective of nature and, thus, the comparison of these data to that of bench-scale or field experiments could be inappropriate. Several researchers (e.g., Sudicky, et al., 1990; MacQuarrie and Sudicky, 1990) evaluated similar scenarios with varying advection rates and observed more dramatic effects in terms of increases in donor mass with increased advection, and therefore dispersion. Nevertheless, these researchers did not utilize the decay coefficient, and a quantitative evaluation through calculation of the total biomass over time was not completed. However, it can be inferred from the results of those studies that use of a decay coefficient of zero in the current study would have also produced more dramatic results in terms of enhanced electron donor contaminant mass removal with increased advection and dispersion than observed in Fig. 6.9.

With regard to the degree of sorption, it is evident that the enhanced advection condition resulted in a reduction in the concentration of sorbed naphthalene due to the increased biodegradation, albeit a small difference as is seen in Fig. 6.12. This small effect was expected because of the input conditions which correspond to relatively weak sorption kinetics.

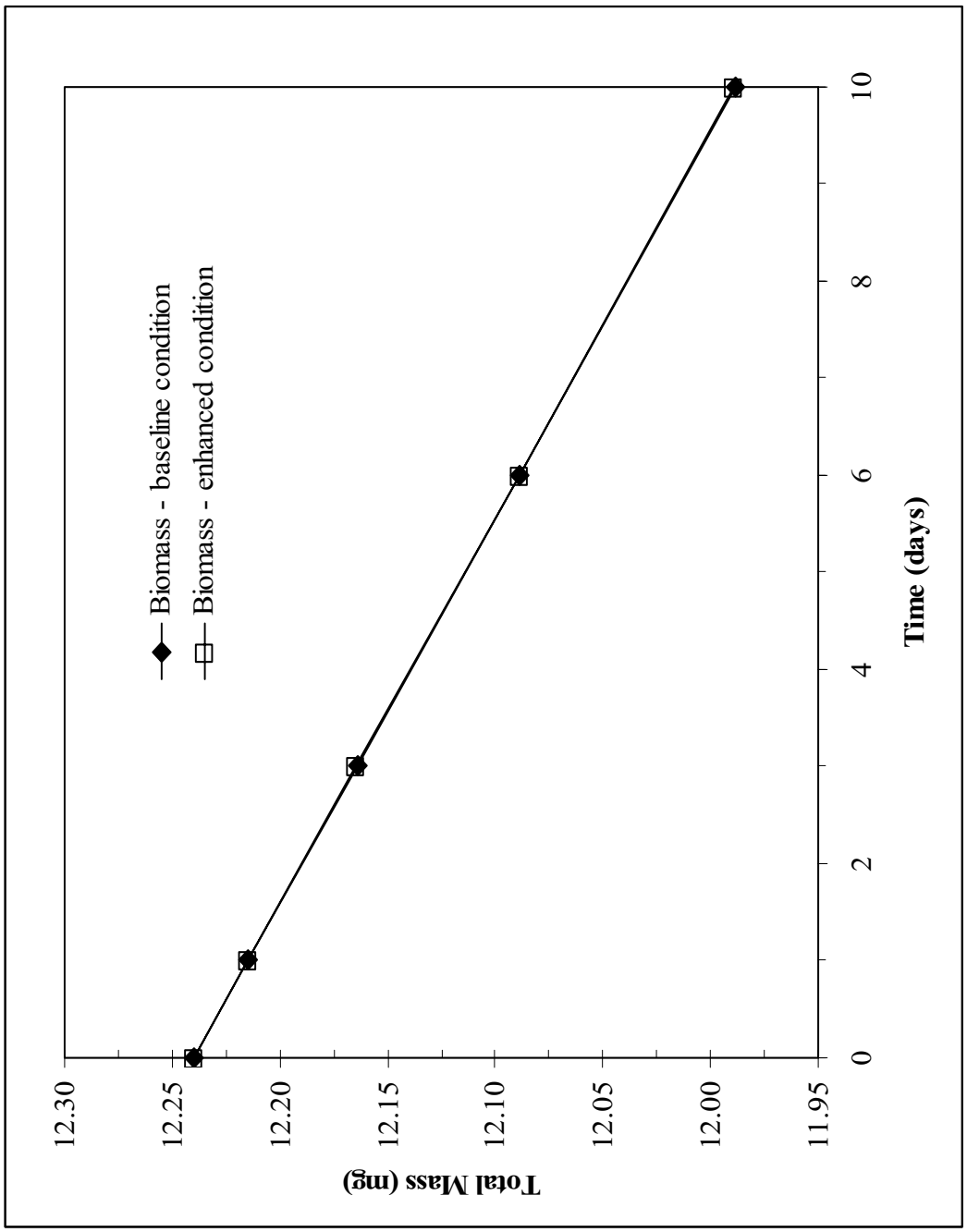

Figure 6.11. Scenario #1(a): Total mass versus time, biomass.

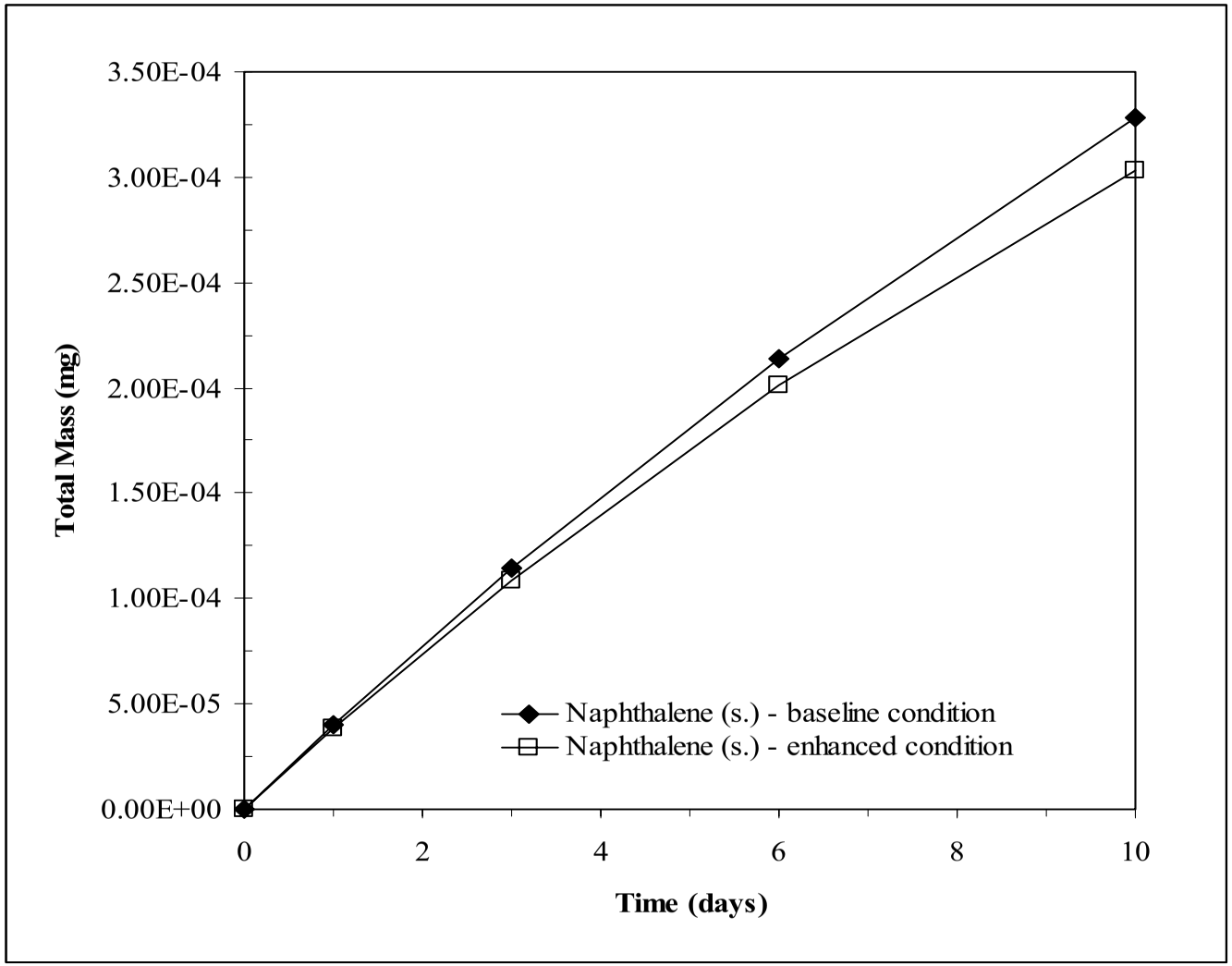

Figure 6.12. Scenario #1(a): Total mass versus time, naphthalene (sorbed).

6.1.4 Evaluation of Alternative Perturbation Results

As discussed in detail in the previous chapter, there are several engineered perturbations that could possibly be used in an effort to alleviate the rate-limiting factor of the baseline conditions and enhance the overall biotransformation rate. In the previous sub-sections, the predicted appropriate enhancement to the baseline conditions of Scenario 1(a), namely increased transverse dispersion as a result of increased advection, was evaluated and compared to the results of the baseline numerical model solution. As discussed in Chap. 5, this predicted appropriate enhancement was selected by using the key dimensionless parameters and the quantitative framework (Fig. 4.2) to determine the rate-limiting processes that needed to be alleviated, thus, allowing for increased biodegradation. Other enhancements (e.g., biokinetic enhancements, or the use of surfactant to increase desorption) while technically feasible, were not predicted to provide useful results because the use of these enhancements would not address the rate-limiting conditions according to the quantitative framework. For example, under Scenario 1(a), where macroscale mass transport controls, and transverse dispersion is limiting, increasing the biokinetics (e.g., an increase in q_{max}) was predicted to have little or no positive impact on the overall biotransformation rate compared to the baseline condition because unlike the predicted enhancement of increased advection and dispersion, the increase in biokinetics would not address the rate-limiting conditions quantified by the value of Da_6. In this subsection, the results of the numerical model runs with the predicted appropriate enhancement are compared to those of the alternate enhancements, which based on the quantitative framework are not predicted to stimulate the overall biotransformation rate. As discussed in Chap. 5.0, the input criteria for these

additional enhancement trials were selected such that the order of the magnitude of parameter variation was at least comparable to or greater than that for the appropriate enhancement in order to provide as near consistent conditions as possible.

Two alternative enhancements were further evaluated. Biokinetic stimulation – here modeled by increasing the substrate utilization rate, q_{max} – could be accomplished in the field by numerous means, including introducing additional biomass or changing the dominant terminal electron acceptor conditions (e.g., changing from anaerobic to aerobic conditions). Enhancement to alleviate rate-limited desorption – here modeled by increasing the mass transfer coefficient – could be accomplished by the addition of a surfactant to promote greater desorption mass transfer. Each of these additional enhancements were run using the same input conditions and run time as the baseline and enhanced runs detailed above, except for the enhancement-specific input variable that was changed. The results of the model runs for each of the three enhancements were compared using the quantitative analysis detailed above. The graphs of aqueous donor, aqueous acceptor, biomass, and sorbed donor, are illustrated in Figs. 6.13 through 6.16, respectively.

The comparison of the three enhancements for aqueous donor is presented in Fig. 6.13. Based on these data, the enhancement predicted to be appropriate (flushing) is seen to have a greater impact on the total mass reduction than for the biokinetic approach, but less of a reduction than for the mass transfer approach. While the former effect was expected, the latter effect was not. The explanation for the effect of increased mass transfer requires a review of the graphs for sorbed donor and for total donor mass reduction over time and is discussed below.

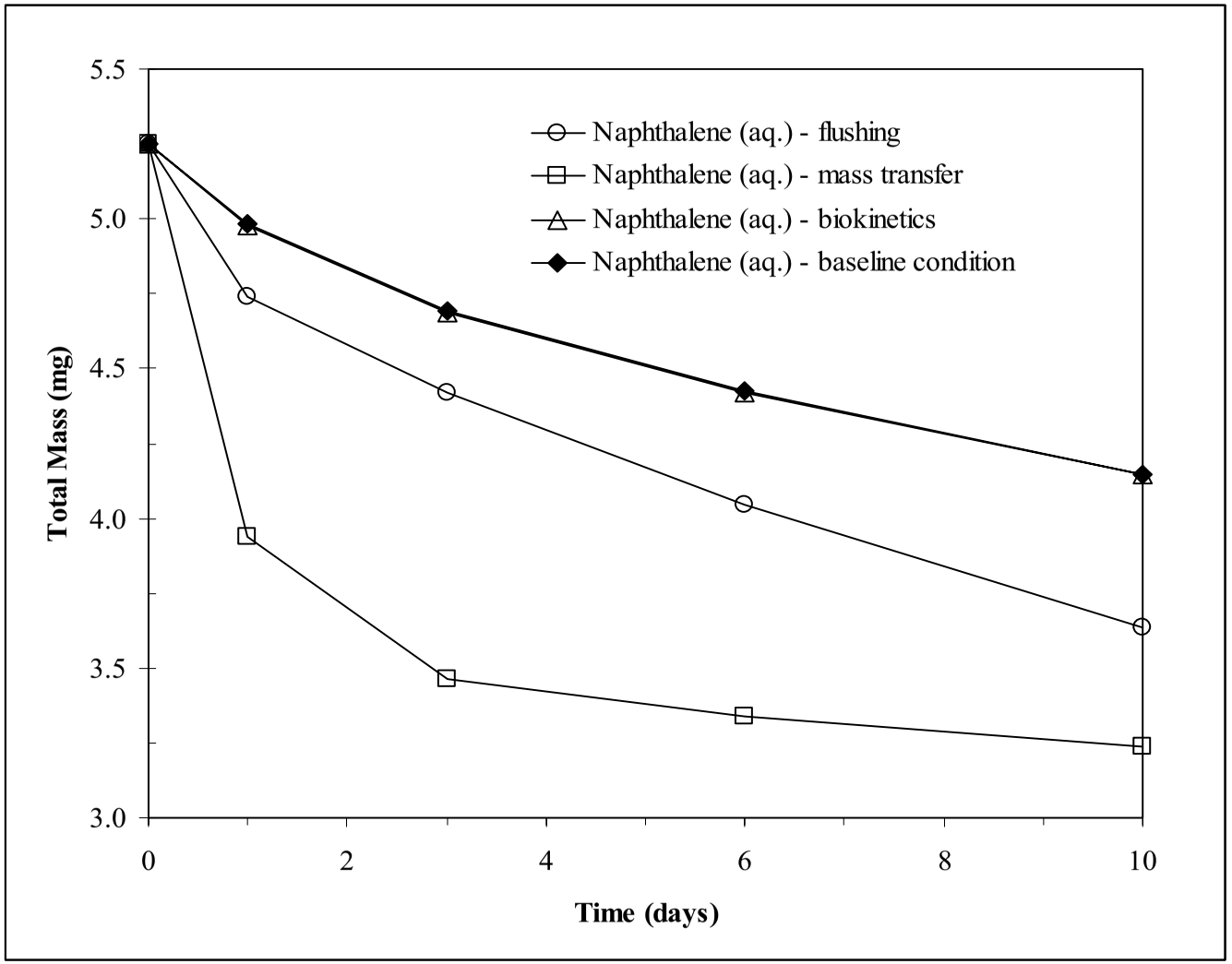

Figure 6.13. Scenario #1(a): Comparison of alternative perturbations - Total mass versus time, naphthalene (aq.).

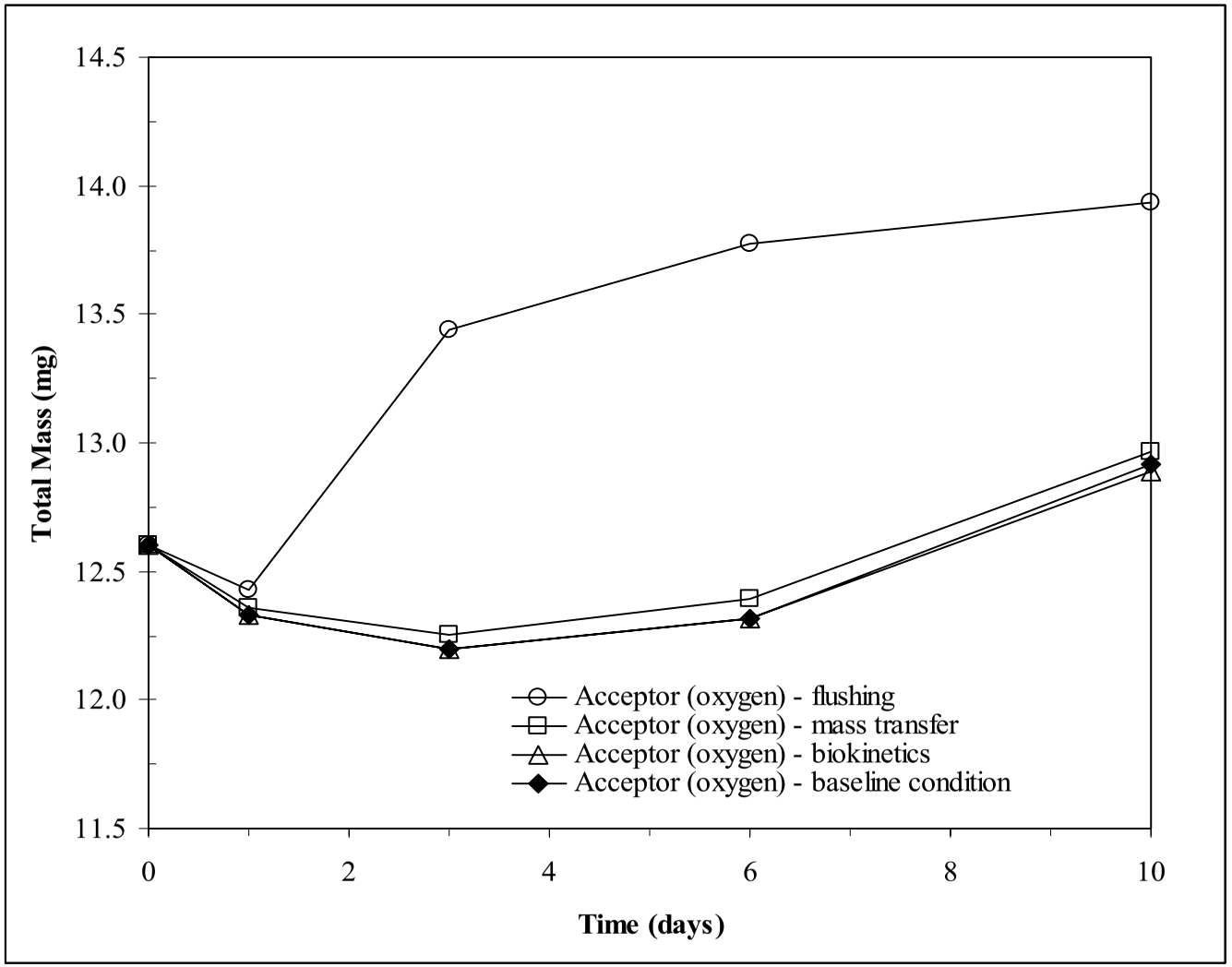

Figure 6.14. Scenario #1(a): Comparison of alternative perturbations - Total mass versus time, electron acceptor.

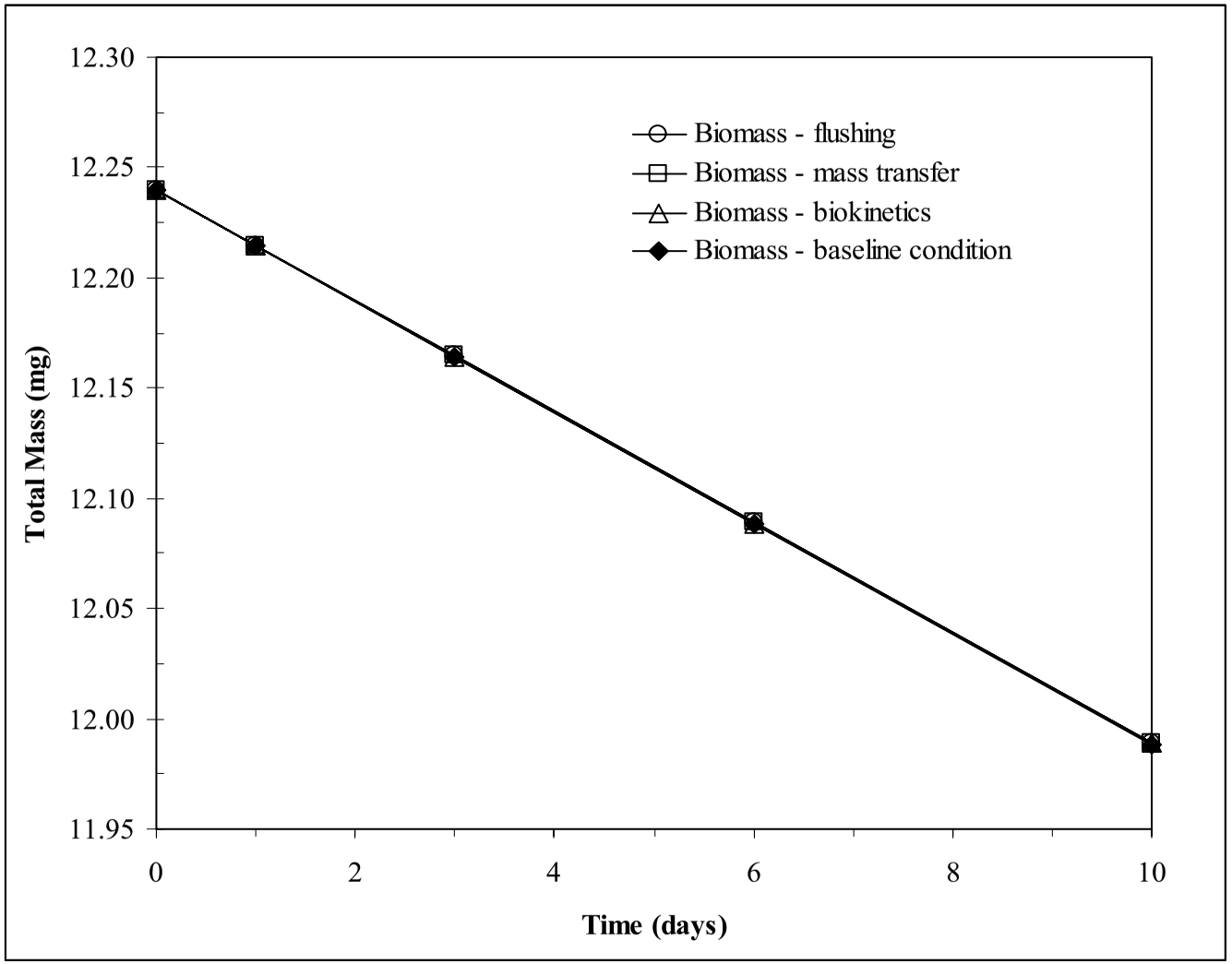

Figure 6.15. Scenario #1(a): Comparison of alternative perturbations - Total mass versus time, biomass.

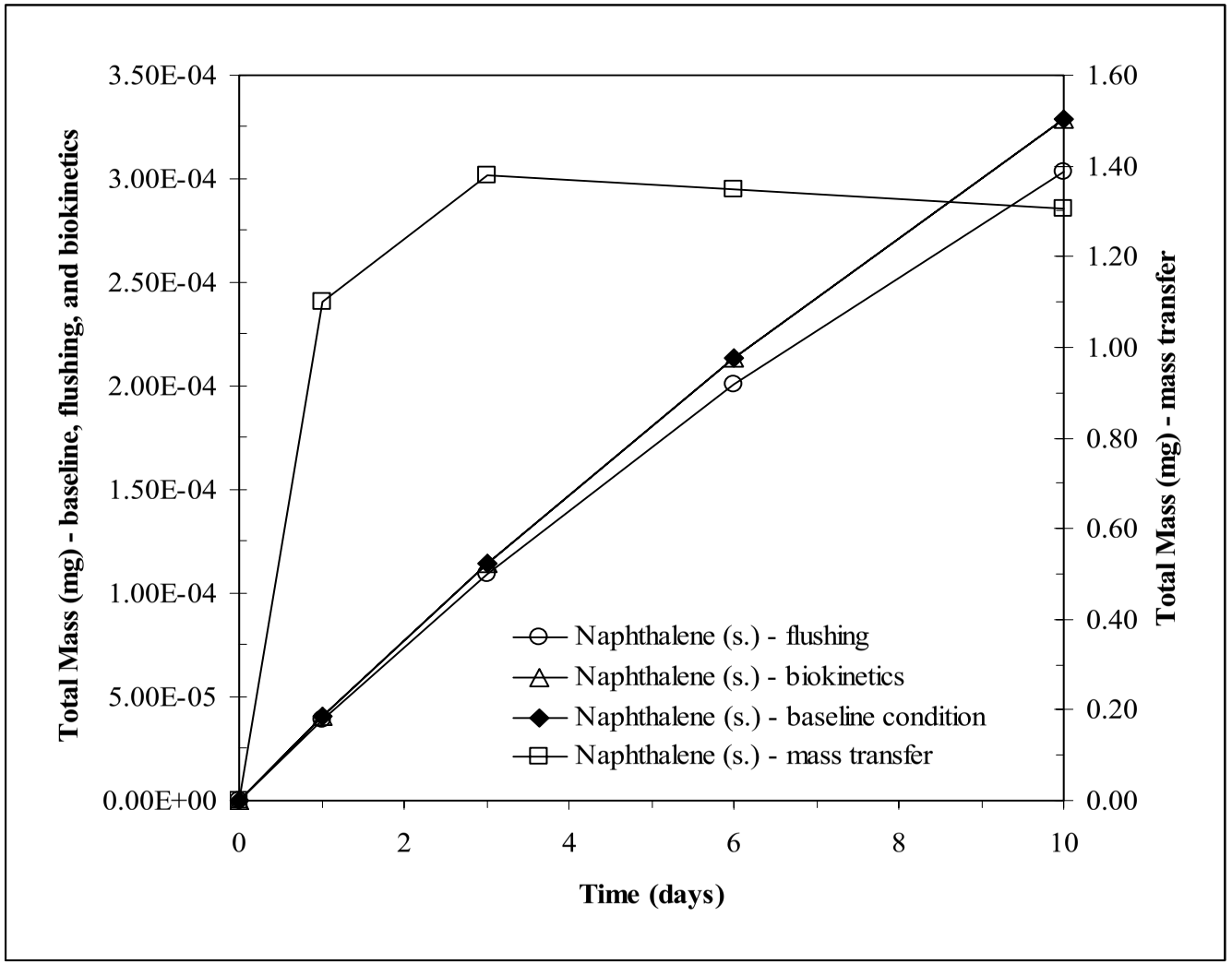

Figure 6.16. Scenario #1(a): Comparison of alternative perturbations - Total mass versus time, naphthalene (sorbed).

Focusing now on a comparison of flushing to biokinetics, clearly the flushing enhancement resulted in an overall increase in the total mass reduction that was nearly two-fold. This was expected when the dimensionless parameters are evaluated and the quantitative framework is inspected. Based on that analysis, only the increase in transverse dispersion, which in turn decreases the scale of Da_6, can be seen to effectively alleviate the rate limiting factor for the scenario. In fact, an examination of Da_6 indicates that improving biokinetics by increasing q_{max} should actually make the system even more limited by transverse dispersion than the baseline case. Thus, if such an enhancement were made, an even larger increase in advection, and, in turn, dispersion would be required to improve the overall biodegradation rate.

Further evidence of the increased overall biokinetics as a result of the flushing is provided by inspection of the graph of total mass of acceptor over time presented in Fig. 6.14. The trends in these data are similar to those presented in Fig. 6.10, the comparison of the baseline conditions to the flushing enhancement. As before, the flushing enhancement produces greater mass loading of acceptor, which would result in greater availability to the biomass than for the biokinetic and mass transfer enhancements. The comparison of biomass for the three enhancements is presented in Fig. 6.15. For the reasons discussed above with regard to Fig. 6.11, the effect of the three enhancements is not readily evident on the total mass of biomass in the system.

Finally, the comparison of total mass of sorbed donor is presented in Fig. 6.16. As discussed above, the graph comparing the total mass of aqueous donor in the system for the three perturbations (Fig. 6.13) indicates that the mass transfer enhancement was effective at reducing the aqueous donor mass; however, this effect needs to be interpreted

in the context of the total mass (aqueous plus sorbed) of naphthalene in the system. A review of Fig. 6.16 clearly shows that the reduction in aqueous donor for the mass transfer case is not a result of biotransformation, but rather can explained as being due to sorption of the naphthalene to the aquifer materials. Indeed the sorption mass increase in the mass transfer case is approximately four orders of magnitude greater than for either the flushing or biokinetic cases. Further, whereas the flushing enhancement indicated a greater mass reduction of aqueous donor (see Fig. 6.13), this is not correlated with an increase in the sorbed mass. In fact, as evidenced by Fig. 6.16, the flushing enhancement actually has a slightly lower degree of sorption than the biokinetic case. This analysis is further supported by a review of the total donor mass (aqueous plus sorbed) in the system for each perturbation, which is presented in Fig. 6.17. Here it is evident that the overall total mass reduction is greater for the case of enhancement by flushing than for either the mass transfer or biokinetic enhancements.

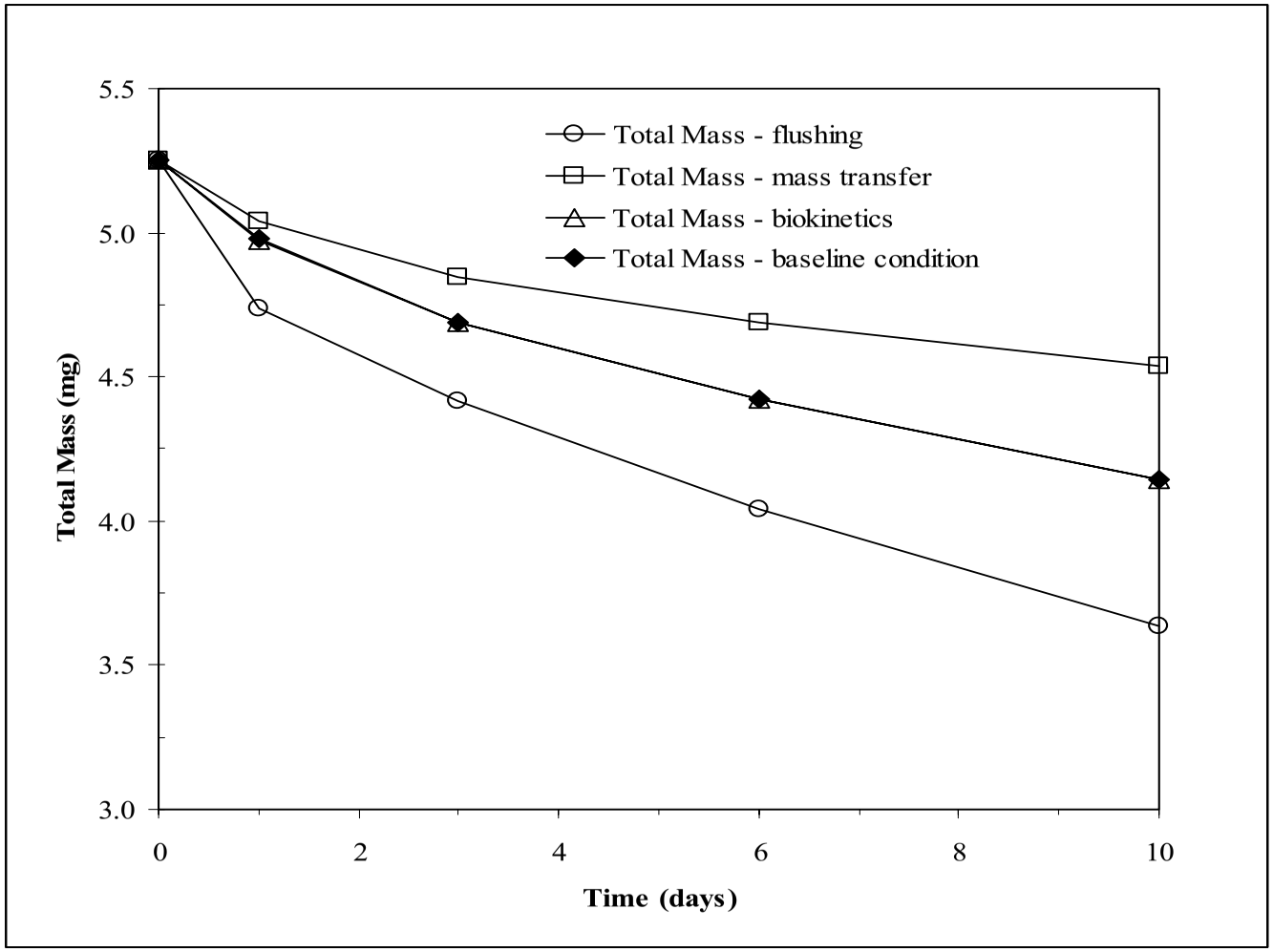

Figure 6.17. Scenario #1(a): Comparison of alternative perturbations - Total mass versus time, total naphthalene (aqueous plus sorbed).

6.2 Scenario 3

6.2.1 Baseline Simulation Results

As described in detail in Chapter 5, the baseline Scenario 3 represents a field site where a low conductivity layer (e.g., a layer of a lower permeability matrix or clay stringer in a stratified sand aquifer) is overlain by a higher conductivity layer. This scenario is similar to Scenario 1(a) in several ways. Specifically for Scenario 3, like Scenario 1(a), the domain consists predominantly of "clean" groundwater, into which a small contaminant plume or slug flows or is present. Nevertheless, there are several key differences between the two scenarios. First, Scenario 1(a) was established with a contaminated lower layer overlain by a "clean" higher conductivity layer. In contrast, Scenario 3 was set-up to be initially free of contamination throughout both layers. Second, whereas oxygen was supplied to the upper layer in Scenario 1(a), the conditions are such in Scenario 3 that the entire two-layer aquifer system is initially deficient in oxygen, with nitrate-reducing anaerobic conditions present. Third, the two-layer system in Scenario 3 became "contaminated" as a finite slug of donor was injected over a discrete time (one day). Based on the quantitative framework outlined in Chapter 4.0, the rate-limiting process in this scenario is the biokinetics for naphthalene degradation, which is predicted to manifest itself primarily in the form of a limited degree of degradation (e.g., anaerobic conditions and a low substrate utilization rate).

Contour plots for aqueous naphthalene, oxygen, biomass, and sorbed naphthalene at 1.25, 2.5, 3.75, and 5 days during the model run are presented in Fig. 6.18 through Fig. 6.21, respectively. As can be seen in Fig. 6.18, the aqueous naphthalene plume moves rapidly across the upper higher conductivity layer, exhibiting a moderate reduction from

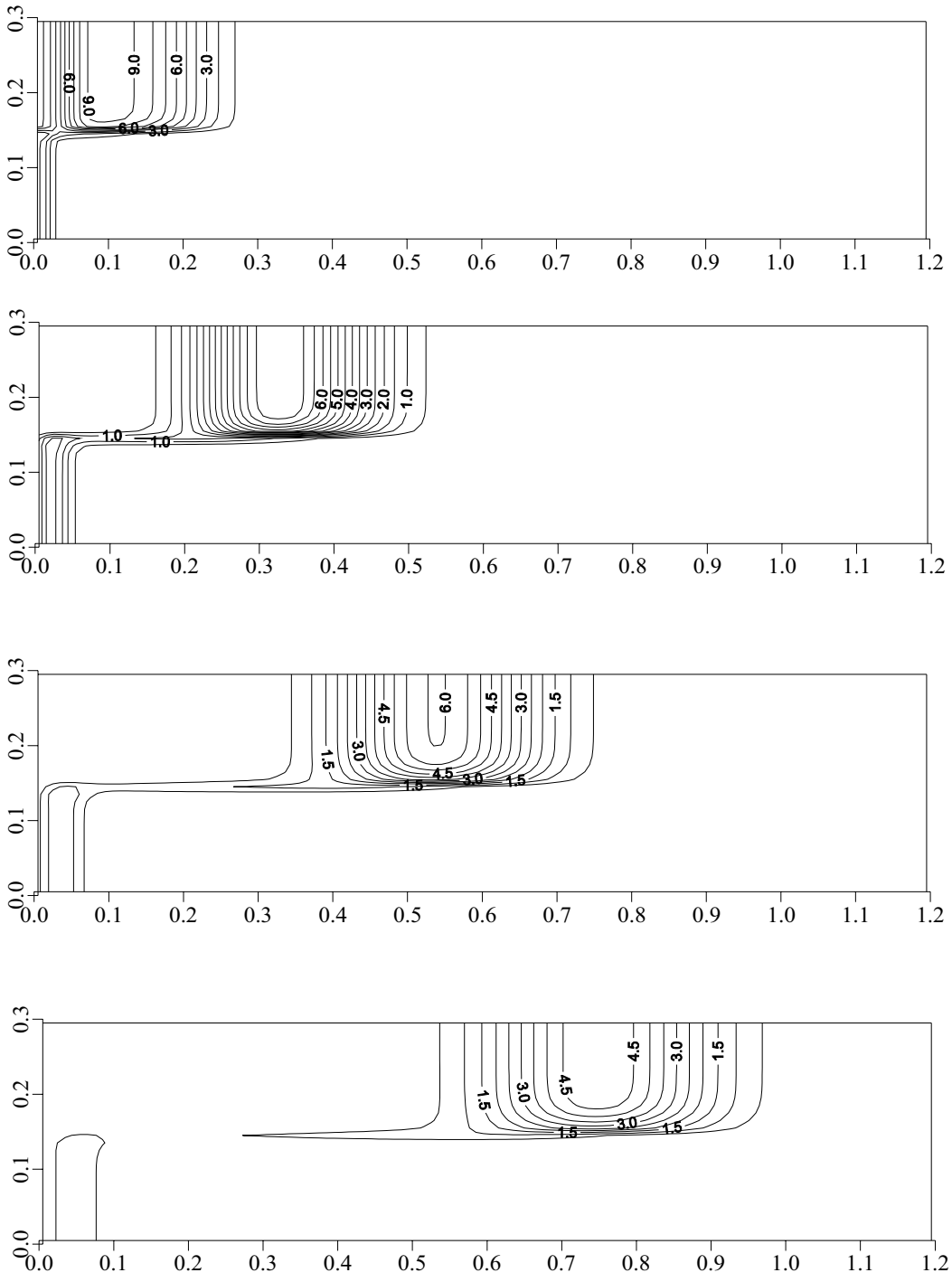

Figure 6.18. Scenario #3: Contour plots of naphthalene (aq.) at 1.25, 2.5, 3.75, and 5 days. Contour interval is 1 mg/l for 1.25 days, and 0.5 mg/l for 2.5, 3.75, and 5 days.

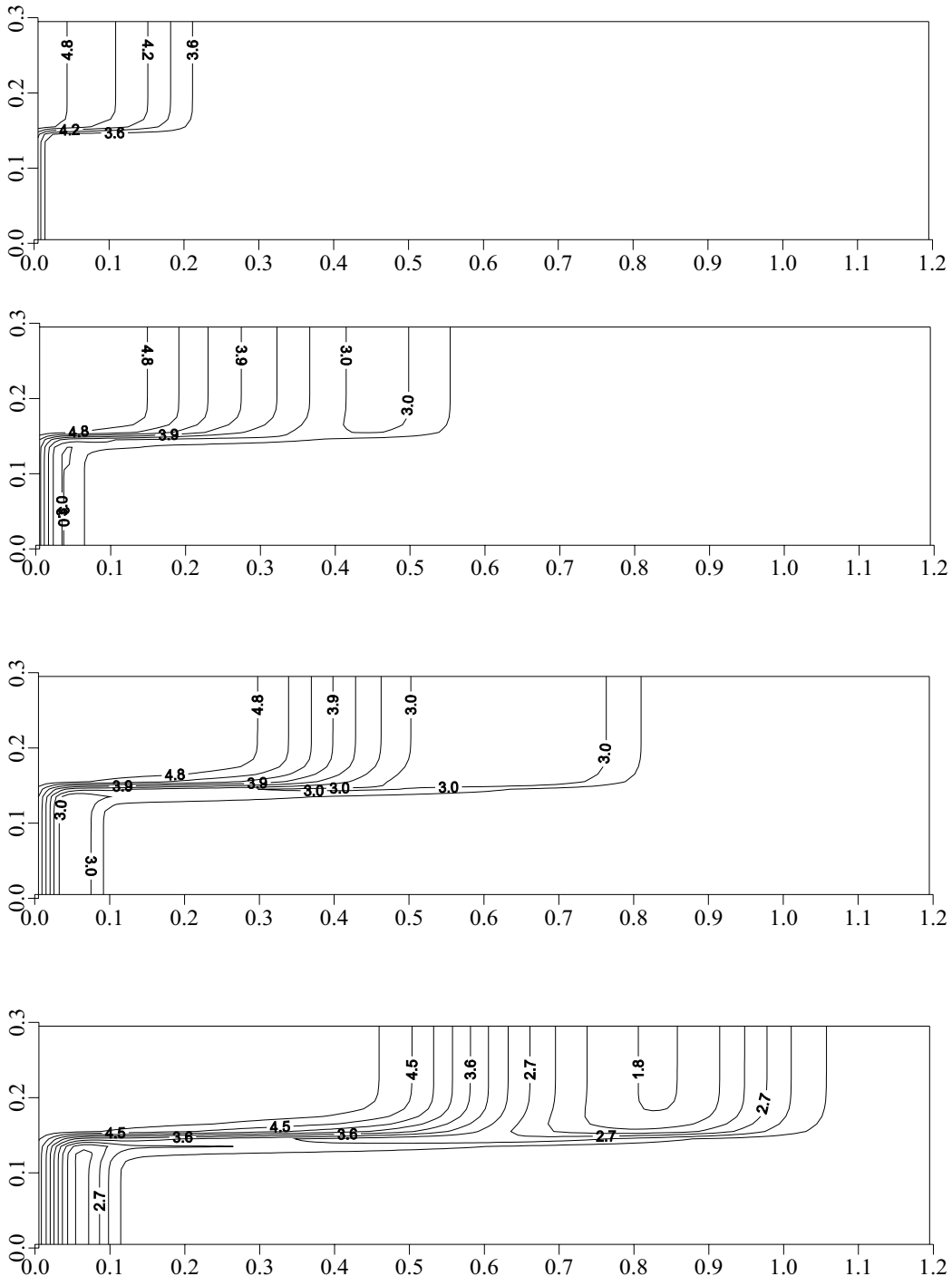

Figure 6.19. Scenario #3: Contour plots of acceptor (nitrate) at 1.25, 2.5, 3.75, and 5 days. Contour interval 0.3 mg/l.

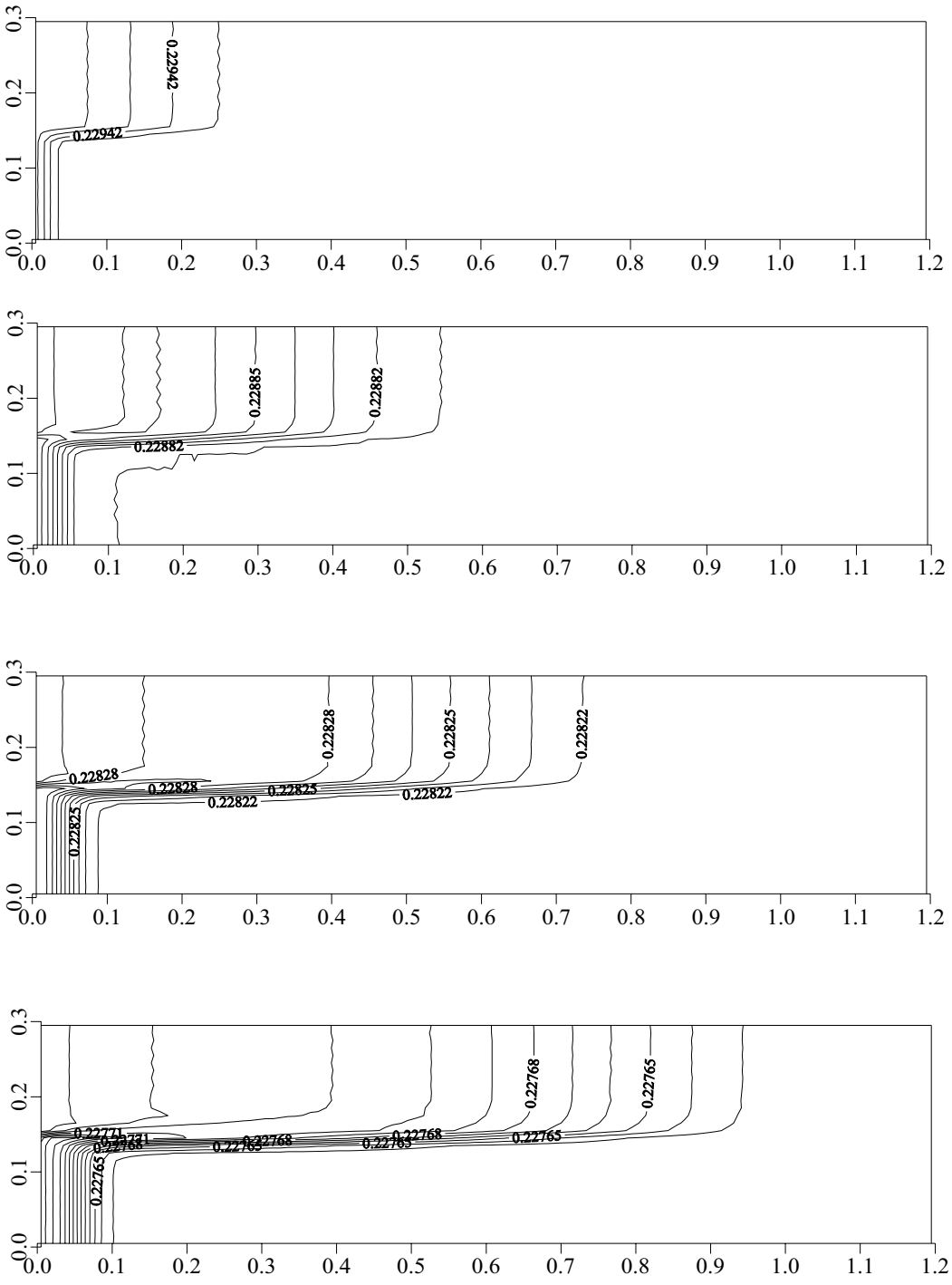

Figure 6.20. Scenario #3: Contour plots of biomass at 1.25, 2.5, 3.75, and 5 days. Contour interval is $1x10^{-5}$ mg/kg.

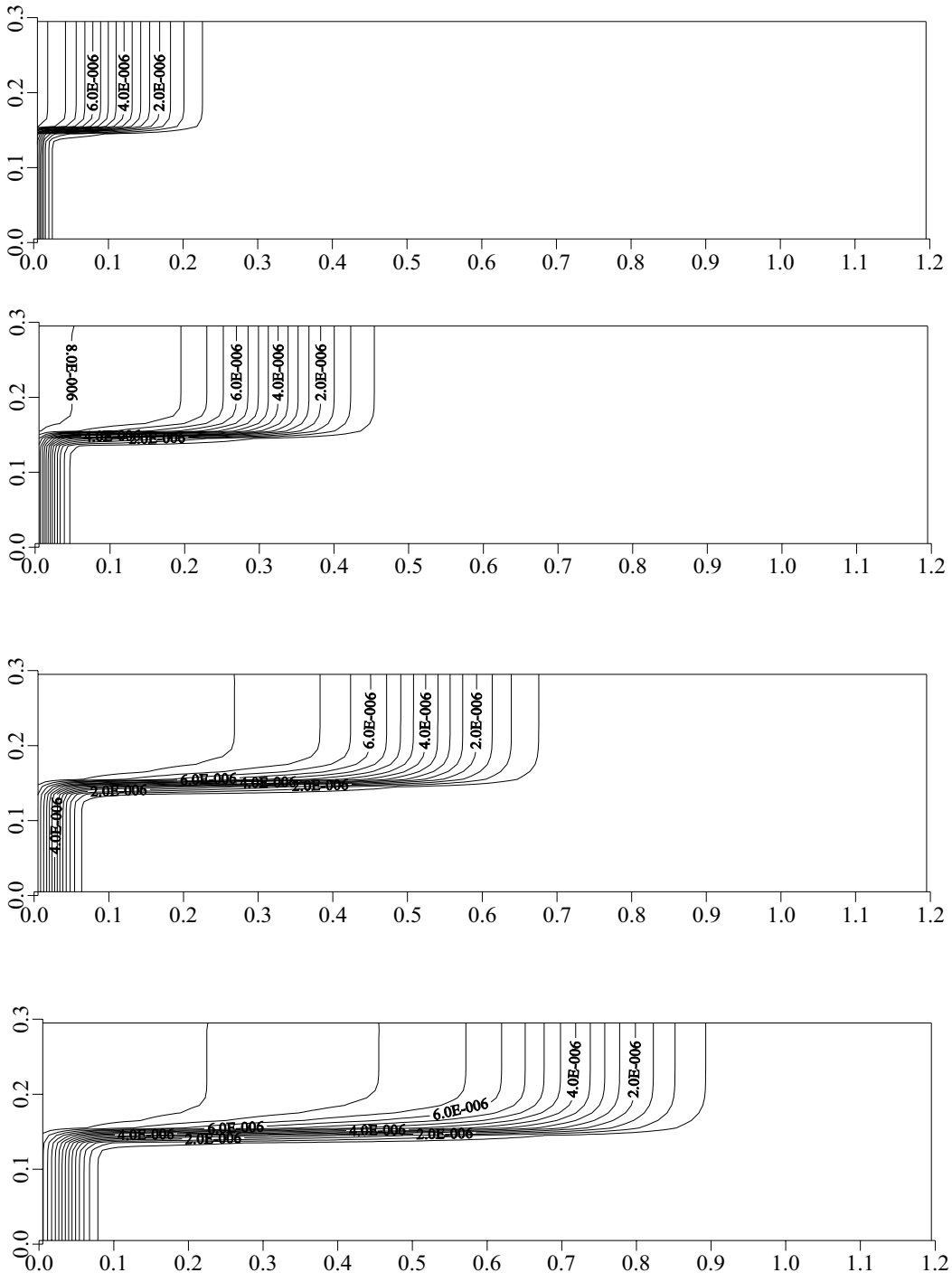

Figure 6.21. Scenario #3: Contour plots of naphthalene (sorbed) at 1.25, 2.5, 3.75, and 5 days. Contour interval is 5×10^{-7} mg/kg.

the 10 mg/l injection concentration over the time period from 0 to 1 day. After a time interval of 5 days, the aqueous plume front has extended to 1.0 m from the source, where the aqueous concentration is 1 mg/l. At this point, the center of the plume in the upper layer is at around 0.75 m where a concentration of approximately 5 mg/l is observed. In the lower layer, there is a much more limited distribution of aqueous naphthalene. This is due in part to the slow advection rate for the layer, along the fact that the slug injection time was for only 1 day. As a result, at 5 days, a small plume (less than 1 mg/l distribution), which is dissociated from the central plume in the upper layer, is found in the lower layer between 0.0 and 1.0 m.

The acceptor (nitrate) concentration profile in the domain is presented in Fig. 6.19. In this series of panels, the nitrate concentration does not show evidence of being significantly reduced from the background conditions (3.5 mg/l) for up to 3.75 days. Even after 5 days, nitrate concentrations at background (3.5 mg/l) or the influent concentration (5 mg/l) are evident throughout the domain with the exception of a limited area around the center of the upper layer aqueous donor plume, between 0.7 m and 1.0 m, where the acceptor concentrations range from 2.7 mg/l down to 1.8 mg/l. A similar but less dramatic reduction in nitrate concentration also occurs in the lower layer in the area of the aqueous naphthalene plume centered around 0.5 m. It is clear from this series of contour plots that the relatively low value of the substrate utilization rate (q_{max}) results in poor biotransformation of the donor, despite the fact that ample mixing of the substrates appears to be occurring, the necessity of which has been observed by several researchers (e.g., Wood, et al., 1994; Cirpka, et al., 1999).

The biomass concentration data are presented in Fig. 6.20. Similar to Scenario 1(a), an overall reduction in domain-wide biomass concentration is evident. As was discussed above, this overall decrease is likely due to the lack of aqueous donor availability throughout the domain coupled with the inclusion of biomass decay. Also similar to Scenario 1(a), the biomass "finger" develops along the interface between the two layers, where a sharp concentration gradient develops. This profile is consistent with a similar numerical model experiment performed by Odencrantz (1992); however, a notable difference between the results of that study and the current study is the fact that despite the presence of well mixed donor and acceptor, the biomass concentrations in this study do not increase, but rather decrease. This could also be explained by the difference in the biokinetic parameters used by Odencrantz (1992) and those used in this study. Again, this is evidence that despite the proper longitudinal and transverse mixing of the donor and acceptor substrates, the biodegradation is inhibited by the rate limiting process, which here, as described above, is the biokinetic transformation rate.

The sorbed concentrations in the domain are presented in Fig. 6.21. Similar to Scenario 1(a), the sorbed phase distribution is seen to correlate with the aqueous phase donor concentrations, as expected. Further, the mass transfer kinetics and partition coefficients of this scenario were also selected such that the system can be characterized as overall having a weak sorption sink and, therefore, the extent of sorption is minimal.

6.2.2 Enhanced Simulation Results – Biokinetic Perturbation

As presented in Chapter 5, the selected engineered perturbation for this scenario was aimed at increasing the rate of biodegradation kinetics, as the biokinetics were established as the process limiting the overall biotransformation rate. In contrast to

Scenario 1(a), transverse dispersion is not the limiting rate in this scenario, as is obvious when reviewing the contour plots of the aqueous donor and acceptor (Figs. 6.18 and 6.19, above). Thus, in this scenario, the engineered perturbation was selected to increase the *in situ* biodegradation rate by improving the biokinetics. This perturbation was accomplished numerically by increasing Da_6 via an increase in the specific substrate utilization rate, q_{max}. In the field, the engineered enhancement that is simulated here may be implemented in several ways. First, the concentration, and/or distribution of the biomass itself could be enhanced via bioaugmentation. Second, nutrients or other amendments, such as co-metabolites, that are found to be deficient in the system could be added to improve the biokinetics or increase the amount of biomass. Third, anaerobic or anoxic conditions can be changed to aerobic conditions. The latter is the practice that is employed here. Specifically, for this enhancement, the electron acceptor is changed from nitrate in the baseline condition, to oxygen in the predicted appropriate simulation. This change is assumed to result in an increased specific substrate utilization rate.

Like the baseline numerical simulation, the enhanced simulation for Scenario 3 was run for 5 days using the VMOD/RT3D model. The input, as before, consisted of an aqueous naphthalene injected across the full height of the upgradient boundary for one day, with a background concentration of 3.5 mg/l acceptor (oxygen) and an influent injection concentration of 5 mg/l oxygen into the upper layer only. Contour plots for aqueous naphthalene, oxygen, biomass, and sorbed naphthalene at 1.25, 2.5, 3.75, and 5 days during the enhanced model run are presented in Fig. 6.22 through Fig. 6.25, respectively.

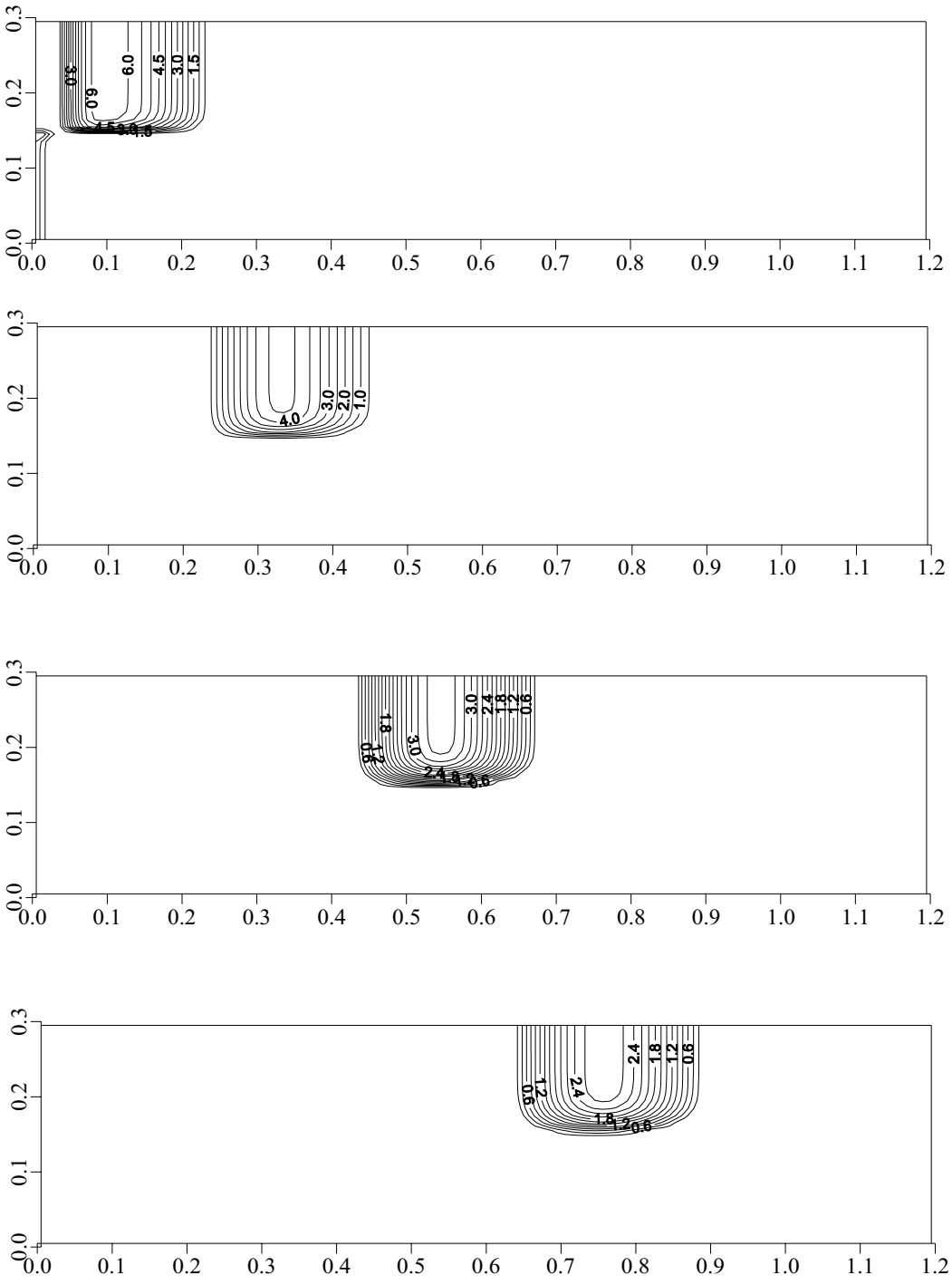

Figure 6.22. Scenario #3 (enhanced): Contour plots of naphthalene (aq.) at 1.25, 2.5, 3.75, and 5 days. Contour interval is 0.5 mg/l for 1.25 and 2.5 days, and 0.2 mg/l for 3.75 and 5 days.

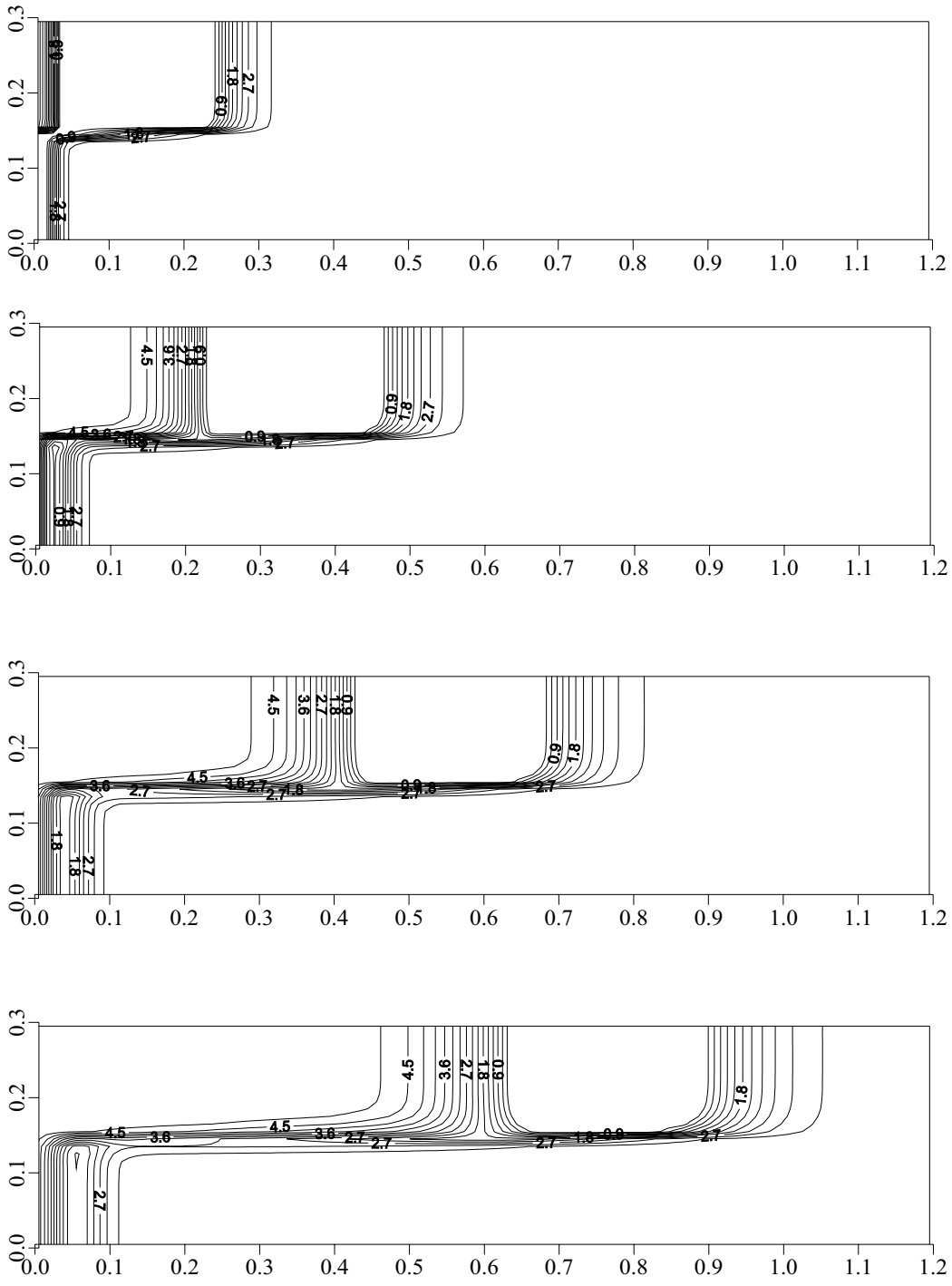

Figure 6.23. Scenario #3 (enhanced): Contour plots of acceptor (oxygen) at 1.25, 2.5, 3.75, and 5 days. Contour interval is 0.3 mg/l.

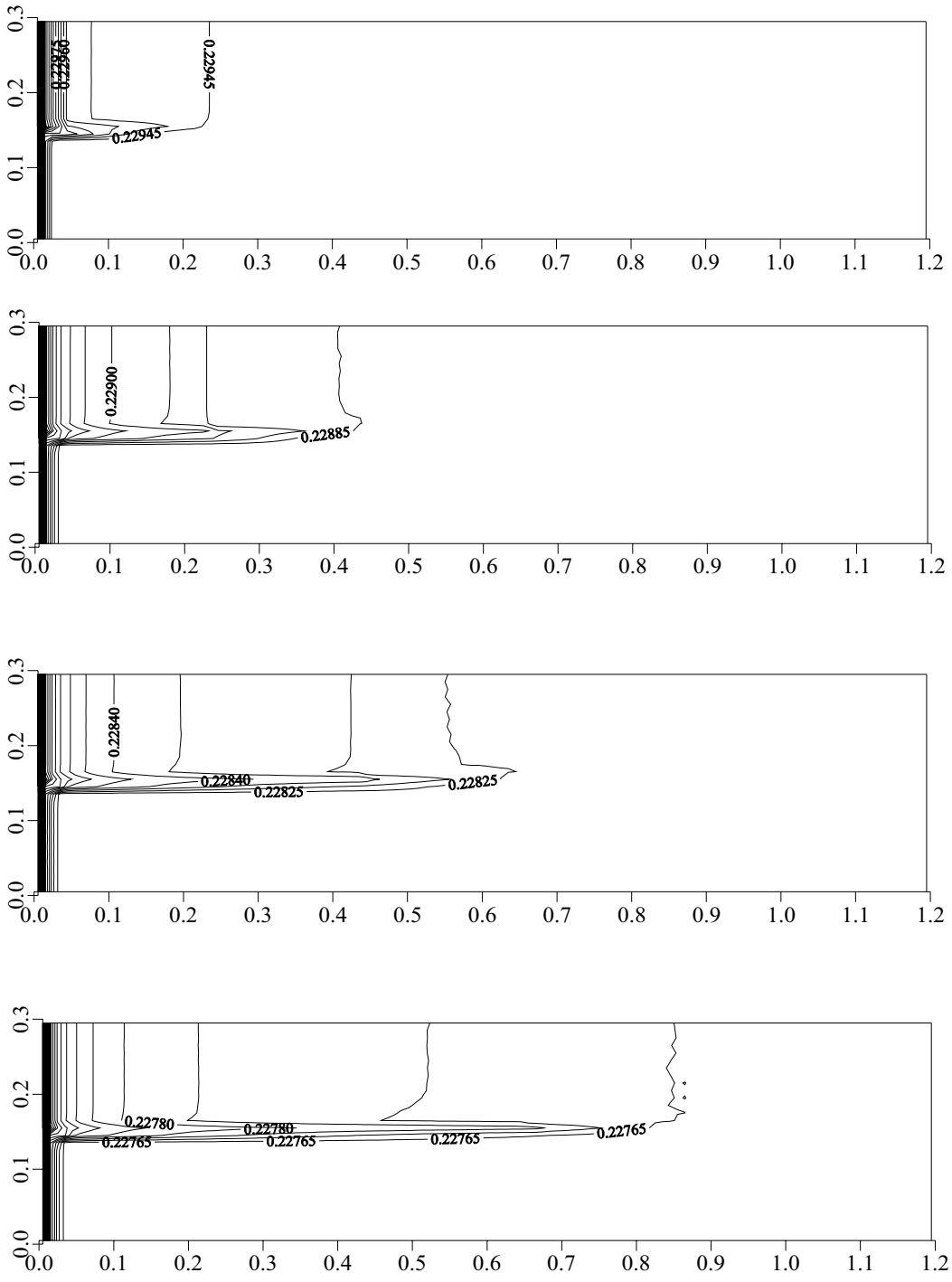

Figure 6.24. Scenario #3 (enhanced): Contour plots of biomass at 1.25, 2.5, 3.75, and 5 days. Contour interval is 5×10^{-5} mg/kg.

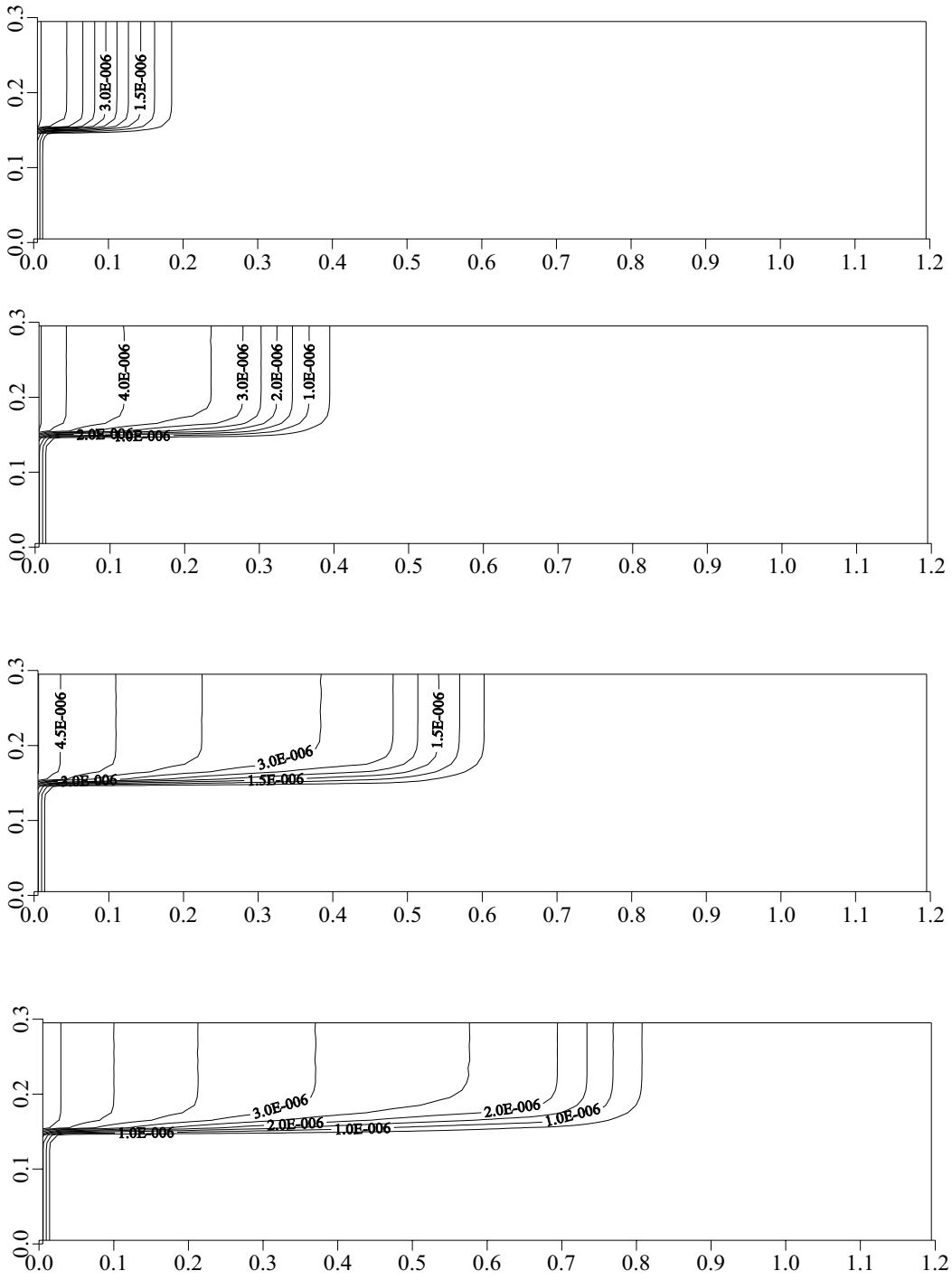

Figure 6.25. Scenario #3 (enhanced): Contour plots of naphthalene (sorbed) at 1.25, 2.5, 3.75, and 5 days. Contour interval is 5×10^{-7} mg/kg.

As can be seen in Fig. 6.22, the longitudinal and vertical extent of the aqueous donor plume has been substantially reduced in each time step compared to the baseline conditions, although the ultimate longitudinal migration of the plume center from the influent injection location is still to approximately 0.75 m after 5 days, as for the baseline condition. However, in the enhanced case, the concentration in the center of the aqueous plume was approximately 2.6 mg/l at 5 days, as compared to 4.5 mg/l for the baseline case. Further, the plume front is also much less dispersed. These results suggest that increased reduction in both the concentration and volume of the plume has occurred due to the increased biomass activity. Vertically, the contaminant source no longer exhibits the dissociated plume remnant in the lower layer. This indicates that what little donor has migrated in the slower layer was rapidly degraded by the biomass. To confirm the interpretations, it is useful to examine the distribution of electron acceptor.

The spatial distribution of the electron acceptor plume for the enhanced case, now oxygen, follows a similar general pattern as for Fig 6.23. However, the acceptor concentration profile in the vicinity of the donor plume in the enhanced cases yields much different results than for the baseline conditions. Whereas in the baseline case the acceptor exhibited only a limited reduction in the immediate vicinity of the donor plume, there is a substantially greater utilization of acceptor in the enhanced case. Specifically, while the background and influent concentrations for the enhanced case were the same as for the baseline conditions, the extent of donor mineralization in the upper layer is significantly greater and, thus, the oxygen is essentially depleted in the upper layer between 0.6 m and 0.9 m, after 5 days. This result of the perturbation was expected,

because there appeared to be sufficient substrate mixing in the baseline case, but the low utilization rate was limiting the overall biotransformation rate.

The result of the enhanced utilization rate on the biomass distribution is illustrated in Fig. 6.24. As for the baseline case, it was expected that the biomass would decrease in the domain given the configuration of background acceptor, the lack of background donor, and the assumption of biomass decay. However, for the enhanced case, after 5 days, there appears to be less of a decrease in the biomass concentrations across the domain. In addition, a very steep concentration gradient (too fine to define individual contour lines) develops along the entire height of the influent injection zone at left of each panel due to significant biodegradation occurring as the acceptor enters the domain. Furthermore, similar to both the baseline condition and Scenario 1(a), fingering of the biomass develops along the interface between the two layers; however, it is not as pronounced in this case, likely due to the fact that the donor is injected across the entire thickness of the domain and, thus, the zone of mixing and dispersion is distributed throughout the domain.

Finally, the concentration profile of sorbed donor is illustrated in Fig. 6.25. In general, the spatially distribution of the sorbed plume is consistent with the baseline condition, with the sorbed phase correlated with the aqueous donor distribution, as expected. In this case however, the corresponding sorbed phase concentrations are lower than the corresponding values in the baseline condition. This further demonstrates that there is increased mass removal of the electron donor (aqueous and sorbed) in the enhanced condition.

6.2.3 Mass Calculations for Scenario 3

In section 6.1.3, above, mass calculations comparing the total mass in the system over time for the baseline and enhanced Scenario 1(a) were presented. Using the same approach (i.e., the methods described in subsection 5.8.1.2), graphs of total mass in the system over the runtime for Scenario 3 (5 days) were generated for the constituents of concern (i.e., aqueous donor, aqueous acceptor, biomass, and sorbed donor). The initial masses in the system were calculated as before (e.g., for aqueous donor, the calculation is 0.0 mg because the domain is assumed "clean").

The total mass of aqueous naphthalene in the system is presented as a function of time in Fig. 6.26 for both the baseline and enhanced conditions. These data clearly show an overall greater decrease in the total mass for the enhanced condition, as expected, with the greater specific substrate utilization rate. Specifically, although for both conditions there is an initially "clean" domain that is "contaminated" by a contaminant slug, the overall increase in aqueous donor after 1 day is smaller in the enhanced case than that of the baseline condition. Specifically, while the mass loading or flux of aqueous donor is the same for both cases, the increased specific substrate utilization rate in the enhanced case results in greater biotransformation of the incoming mass during the injection time (from 0 to 1 day) than for the baseline case. However, after day one, biotransformation continues and the total mass decreases in both cases. To evaluate the total mass removal during this phase of the run, it is also instructive here to examine the rate of mass change (see Table 6.2), as was done with Scenario 1(a).

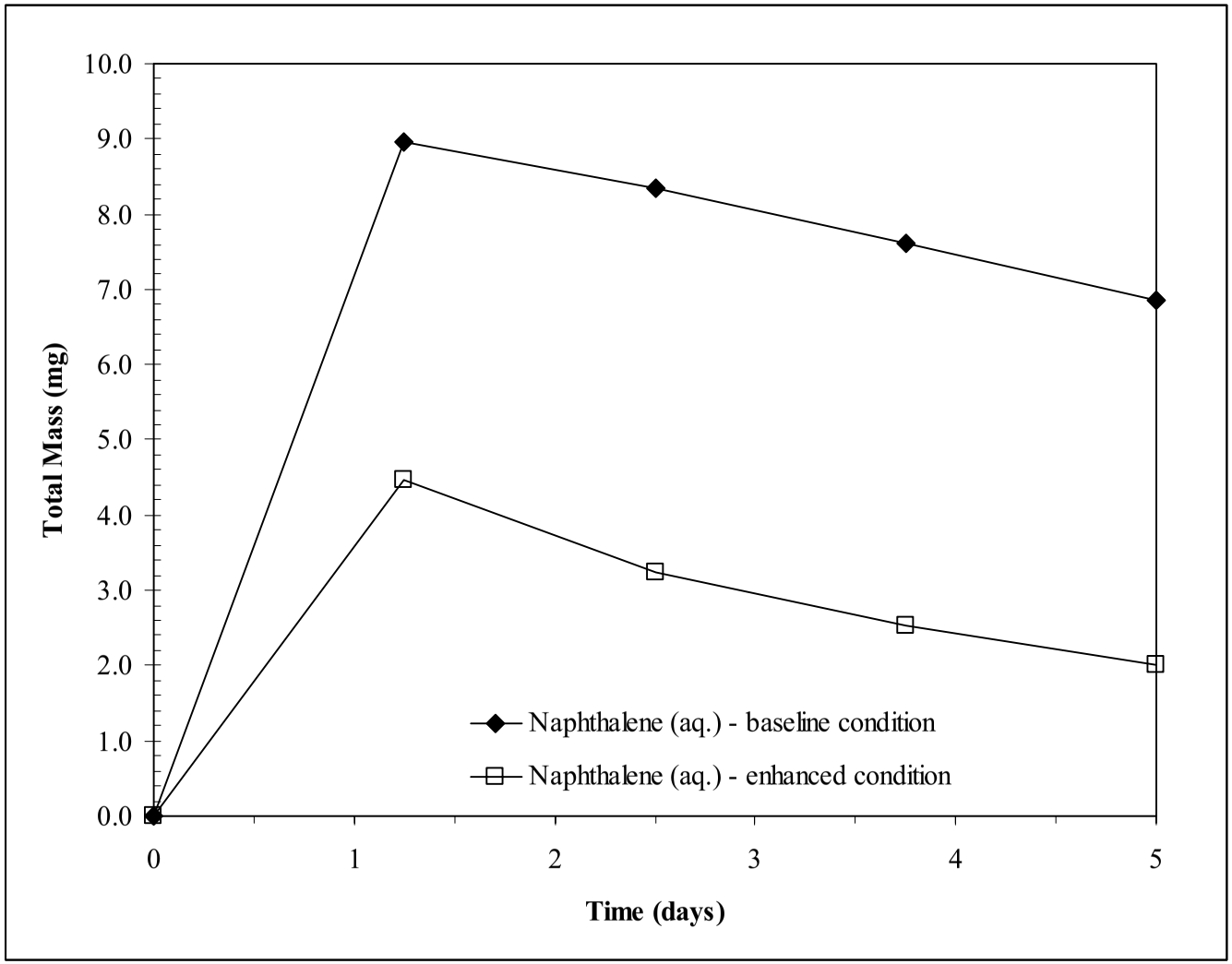

Figure 6.26. Scenario #3: Total mass over time, naphthalene (aq.).

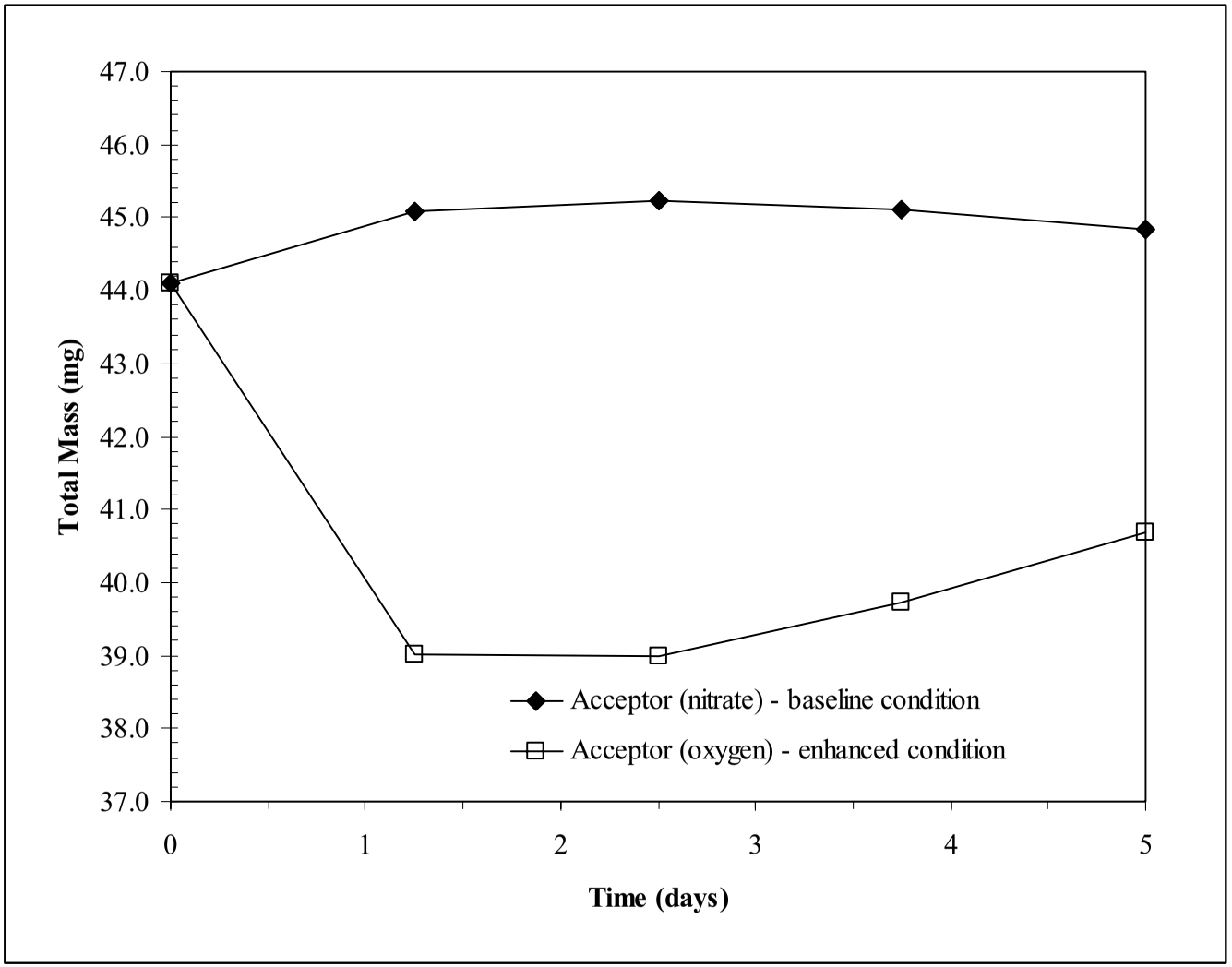

Figure 6.27. Scenario #3: Total mass over time, oxygen.

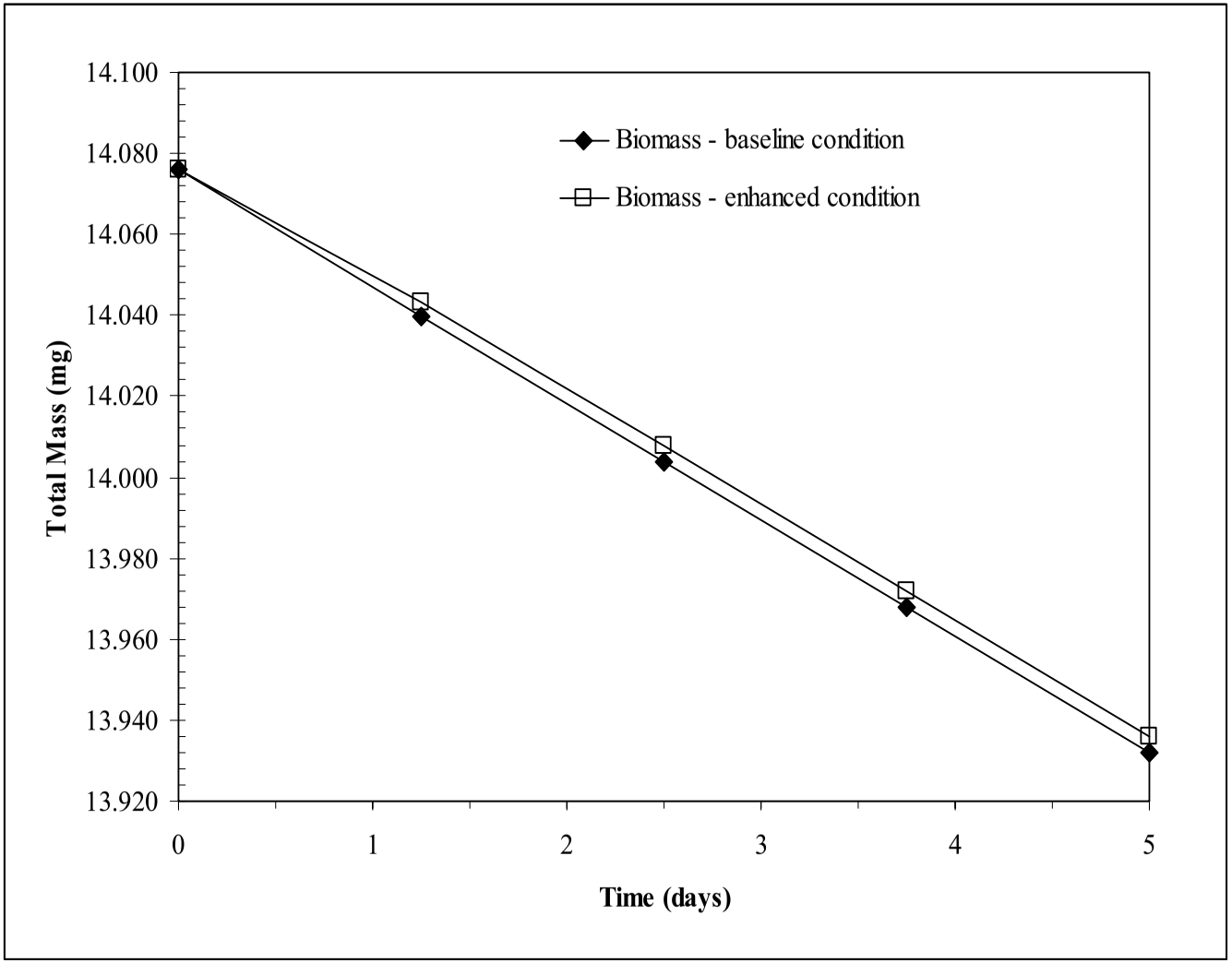

Figure 6.28. Scenario #3: Total mass over time, biomass.

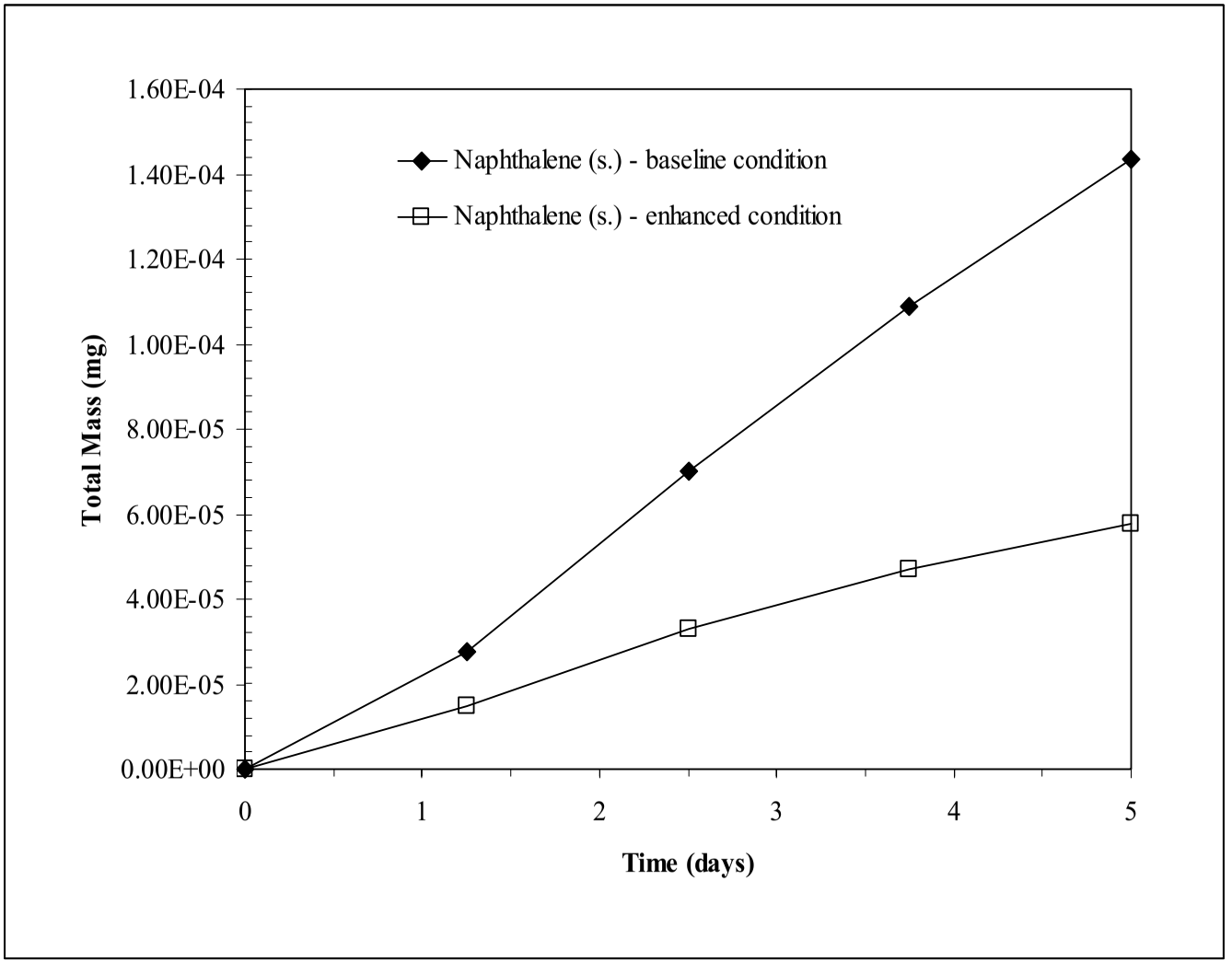

Figure 6.29. Scenario #3: Total mass over time, naphthalene (sorbed).

Table 6.2. Scenario 3: comparison of removal rates of aqueous naphthalene.

Day	Baseline Rate (mg/day)	Enhanced Rate (mg/day)
1.25-2.5	0.492	0.980
2.5-3.75	0.575	0.564
3.75-5	0.613	0.429

Similar to the pattern seen in the comparison of baseline to enhanced conditions for Scenario 1(a), the values in Table 6.2 indicate the initial removal rate of naphthalene is significantly greater in the enhanced condition early in the model run (day 0 to 1). Similar to Scenario 1(a) this can be explained by the initial proximity of the electron donor substrate to the electron acceptor along the injection front and the increased utilization rate in the enhanced case. However, the time series progresses, the concentration gradients are reduced with time, and therefore, the difference in the mass removal rates between the baseline and enhanced conditions becomes less over time.

The interpretation of the aqueous naphthalene data is reinforced by a review of the graph of electron acceptor mass data presented in Fig. 6.27. In this graph, the acceptor changes little in the baseline condition where the nitrate is subject to mass loss out of the domain due to advection and biodegradation, as well as increases in mass due to loading from the injection front. The overall result is a moderate increase of nitrate mass over the first few time steps. In sharp contrast, the acceptor oxygen in the enhanced case significantly decreases during the injection period from time 0 to day 1 (see Fig. 6.26). In this case, the background concentrations in the vicinity of the injection front, as well as much of the influent acceptor are consumed during the biotransformation of the influent donor up to day 1. Once the injection of donor is stopped at day 1, the mass of

acceptor slowly rebounds in the enhanced case as the injection of oxygen continues while there is decreasing donor available with which to mix and continue the biotransformation process.

The total mass of biomass over time for the baseline and enhanced conditions is compared in Fig. 6.28. As discussed before, there is an overall decrease in the total mass of biomass under both conditions; however, there is less of a decrease, albeit small, in the enhanced condition. This trend of increased biomass is consistent with the results of other researchers (e.g., Odencrantz, 1992), and is expected based on the selected perturbation's effects on substrate utilization and correspondingly on the biomass growth. If, as previously discussed, the decay term was not used, or perhaps an alternate contaminant profile was used, a greater increase in the mass of biomass would be expected for the enhanced condition.

In Fig. 6.29, the total mass data for the sorbed donor is presented for the baseline and enhanced conditions. Inspection of the data indicates that sorption continues to increase of sorbed mass in both conditions, but that the rate and magnitude of the increase in the baseline condition is much greater than for the enhanced case. This is in contrast to the results of Scenario 1(a) where the sorbed mass increased at similar rates and magnitudes for the two conditions. This could be due to the fact that increasing the biokinetics directly impacted the substrate utilization rate in scenario 3, whereas increasing the advection in scenario 1(a) was not directly tied to the biodegradation rate, but rather increased the overall biotransformation rate by indirectly increasing the transverse dispersion and thereby increasing substrate mixing which increased the utilization rate.

6.2.3 Evaluation of Alternative Perturbation Results

Following the same approach as used for scenario 1(a), alternative engineering enhancements that might be considered as possible options for increasing the overall biotransformation rate were compared to the predicted appropriate enhancement. In the case of Scenario 3, the alternative enhancements considered were flushing (increased transverse dispersion through increased advection) and mass transfer (increased desorption). These alternative enhancements were evaluated by comparison to the biokinetics enhancement (direct biostimulation) for each constituent: aqueous donor, aqueous acceptor, biomass, and sorbed donor. The results of the additional numerical trials for the alternative enhancements were compiled in the manner as above for comparison of total mass of the constituents aqueous donor, acceptor, biomass, and sorbed donor, in the system, as illustrated in Figs. 6.30 through 6.34, respectively.

The comparison of the three enhancements for aqueous donor mass is presented in Fig. 6.30. Inspection of the graph indicates that the biokinetics enhancement results in a greater mass reduction over time compared to enhanced mass transfer. The result of the mass calculation for the flushing perturbation indicates a greater mass removal rate after an initial period of much greater mass increase. This pattern may be due to the fact that initially the advection rate is so large that $Da_2 << 1$, in which case the rate of advection of substrate is so fast compared to the biodegradation rate that there is insufficient time for biodegradation. As a result, the naphthalene mass transiently increases in the system. However, after approximately 1.5 days, breakthrough occurs for this higher advection rate and thus mass is lost via advection out of the domain. The resulting mass loss is considerable, but it does not represent mass removal through biodegradation as other

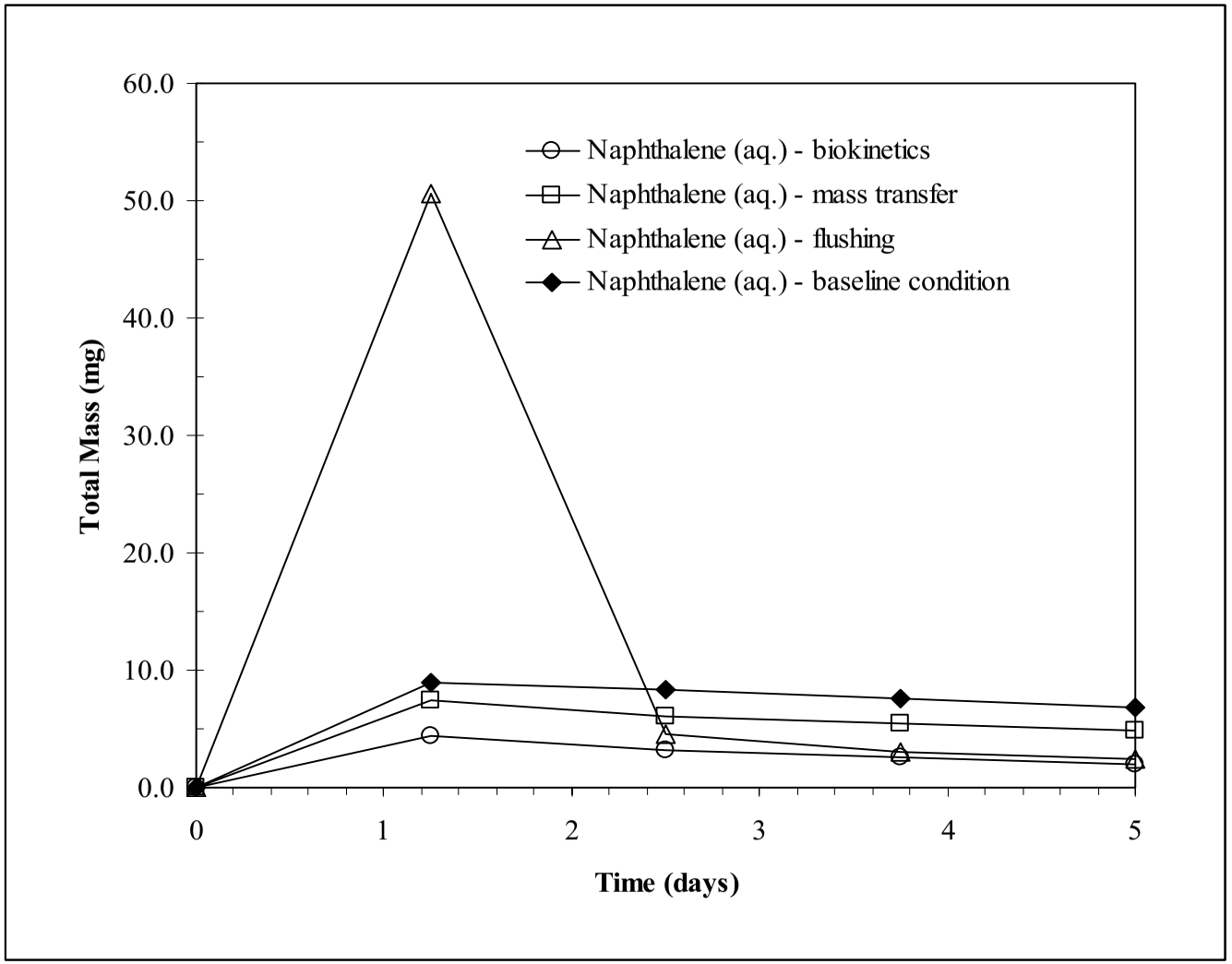

Figure 6.30. Scenario #3: Comparison of alternative perturbations - Total mass versus time, naphthalene (aq.).

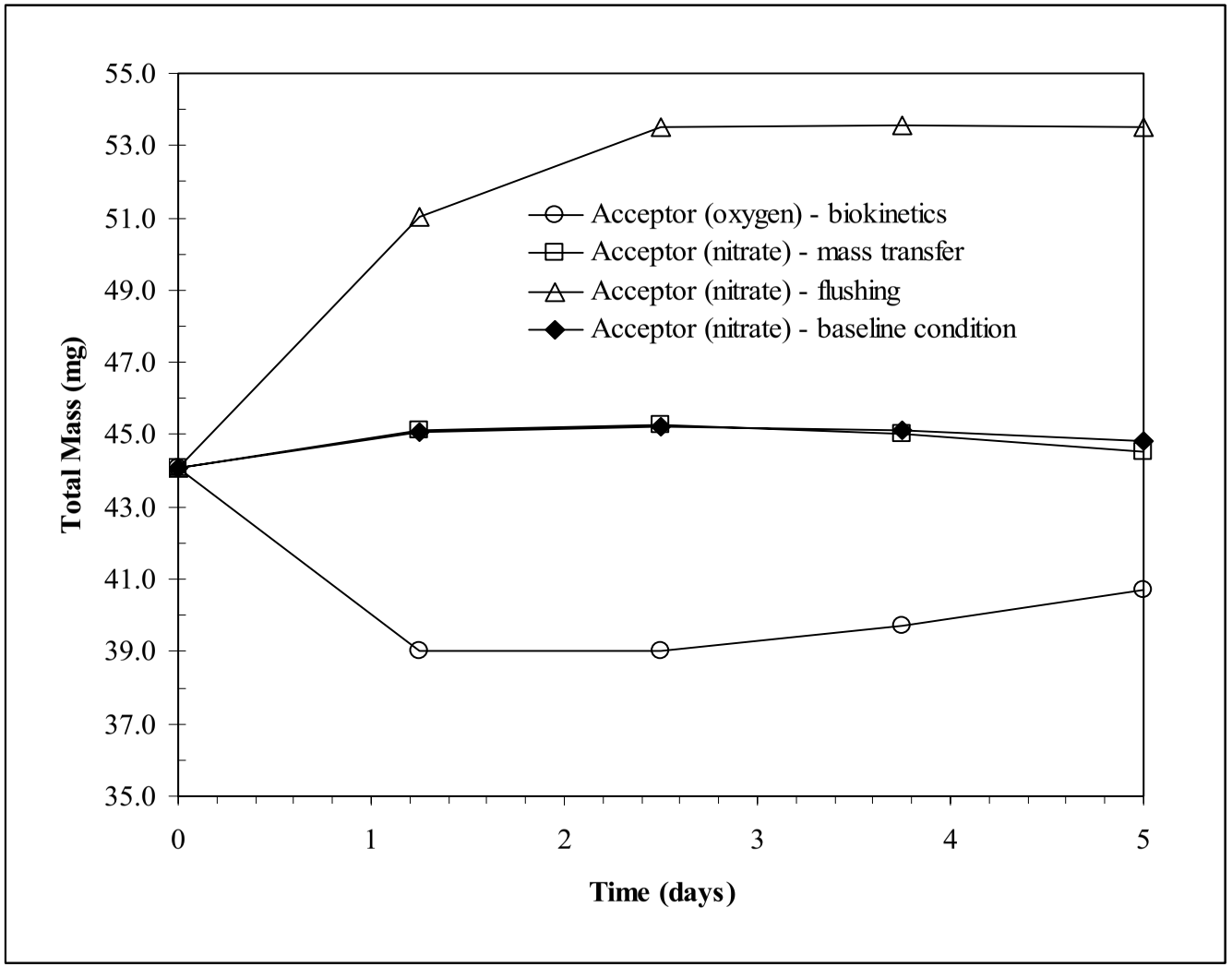

Figure 6.31. Scenario #3: Comparison of alternative perturbations - Total mass versus time, electron acceptor.

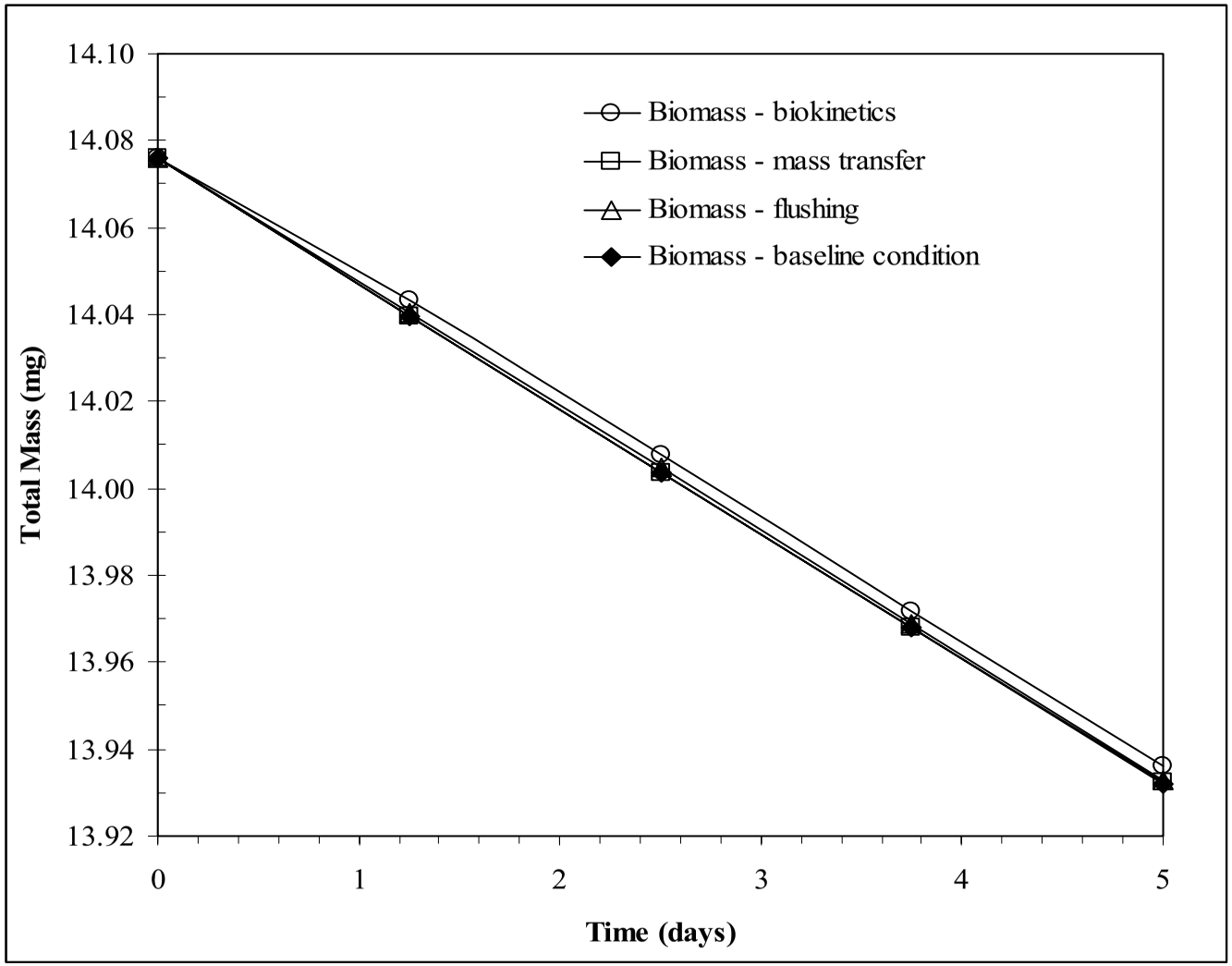

Figure 6.32. Scenario #3: Comparison of alternative perturbations - Total mass versus time, biomass.

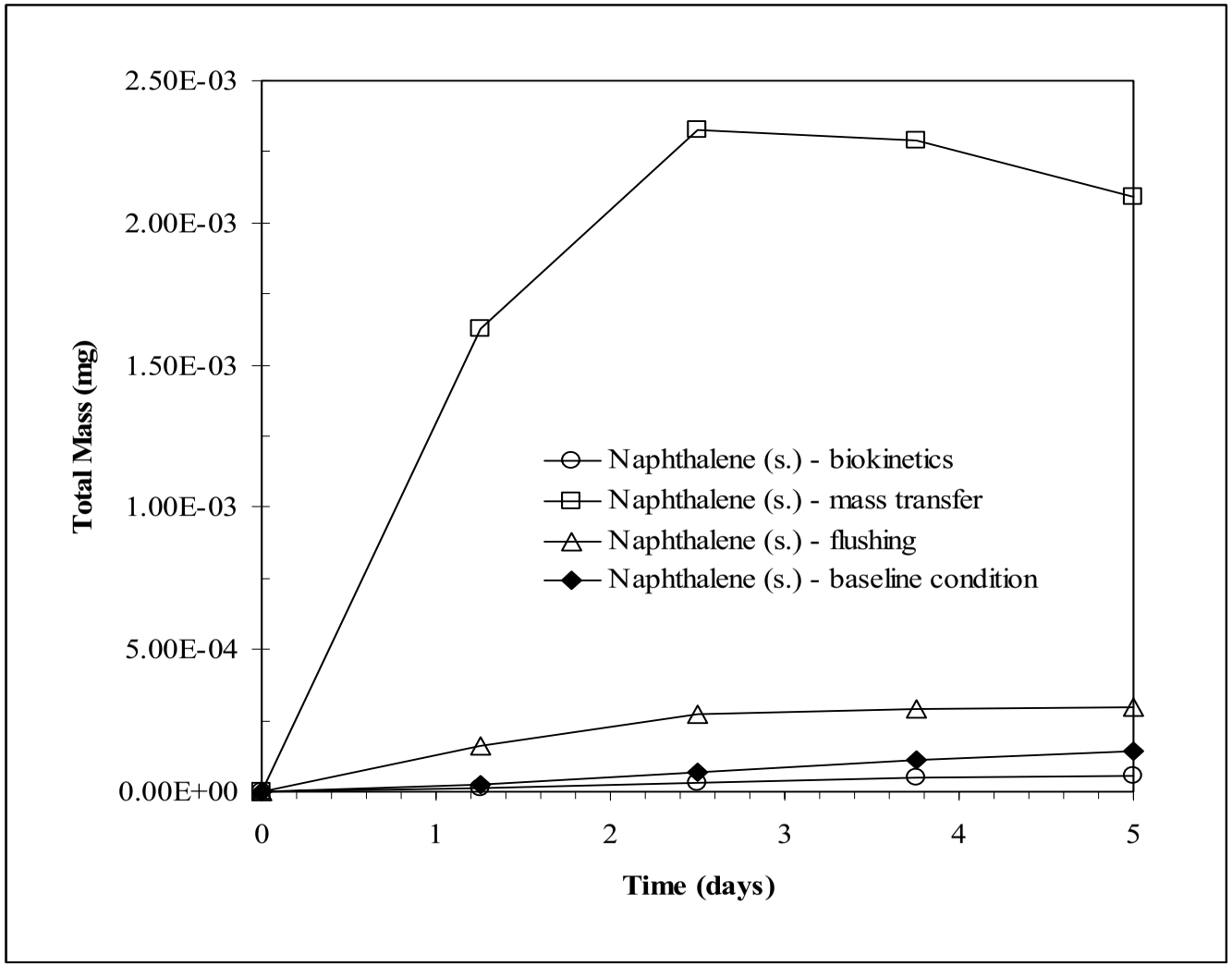

Figure 6.33. Scenario #3: Comparison of alternative perturbations - Total mass versus time, naphthalene (sorbed).

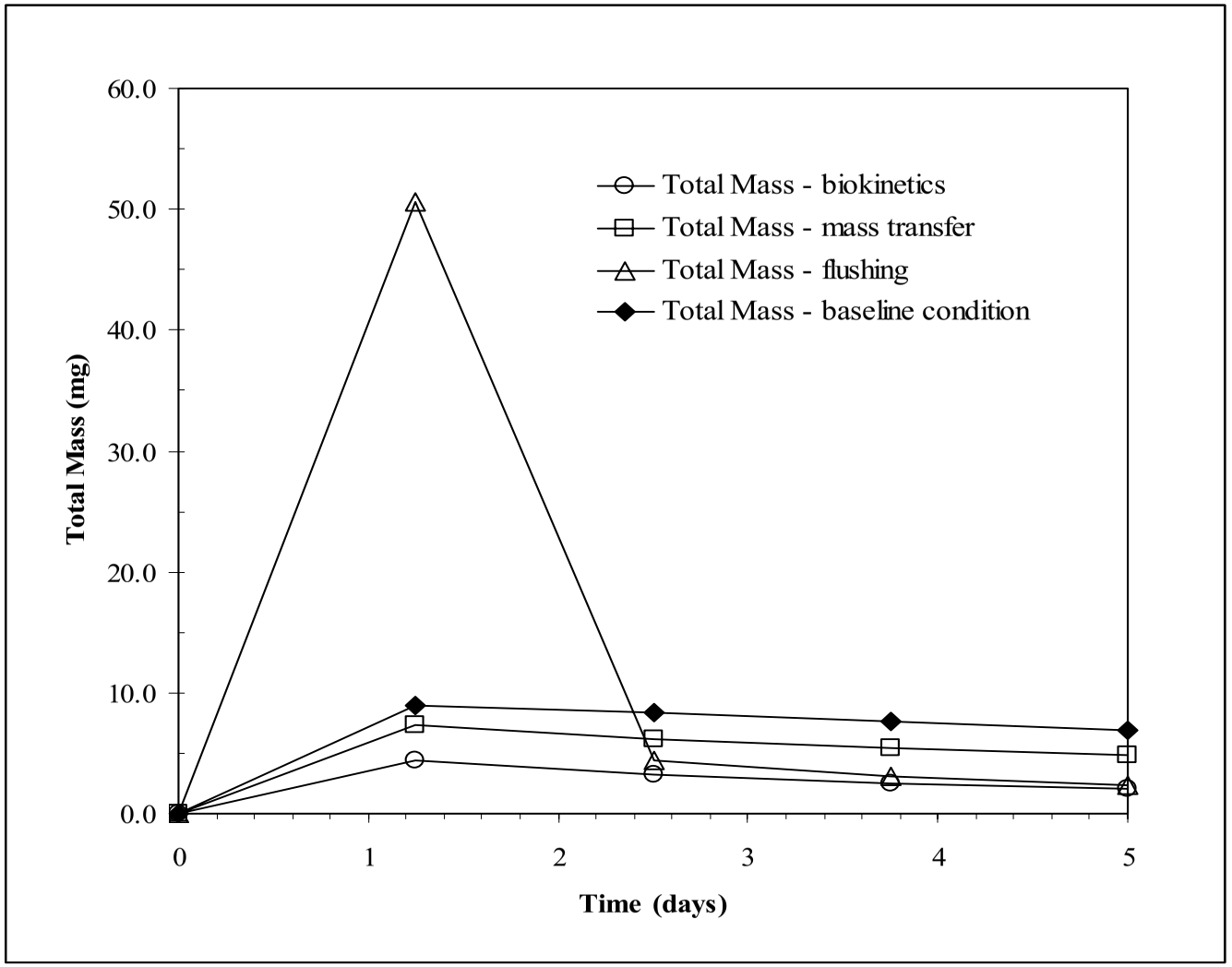

Figure 6.34. Scenario #3: Comparison of alternative perturbations - Total mass versus time, total naphthalene (aqueous plus sorbed).

mass data presented below will confirm. This mass loss due to breakthrough has been documented by others (e.g., Odencrantz, 1992) and was discussed in detail above. The comparison of electron acceptor mass in the system is presented in Fig. 6.31. Based on these data, it is clear that the greatest utilization of acceptor, which is indicative of the greatest amount of donor biotransformation, occurs for the predicted appropriate enhancement, biokinetic enhancement. In fact, the biokinetic enhancement case is the only one of the three that results in acceptor mass loss confirming the interpretation of the electron donor data during the one day injection period, as expected. After day one, the mass of acceptor for the biokinetic case begins to increase slightly because, as indicated above, once the concentration gradient begins to decrease so to does the rate of degradation.

In Fig. 6.32, the total mass over time of biomass is presented. As discussed before, all three enhancements (and the baseline condition) exhibit an overall decrease in mass over time. The overall decrease in biomass for the biokinetics enhancement is less than that for the mass transfer and flushing enhancement albeit by only a relatively small amount.

The data for the total mass of sorbed donor over time is presented in Fig. 6.33. As with the case for the aqueous donor, the biokinetic enhancement case exhibits a smaller mass increase in the sorbed phase mass than that of the mass transfer and flushing enhancements. As discussed above, this result is due to the fact that the predicted appropriate enhancement indeed has the greatest impact on mass removal of the aqueous phase donor, which in turn will result in a small amount of sorption as there is less total mass available for partitioning into the solid phase. Here, as for Scenario 1(a), the mass

transfer enhancement approach results in the greatest increase in sorbed phase due to the increased mass transfer coefficient. While under alternative scenarios this increased mass transfer may result in increased *desorption*, under the current conditions it has the opposite effect of increasing sorption because the aquifer is initially free of both aqueous and solid phase contaminant.

Finally, in Fig. 6.34, the results of the total donor mass (both aqueous and sorbed) analyses are presented. The results, as expected, indicate that the predicted appropriate enhancement has the greatest overall impact on reducing the mass of electron donor contaminant in the system.

7.0 SUMMARY AND CONCLUSIONS

This research examined the complex interrelationships between physical, chemical, and biological processes under heterogeneous subsurface conditions and their effect on the intrinsic *in situ* biodegradation of contaminants as well as the efficacy of engineered approaches for enhancing *in situ* bioremediation. Specifically, the goal of the current research was to develop a fundamental quantitative approach for understanding the impact of these physical, chemical, and biological heterogeneities, and the interfacial interactions resulting from these heterogeneities, on the biodegradation of subsurface contaminants. To elucidate the effects of these heterogeneities, this research first developed a quantitative framework comprised of a set of dimensionless parameters based on the relevant subsurface heterogeneities and interfaces. These parameters were defined so as to capture the effects of competing physiochemical and biokinetic processes (e.g., dispersion, sorption, and biodegradation). Secondly, this framework was examined using a series of systematic numerical modeling experiments to determine the impacts of these heterogeneities on *in situ* bioremediation, and to use the quantitative framework to determine what, if any, engineered actions will augment the intrinsic *in situ* biodegradation rate. Thus, the quantitative framework could be utilized in practice to both determine what are the potential rate-limiting reaction(s) in an environment, and to also assist in determining what field actions (e.g., flushing or pumping, surfactant addition, and/or biostimulation) could be used to alleviate the effects of the rate-limiting condition. This research subject is part of a larger integrated project, combining the theoretical evaluation presented here with experimental investigations that are being completed by others in the Department of Civil and Environmental Engineering at the

University of Maryland, College Park. Thus, the results of this research will have an immediate impact on other researchers.

In the first component of this research, A FORTRAN-based numerical model that incorporated kinetic mass transfer and dual-substrate limiting biokinetics was developed by modifying a commercially-available product, RT3D, developed by the Battelle Pacific Northwest National Laboratory with the assistance of programmers at Waterloo Hydrogeologic, Inc. This "used-defined" module was loaded into Visual MODFLOW, a WINDOWS®-based GUI for running the RT3D program.

Subsequently, several test scenarios for examining the quantitative framework were developed in concert with the ongoing laboratory bench-scale sand tank reactor experiments. Each of these scenarios was specifically designed to simulate a realistic subsurface condition, in which one particular process (physical, chemical, or biological) was limiting the overall biotransformation rate. Two of the scenarios were examined in this study. These scenarios were examined in three steps. First, a baseline condition was established where a contaminant was introduced to the two-layered model domain under background conditions. The baseline conditions were used to examine the impact of the given rate-limiting condition on the intrinsic biotransformation of the contaminants. Second, a specifically selected enhancement to the baseline condition was introduced. Specifically, this engineered enhancement, e.g., flushing (increased advection and dispersion), mass transfer increase (enhanced desorption) or biostimulating amendment (improved biokinetics), was selected because it was predicted to enhance the baseline condition by alleviating the rate limiting condition. This selection was based on the use of the quantitative framework, and an examination of the particular dimensionless

parameters that would be altered as a result of the enhancement. Subsequently, the enhanced numerical runs were compared to the results of the baseline conditions. If the physico-chemical rate-limiting process(es) can be alleviated by implementing the appropriate engineered perturbations, then the biokinetics become the overall rate-controlling process. This condition can be considered optimal in the sense that at that point, conventional amendments to enhance the biological activity (e.g., nutrients, electron donors or acceptors, cosubstrates, etc.) can be added to achieve the greatest overall biotransformation rate achievable by the native organisms. Third, and finally, alternative enhancements were selected that while beneficial under certain circumstances, were not predicted to be effective at alleviating the rate-limiting condition based on the dimensionless parameters of the quantitative framework. These alternate enhancements were compared then to the predicted appropriate enhancement as well as the baseline condition.

In Scenario 1(a), the relevant were established such that the dimensionless parameters resulted in the following conditions: $Pe_T >> 1$, $Da_6 >> 1$, and $Sh'_2 >> 1$. This caused a situation in which dispersion was the rate-limiting process. The baseline condition was established such that a portion of the lower conductivity layer of the domain was contaminated with the electron donor substrate, and was deficient in electron acceptor. Furthermore, electron acceptor (oxygen) was flushed into the system only via the higher conductivity layer overlying the contaminated zone at a rate of 0.165 m/day. As a result, degradation of the electron donor was dependant upon the contact and mixing of the electron donor and acceptor across the interface between the two regions of different hydraulic conductivity. Specifically, successful degradation required dispersion

of the oxygen acceptor from the higher conductivity layer into the lower conductivity layer, and conversely, dispersion of the electron donor from the lower conductivity layer into the higher conductivity oxygen bearing zone. The enhancement that was predicted to be appropriate for this scenario was an increase in the rate of advection, which in turn would result in greater transverse dispersion of the two substrates across the interface, leading to greater mixing and, thus, greater biotransformation. Increasing the advection had a direct effect on the dimensionless parameter Da_6. Whereas under the baseline condition $Da_6 >> 1$ resulted in the rate of dispersion controlling, for the enhanced condition, the advection rate was increased six-fold to approximately 0.98 m/day which caused Da_6 to decrease from 3 to 0.5 in the faster layer, such that dispersion was no longer rate-controlling, based on the quantitative framework. The effect on the transverse dispersion was an increase from 2.6×10^{-4} m/day to 1.5×10^{-3} m/day. It was further found that alternative enhancements, i.e., increased mass transfer (desorption) and biostimulation, resulted in either less donor removal or removal at lower rates than for the predicted appropriate enhancement. This was the predicted result since according to the quantitative framework, only by alleviating the rate-limiting process of dispersion (Da_6) could the overall biotransformation rate be increased.

In Scenario 3, the baseline conditions were established such that the domain was operating under background anaerobic conditions with a only a low rate of biotransformation possible (e.g., due to a low specific substrate utilization rate). Specifically, the dimensionless parameters were selected such that $Pe_T >> 1$, $Da_6 << 1$, and $Sh'_2 >> 1$, indicating that biokinetics were the overall rate-limiting process. In this case, a contaminant plume (electron donor) and acceptor were injected into the domain

for a set time. This would be comparable to a field site where a pristine aquifer becomes contaminated by the leading front of the plume. As with Scenario 1(a), several enhancements were feasible, but only one was predicted to alleviate the rate-limiting process. In this case, only the enhancement of the biokinetics would result in greater biotransformation, by enhancing the degree to which Da_6 was >>1. Therefore to enhance the biotransformation rate, the substrate utilization rate (q_{max}) was increased from 0.000238 day^{-1} to 0.238 day^{-1}. In contrast, the alternative enhancements of flushing to increase transverse dispersion and mass transfer enhancement to enhance desorption did not have an appreciable effect on the overall biotransformation rate as predicted.

The results of these numerical modeling experiments indicate that the quantitative framework was a useful tool for identifying which of the relevant system processes is rate-limiting. As previously noted, in each test scenario, the baseline conditions were established such that one process was rate-limiting. In each case, in accordance with the framework, the specific enhancement predicted to alleviate the rate-limiting process resulted in an increase in the overall rate and extent of biotransformation. The correctness of this selection was further demonstrated by comparison of the predicted appropriate enhancement to the alternative enhancements, with the result that the predicted appropriate perturbation had the greatest effect on increasing the rate and extent of total contaminant mass removal.

Another significant observation made while performing the numerical experiments was the degree of difficulty associated with appropriately selecting the underlying variables (e.g., D_T, q_{max}, and k_m) of the dimensionless parameters to conform to the requirements of the framework. For example it was found that the model was very

sensitive to discrete changes in the variables. In other words, small changes in certain values resulted in unstable model performance (e.g., a failure to converge within the set time limits and spatial constraints of the domain). Further, selection of the individual variables and criteria was also difficult in that often changes in one variable to shift the dimensionless parameters appropriately at the third tier of the quantitative framework (e.g., where advection, sorption, dispersion, or biokinetics is determined to be controlling), often resulted in changes to the dimensionless criteria of the second or first tier as well. This was an important observation as it highlights the fact that in practice, engineered remedies can be selected and implemented in the field, but with little or no success because the selected remedy also caused another unintended change in some other condition, rendering the remedy less effective.

In conclusion, the results of these modeling experiments have successfully documented the utility of the quantitative framework as a predictive tool for guiding in the selection of a site remedy that will be successful at enhancing *in situ* bioremediation. Although application to actual field conditions remains to be demonstrated, the selected model scenarios did incorporate a significant degree of complexity and heterogeneity, representative of the field. Finally, the results of this study indicate that care must be taken in selecting engineered enhancements, as system changes based on criteria that are geared toward alleviating one rate-limiting process can have unforeseen consequences on another.

8.0 RECOMMENDATIONS FOR FURTHER WORK

As discussed above, the modeling results of this study confirmed the hypothesis that the quantitative framework developed as part of this research could successfully be utilized to predict the rate-limiting process hindering intrinsic bioremediation, as well as to aid in selecting the appropriate engineering technique(s) to enhance natural conditions.

The examination of the quantitative framework under this research was theoretical in nature, relying on numerical modeling techniques. Thus, one obvious recommendation for further work is to complete laboratory-scale experimentation to support the theoretical numerical experiments completed as part of this research. As discussed above, this experimentation is currently in progress, being completed by Ms. Xin Song, a Ph.D. candidate in the Department of Civil and Environmental Engineering.

In addition, numerical modeling presented here could be expanded to apply the evaluation of the quantitative framework and the selection of enhancement processes to a larger experimental domain. Whereas the model domain used in this research conformed to the dimensions of the sand tank used for the ongoing laboratory experimentation, a larger domain would be helpful to show changes over a greater spatial distribution and longer timeframe, and perhaps over multiple layers of varying hydraulic conductivity rather than the two layered model examined herein.

Another useful exercise would be to evaluate an actual field site where numerous data have been collected such as the well-studied Borden Aquifer, Ontario, Canada, or the Massachusetts Military Reservation Site, Cape Cod, Massachusetts. For such sites, sufficient data have been compiled such that a numerical model domain could be established, and the input criteria could be selected from the existing data. Information

from sites where a remedy has been selected and implemented could also be used to further evaluate the quantitative framework; especially where data exist in support of successful *in situ* bioremediation.

Finally, the incorporation into the numerical model of NAPL source zones (blobs or pools) or kinetic expressions for transfer of oxygen from the vadose zone to the saturated zone could support further studies of application of the techniques presented here to site scenarios involving these types of contamination.

Appendix I: Custom User-Define RT3D Reaction Module – UMD Biokinetics

```
C*****Reaction model for University of Maryland, College Park************************************
c     Biomass transport and rate-limited degradation are simulated
c     set ncomp = 4 and mcomp = 2
c*********************************************************************
      SUBROUTINE Rxns(ncomp,nvrxndata,j,i,k,y,dydt,poros,rhob,reta,rc,nlay,nrow,ncol,vrc)
C*Block 1:*************************************************************
c List of calling arguments
c ncomp - Total number of components
c nvrxndata - Total number of variable reaction parameters to be input via RCT file
c J, I, K - node location (used if reaction parameters are spatially variable)
c y - Concentration value of all component at the node [array variable y(ncomp)]
c dydt - Computed RHS of your differential equation [array variable dydt(ncomp)]
c poros - porosity of the node
c reta -  Retardation factor [ignore dummy reta values of immobile species]
c rhob -  bulk density of the node
c rc - Stores spatially constant reaction parameters (can dimension upto 100 values)
c nlay, nrow, ncol - Grid size (used only for dimensioning purposes)
c vrc - Array variable that stores spatially variable reaction parameters
C*End of block 1*******************************************************

C*Block 2:*************************************************************
c*    *Please do not modify this standard interface block*
      !MS$ATTRIBUTES DLLEXPORT, ALIAS: 'rxns' :: rxns
      IMPLICIT NONE
      INTEGER ncol,nrow,nlay
      INTEGER ncomp,nvrxndata,j,i,k
      !INTEGER, SAVE :: First_time=1
      DOUBLE PRECISION y,dydt,poros,rhob,reta
      DOUBLE PRECISION rc,vrc
      DIMENSION y(ncomp),dydt(ncomp),rc(50)
      DIMENSION vrc(ncol,nrow,nlay,nvrxndata),reta(ncomp)
C*End of block 2*******************************************************
```

Appendix I: Custom User-Define RT3D Reaction Module – UMD Biokinetics

```
C*Block 3:************************************************************
c      *Declare your problem-specific new variables here*
c     INTEGER
       DOUBLE PRECISION rdonors,racceps,rsorbed,rgrows
C*End of block 3******************************************************
C*Block 4:************************************************************
c      *Initilize reaction parameters here, if required*
c       IF (First_time .EQ. 1) THEN
c         None
c         First_time = 0 !reset First_time to skip this block later
c       END IF
C*End of block 4******************************************************

C*Block 5:************************************************************
c      *Assign or compute values for new variables, if required*
c     None
C*End of block 5******************************************************

C*Block 6:************************************************************
c      *Differential Reaction Equations*
c       Definition of values in the rc(8) and y(4) arrays
c     rc(1)  = Specific utilization rate, umax
c     rc(2)  = Monod half saturation constant for donor, Ks
c     rc(3)  = Monod half saturation constant for acceptor, Ka
c      rc(4)  = yield (amount of biomass produced to the amount of carbon utilized)
c      rc(5)  = yield (amount of oxygen consumed to the amount of carbon utilized)
c      rc(6)  = First-order, bacterial death or decay rate
c      rc(7)  = Mass transfer coefficient (Km)
c      rc(8)  = Partitioning coefficient (Kp)
c      rc(9)  = Freundlich sorption parameter (n)
c      y(1)  = Elec Donor (Aqueous Naphthalene) [M/L3]
```

Appendix I: Custom User-Define RT3D Reaction Module – UMD Biokinetics

```
c       y(2)  = Elec Acceptor (Aqueous Nitrate) [M/L3]
c      y(3)  = Sorbed phase, Donor/Naphthalene [M/M]
c       y(4)  = Attached bacteria (mass of bacteria per mass of soil [M/M])
        IF (nvrxndata .EQ. 0) THEN
c
c         Soil phase kinetic expressions (for constant rxn parameters)
          rgrows = (rc(1)*y(4)*rc(4)*y(1)*y(2)*
     &             (1.0/(rc(2)+y(1)))*(1.0/(rc(3)+y(2))))-(rc(6)*y(4))
          rdonors = rc(1)*y(4)*y(1)*y(2)*
     &             (1.0/(rc(2)+y(1)))*(1.0/(rc(3)+y(2)))
          racceps = rc(1)*rc(5)*y(4)*y(1)*y(2)*
     &             (1.0/(rc(2)+y(1)))*(1.0/(rc(3)+y(2)))
          rsorbed = rc(7)*(rc(8)*y(1)**rc(9)-y(3))
c
c         Reaction kinetic expressions (for constant rxn parameters)
          dydt(1) = -((rhob*rdonors/poros)/reta(1))-(rhob/poros*rsorbed)
          dydt(2) = -(rhob*racceps/poros)
          dydt(3) = rsorbed
          dydt(4) = rgrows
c
       ELSE
c
c         Soil phase kinetic expressions (for variable rxn parameters)
          rgrows = (vrc(j,i,k,1)*y(4)*vrc(j,i,k,4)*y(1)*y(2)*
     &             (1.0/(vrc(j,i,k,2)+y(1)))*
     &             (1.0/(vrc(j,i,k,3)+y(2))))-(vrc(j,i,k,6)*y(4))
          rdonors = vrc(j,i,k,1)*y(4)*y(1)*y(2)*
     &             (1.0/(vrc(j,i,k,2)+y(1)))*
     &             (1.0/(vrc(j,i,k,3)+y(2)))
          racceps = vrc(j,i,k,1)*vrc(j,i,k,5)*y(4)*y(1)*y(2)*
     &             (1.0/(vrc(j,i,k,2)+y(1)))*
     &             (1.0/(vrc(j,i,k,3)+y(2)))
```

Appendix I: Custom User-Define RT3D Reaction Module – UMD Biokinetics

```
        rsorbed = vrc(j,i,k,7)*(vrc(j,i,k,8)*
     &           y(1)**vrc(j,i,k,9)-y(3))
c
c       Reaction kinetic expressions (for variable rxn parameters)
        dydt(1) = -((rhob*rdonors/poros)/reta(1))-(rhob/poros*rsorbed)
        dydt(2) = -(rhob*racceps/poros)
        dydt(3) = rsorbed
        dydt(4) = rgrows
      END IF
C*End of block 6*********************************************************
        RETURN
        END
```

Appendix II: Analytical Verification Input Parameters

Two Dimensional Analytical Solution to Solute Transport

References: Domenico & Schwartz
Domenico, 1987
Odencrantz, 1992
MacQuarrie et al, 1990

CONDITIONS:

t =	10	days
z =	0.0	m

		Value	Units	Reference for value	
Seepage velocity	υ_x	0.090	m/day	MacQuarrie et al, 1990; Odencrantz, 1992	
Retarded velocity (lin. equil. ads.)	υ'_x	0.090	m/day	calculated by R=Vx/V'x	z = 0 for entire domain
Longitudinal Dispersivity	α_L	0.600	m	MacQuarrie et al, 1990; Odencrantz, 1992	Longitudinal = x-direction
Transverse Dispersivity	α_T	0.005	m	MacQuarrie et al, 1990; Odencrantz, 1992	Transverse = y-direction
Molecular Diffusion	D_m	0.000	m^2/day	MacQuarrie et al, 1990; Odencrantz, 1992	
Long. Dispersion coefficient	D_L	0.054	m^2/day	$D_L = \alpha_L\upsilon + D_m$	
Trans. Dispersion coefficient	D_T	0.000450	m^2/day	$D_T = \alpha_T\upsilon + D_m$	
Decay	λ	0.007	/day	MacQuarrie et al, 1990; Odencrantz, 1992	
Soil bulk density	ρ_b	2.650E+03	g/L		
Porosity	n	0.35	--		
Soil partition coeff.	Kd	2.642E-05	L/g		
Retardation	R	1.20004		MacQuarrie et al, 1990; Odencrantz, 1992 (calculated)	

	Value	Unit
Initial t	0.0	day
Final t	10.0	day
δt	1.0	day
Initial x	0.0	m
δx	0.5	m

Y (m) =	2.00

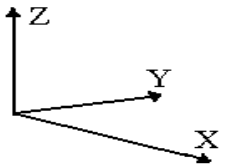

Criteria for controlling numerical dispersion and oscillation

Courant No. =	0.180	Co <= 1 ?
Peclet No. =	0.833	Pe <= 2 ?

$$\frac{C(x,y,z,t)}{C_o} = \left(\frac{1}{2}\right)\exp\left\{\left(\frac{x}{2\alpha_x}\right)\left[1-\left(1+\frac{4\lambda\alpha_x}{v}\right)^{1/2}\right]\right\} erfc\left[\frac{x - vt\left(1+4\lambda\alpha_x/v\right)^{1/2}}{2\left(\alpha_x vt\right)^{1/2}}\right]$$

$$\left\{erf\left[\frac{Y}{4\left(\alpha_y x\right)^{1/2}}\right]\right\}$$

Appendix II: Analytical Verification Input Parameters

Two Dimensional Analytical Solution to Solute Transport

References: Domenico & Schwartz
Domenico, 1987
Odencrantz, 1992
MacQuarrie et al, 1990

CONDITIONS:

t =	40	days
z =	0.0	m

		Value	Units	Reference for value	
Seepage velocity	υ_x	0.090	m/day	MacQuarrie et al, 1990; Odencrantz, 1992	
Retarded velocity (lin. equil. ads.)	υ'_x	0.090	m/day	calculated by R=Vx/V'x	z = 0 for entire domain
Longitudinal Dispersivity	α_L	0.600	m	MacQuarrie et al, 1990; Odencrantz, 1992	Longitudinal = x-direction
Transverse Dispersivity	α_T	0.005	m	MacQuarrie et al, 1990; Odencrantz, 1992	Transverse = y-direction
Molecular Diffusion	D_m	0.000	m^2/day	MacQuarrie et al, 1990; Odencrantz, 1992	
Long. Dispersion coefficient	D_L	0.054	m^2/day	$D_L = \alpha_L\upsilon + D_m$	
Trans. Dispersion coefficient	D_T	0.000450	m^2/day	$D_T = \alpha_T\upsilon + D_m$	
Decay	λ	0.007	/day	MacQuarrie et al, 1990; Odencrantz, 1992	
Soil bulk density	ρ_b	2.650E+03	g/L		
Porosity	n	0.35	--		
Soil partition coeff.	Kd	2.642E-05	L/g		
Retardation	R	1.20004		MacQuarrie et al, 1990; Odencrantz, 1992 (calculated)	

	Value	Unit
Initial t	0.0	day
Final t	40.0	day
δt	1.0	day
Initial x	0.0	m
δx	0.5	m

Y (m) =	2.00

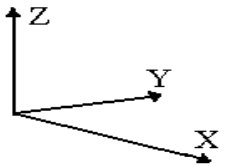

Criteria for controlling numerical dispersion and oscillation

Courant No. =	0.180	Co <= 1 ?
Peclet No. =	0.833	Pe <= 2 ?

$$\frac{C(x,y,z,t)}{C_o} = \left(\frac{1}{2}\right)\exp\left\{\left(\frac{x}{2\alpha_x}\right)\left[1-\left(1+\frac{4\lambda\alpha_x}{v}\right)^{1/2}\right]\right\} erfc\left[\frac{x - vt\left(1+4\lambda\alpha_x/v\right)^{1/2}}{2\left(\alpha_x vt\right)^{1/2}}\right]$$

$$\left\{erf\left[\frac{Y}{4\left(\alpha_y x\right)^{1/2}}\right]\right\}$$

Appendix II: Analytical Verification Input Parameters

Two Dimensional Analytical Solution to Solute Transport

References:
Domenico & Schwartz
Domenico, 1987
Odencrantz, 1992
MacQuarrie et al, 1990

CONDITIONS:

t =	120	days
z =	0.0	m

		Value	Units	Reference for value	
Seepage velocity	υ_x	0.090	m/day	MacQuarrie et al, 1990; Odencrantz, 1992	
Retarded velocity (lin. equil. ads.)	υ'_x	0.090	m/day	calculated by R=Vx/V'x	z = 0 for entire domain
Longitudinal Dispersivity	α_L	0.600	m	MacQuarrie et al, 1990; Odencrantz, 1992	Longitudinal = x-direction
Transverse Dispersivity	α_T	0.005	m	MacQuarrie et al, 1990; Odencrantz, 1992	Transverse = y-direction
Molecular Diffusion	D_m	0.000	m^2/day	MacQuarrie et al, 1990; Odencrantz, 1992	
Long. Dispersion coefficient	D_L	0.054	m^2/day	$D_L = \alpha_L\upsilon + D_m$	
Trans. Dispersion coefficient	D_T	0.000450	m^2/day	$D_T = \alpha_T\upsilon + D_m$	
Decay	λ	0.007	/day	MacQuarrie et al, 1990; Odencrantz, 1992	
Soil bulk density	ρ_b	2.650E+03	g/L		
Porosity	n	0.35	--		
Soil partition coeff.	Kd	2.642E-05	L/g		
Retardation	R	1.20004		MacQuarrie et al, 1990; Odencrantz, 1992 (calculated)	

	Value	Unit
Initial t	0.0	day
Final t	120.0	day
δt	1.0	day
Initial x	0.0	m
δx	0.5	m

Y (m) =	2.00

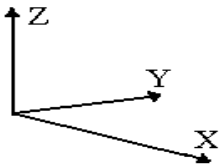

Criteria for controlling numerical dispersion and oscillation

Courant No. =	0.180	Co <= 1 ?
Peclet No. =	0.833	Pe <= 2 ?

$$\frac{C(x,y,z,t)}{C_o} = \left(\frac{1}{2}\right)\exp\left\{\left(\frac{x}{2\alpha_x}\right)\left[1-\left(1+\frac{4\lambda\alpha_x}{v}\right)^{1/2}\right]\right\} erfc\left[\frac{x - vt\left(1+4\lambda\alpha_x/v\right)^{1/2}}{2\left(\alpha_x vt\right)^{1/2}}\right]$$

$$\left\{erf\left[\frac{Y}{4\left(\alpha_y x\right)^{1/2}}\right]\right\}$$

Appendix II: Analytical Verification Input Parameters

Two Dimensional Analytical Solution to Solute Transport

References: Domenico & Schwartz
Domenico, 1987
Odencrantz, 1992
MacQuarrie et al, 1990

CONDITIONS:

t =	280	days
z =	0.0	m

		Value	Units	Reference for value	
Seepage velocity	υ_x	0.090	m/day	MacQuarrie et al, 1990; Odencrantz, 1992	
Retarded velocity (lin. equil. ads.)	υ'_x	0.090	m/day	calculated by R=Vx/V'x	z = 0 for entire domain
Longitudinal Dispersivity	α_L	0.600	m	MacQuarrie et al, 1990; Odencrantz, 1992	Longitudinal = x-direction
Transverse Dispersivity	α_T	0.005	m	MacQuarrie et al, 1990; Odencrantz, 1992	Transverse = y-direction
Molecular Diffusion	D_m	0.000	m^2/day	MacQuarrie et al, 1990; Odencrantz, 1992	
Long. Dispersion coefficient	D_L	0.054	m^2/day	$D_L = \alpha_L\upsilon + D_m$	
Trans. Dispersion coefficient	D_T	0.000450	m^2/day	$D_T = \alpha_T\upsilon + D_m$	
Decay	λ	0.007	/day	MacQuarrie et al, 1990; Odencrantz, 1992	
Soil bulk density	ρ_b	2.650E+03	g/L		
Porosity	n	0.35	--		
Soil partition coeff.	Kd	2.642E-05	L/g		
Retardation	R	1.20004		MacQuarrie et al, 1990; Odencrantz, 1992 (calculated)	

	Value	Unit
Initial t	0.0	day
Final t	280.0	day
δt	1.0	day
Initial x	0.0	m
δx	0.5	m

Y (m) = 2.00

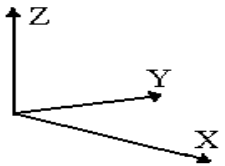

Criteria for controlling numerical dispersion and oscillation

Courant No. =	0.180	Co <= 1 ?
Peclet No. =	0.833	Pe <= 2 ?

$$\frac{C(x,y,z,t)}{C_o} = \left(\frac{1}{2}\right)\exp\left\{\left(\frac{x}{2\alpha_x}\right)\left[1-\left(1+\frac{4\lambda\alpha_x}{v}\right)^{1/2}\right]\right\} erfc\left[\frac{x - vt\left(1+4\lambda\alpha_x/v\right)^{1/2}}{2\left(\alpha_x vt\right)^{1/2}}\right]$$

$$\left\{erf\left[\frac{Y}{4\left(\alpha_y x\right)^{1/2}}\right]\right\}$$

Appendix III: Numerical Modeling Input Parameters				Scenario (1A) Macro scale mass transport controls Pet >> 1 Sh2' >> 1 Da6 >> 1		(1A) Enhanced ++ Flushing		(1A) Enhanced ++ Biokinetics		(1A) Enhanced ++ Mass Transfer	
	Dimensionless Parameters			**FAST Layer**	**SLOW Layer**	**FAST**	**SLOW**	**FAST**	**SLOW**	**FAST**	**SLOW**
		Transverse Peclet No.	Pet	748	557	791	1547	748	557	748	557
		Damkohler No. 2	Da2	3.47E-03	5.55E-02	5.78E-04	9.26E-03	3.47E-02	5.55E-01	3.47E-03	5.55E-02
		Damkohler No. 6	Da6	3	31	0.5	14.3	26.0	309.6	2.6	31.0
		Damkohler No. 5	Da5	2.38E-02	2.38E-02	2.38E-02	2.38E-02	2.38E-01	2.38E-01	4.76E-04	4.76E-04
		Stanton No. 2	St2	0.1458	2.3333	0.0243	0.3889	0.1458	2.3333	7.2917	116.6667
		Modified Sherwood No. 2	Sh2'	109	1301	19.2	601.8	109.1	1300.6	5457.5	65032.3
		Courant	<= 1	0.102	0.006	0.609	0.038	0.102	0.006	0.102	0.006
		Peclet	<=2	3.222	3.770	3.314	7.840	3.222	3.770	3.222	3.770
	Parameter	**Dimensions/ Units**	**Reference/Notes**								
X length	x	m	tank dimension	1.2	1.2	1.2	1.2	1.2	1.2	1.2	1.2
delta x	dx	m		0.01	0.01	0.01	0.01	0.01	0.01	0.01	0.01
Y length	y	m	tank dimension	0.3	0.3	0.3	0.3	0.3	0.3	0.3	0.3
delta y	dy	m		0.01	0.01	0.01	0.01	0.01	0.01	0.01	0.01
Characteric length	L	m	domain	1.2	1.2	1.2	1.2	1.2	1.2	1.2	1.2
total porosity	θ	--		0.35	0.35	0.35	0.35	0.35	0.35	0.35	0.35
bulk density	ρb	mg/L		1.700E+06	1.700E+06	1.700E+06	1.700E+06	1.700E+06	1.700E+06	1.700E+06	1.700E+06
seepage velocity	vx	m/day	calculated	0.165	0.010	0.987	0.062	0.165	0.010	0.165	0.010
Hyd. Cond.	K	m/day	sand tank data	345.6	21.6	345.6	21.6	345.6	21.6	345.6	21.6
dispersivity (trans)	αT	m	(8)	0.0015	0.0005	0.0015	0.0005	0.0015	0.0005	0.0015	0.0005
dispersivity (long)	αL	m	(8)	0.003	0.001	0.003	0.001	0.003	0.001	0.003	0.001
long. dispersion	DL	m^2/day	calculated	5.11E-04	2.73E-05	2.98E-03	7.87E-05	5.11E-04	2.73E-05	5.11E-04	2.73E-05
trans. dispersion	DT	m^2/day	calculated	2.64E-04	2.21E-05	1.50E-03	4.79E-05	2.64E-04	2.21E-05	2.64E-04	2.21E-05
molec. diffusion	Dm	m^2/day	(10)	1.70E-05	1.70E-05	1.70E-05	1.70E-05	1.70E-05	1.70E-05	1.70E-05	1.70E-05
Half-Saturation (Substrate)	Ks	mg/L	(10)	0.654	0.654	0.654	0.654	0.654	0.654	0.654	0.654
Half-Saturation (Acceptor)	Ka	mg/L	(5)	0.146	0.146	0.146	0.146	0.146	0.146	0.146	0.146
Specific utiliz. Rate	qmax	day^{-1}	(3) & (4)	0.0238	0.0238	0.0238	0.0238	**0.238**	**0.238**	0.0238	0.0238
Acceptor consumed/donor used	Yield (A/S)	unitless, mass-based for RT3D	stoichiometric, (9)	1.46	1.46	1.46	1.46	1.46	1.46	1.46	1.46
biomass decay	kd	day^{-1}	(3)	0.00208	0.00208	0.00208	0.00208	0.00208	0.00208	0.00208	0.00208
Biomass produced/donor consumed	Yield (X/S)	unitless, mass-based for RT3D	stoichiometric, (9)	0.78	0.78	0.78	0.78	0.78	0.78	0.78	0.78
Partitioning coeff.	Kp	L/mg	calculated	8.235E-08	8.235E-08	8.235E-08	8.235E-08	8.235E-08	8.235E-08	8.235E-08	8.235E-08
Mass transfer coeff.	km	day^{-1}	varies	0.020	0.020	0.020	0.020	0.020	0.020	**1.000**	**1.000**
initial donor	So (C initial)	mg/L	varies	10.0	10.0	10.0	10.0	10.0	10.0	10.0	10.0
initial biomass	Xo (initial biomass)	mg/kg	(10)	0.200	0.200	0.200	0.200	0.200	0.200	0.200	0.200
input acceptor	Ai (A input)	mg/L		2.0	0.0	2.0	0.0	2.0	0.0	2.0	0.0
initial acceptor	Ao (initial acceptor)	mg/L	(10)	2.0	0.0	2.0	0.0	2.0	0.0	2.0	0.0
initial sorbed donor	Si (initial sorbed)	mg/kg		0.0	0.0	0.0	0.0	0.0	0.0	0.0	0.0

Appendix III: Numerical Modeling Input Parameters				Scenario (3) Biokinetics controls Pet >> 1 Sh2' >> 1 Da6 << 1		(3) Enhanced ++biokinetics	(3) Enhanced	(3) Enhanced ++ Flushing	(3) Enhanced	(3) Enhanced ++ Desorption	(3) Enhanced
	Dimensionless Parameters			**FAST**	**SLOW**	**FAST**	**SLOW**	**FAST**	**SLOW**	**FAST**	**SLOW**
		Transverse Peclet No.	Pet	2975	685	2975	615	3783	2085	2975	615
		Damkohler No. 2	Da2	3.99E-05	6.39E-04	3.99E-02	6.39E-01	6.65E-06	1.06E-04	3.99E-05	6.39E-04
		Damkohler No. 6	Da6	0.12	0.44	118.76	392.45	0.03	0.22	0.12	0.39
		Damkohler No. 5	Da5	5.47E-04	5.47E-04	5.47E-01	5.47E-01	5.47E-04	5.47E-04	5.47E-06	5.47E-06
		Stanton No. 2	St2	0.1	1.2	0.1	1.2	0.0	0.2	7.3	116.7
		Modified Sherwood No. 2	Sh2'	217	799	217	717	46	405	21696	71693
		Courant	<= 1	0.033	0.002	0.033	0.002	0.197	0.012	0.033	0.002
		Peclet	<=2	3.222	3.770	3.222	2.149	3.314	3.053	3.222	2.149
	Parameter	**Dimensions/ Units**	**Reference/Notes**								
X length	x	m	tank dimension	1.2	1.2	1.2	1.2	1.2	1.2	1.2	1.2
delta x	dx	m		0.01	0.01	0.01	0.01	0.01	0.01	0.01	0.01
Y length	y	m	tank dimension	0.3	0.3	0.3	0.3	0.3	0.3	0.3	0.3
delta y	dy	m		0.01	0.01	0.01	0.01	0.01	0.01	0.01	0.01
Characteric length	L	m	domain	1.2	1.2	1.2	1.2	1.2	1.2	1.2	1.2
total porosity	θ	--		0.35	0.35	0.35	0.35	0.35	0.35	0.35	0.35
bulk density	ρb	mg/L		1.700E+06	1.700E+06	1.700E+06	1.700E+06	1.700E+06	1.700E+06	1.700E+06	1.700E+06
seepage velocity	vx	m/day	calculated	0.165	0.010	0.165	0.010	0.987	0.062	0.165	0.010
Hyd. Cond.	K	m/day	sand tank data	345.6	21.6	345.6	21.6	345.6	21.6	345.6	21.6
dispersivity (trans)	αT	m	(8)	0.0003	0.0001	0.0003	0.0003	0.0003	0.0003	0.0003	0.0003
dispersivity (long)	αL	m	(8)	0.003	0.001	0.003	0.003	0.003	0.003	0.003	0.003
long. dispersion	DL	m^2/day	calculated	5.11E-04	2.73E-05	5.11E-04	4.79E-05	2.98E-03	2.02E-04	5.11E-04	4.79E-05
trans. dispersion	DT	m^2/day	calculated	6.64E-05	1.80E-05	6.64E-05	2.01E-05	3.13E-04	3.55E-05	6.64E-05	2.01E-05
molec. diffusion	Dm	m^2/day	(10)	1.70E-05	1.70E-05	1.70E-05	1.70E-05	1.70E-05	1.70E-05	1.70E-05	1.70E-05
Half-Saturation (Substrate)	Ks	mg/L	(10)	0.654	0.654	0.654	0.654	0.654	0.654	0.654	0.654
Half-Saturation (Acceptor)	Ka	mg/L	(5)	0.146	0.146	0.146	0.146	0.146	0.146	0.146	0.146
Specific utiliz. Rate	qmax	day^{-1}	(3) & (4)	**0.000238**	**0.000238**	**0.238**	**0.238**	0.000238	0.000238	0.000238	0.000238
Acceptor consumed/donor used	Yield (A/S)	unitless, mass-based for RT3D	stoichiometric, (9)	**2.74**	**2.74**	**1.46**	**1.46**	2.74	2.74	2.74	2.74
biomass decay	kd	day^{-1}	(3)	0.00208	0.00208	0.00208	0.00208	0.00208	0.00208	0.00208	0.00208
Biomass produced/donor consumed	Yield (X/S)	unitless, mass-based for RT3D	stoichiometric, (9)	**0.76**	**0.76**	**0.78**	**0.78**	0.76	0.76	0.76	0.76
Partitioning coeff.	Kp	L/mg	calculated	8.235E-08	8.235E-08	8.235E-08	8.235E-08	8.235E-08	8.235E-08	8.235E-08	8.235E-08
Mass transfer coeff.	km	day^{-1}	varies	0.01	0.01	0.01	0.01	0.01	0.01	**1.00**	**1.00**
initial donor	So (C initial)	mg/L	varies	10.0	10.0	10.0	10.0	10.0	10.0	10.0	10.0
initial biomass	Xo (initial biomass)	mg/kg	(10)	0.230	0.230	0.230	0.230	0.230	0.230	0.230	0.230
input acceptor	Ai (A input)	mg/L		5.0	5.0	5.0	5.0	5.0	5.0	5.0	5.0
initial acceptor	Ao (initial acceptor)	mg/L	(10)	3.5	3.5	3.5	3.5	3.5	3.5	3.5	3.5
initial sorbed donor	Si (initial sorbed)	mg/kg		0.0	0.0	0.0	0.0	0.0	0.0	0.0	0.0

Apendix III: Numerical Modeling Input Parameters

References for Input Values

(1) Priddle and MacQuarrie, 1994
(2) Wilson, et al, 1985
(3) Odencrantz, 1992
(4) Mihelcic and Luthy, 1991
(5) Rittmann et al, 1988
(6) CRC Handbook, 1999
(7) Starr, et al, No. 2, 1985
(8) Gelhar, et al, 1992
(9) Durant et al, 1997; after McCarty, 1975
(10) McQuarrie and Sudicky, 1990

REFERENCES

Anderson, M.P. and Woessner, W.W. 1992. Assigning parameter values. Applied Groundwater Modeling; Simulation of Flow and Advective Transport. Academic Press, Boston, MA. 73-77.

Baker, J.H. 1986. Relationship between microbial activity of stream sediments, determined by three different methods, and abiotic variables. Microbial Ecology. 12:193-203.

Balkwill, D.L. et al. 1989. Vertical and horizontal variations in the physiological diversity of the aerobic chemoheterotrophic bacterial microflora in deep southeast coastal plain subsurface sediments. Applied and Environmental Microbiology. 55:1058-1065.

Balkwill, D.L. and Fredrickson, J.K. and Thomas, J.M. 1989. Vertical and Horizontal Variations in the Physiological Diversity of the Aerobic Chemoheterotrophic Bacterial Microflora in Deep Southeast Coastal Plain Subsurface Sediments. Applied and Environmental Microbiology. 55(5): 1058-1065.

Baveye, P. and Valocchi, A., 1989. An evaluation of mathematical models of the transport of biologically reacting solutes in saturated soils and aquifers. Water Resources Research, 25 (6), 1413-1421.

Bosma, T.N.P. and Middeldorp, P.J.M. and Schraa, G. and Zehnder, A.J.B. 1997. Mass transfer limitation of biotransformation: quantifying bioavailability. Environmental Science and Technology. 31(1): 248-252.

Brockman, F.J. and Murray, C.J. 1997. Microbiological heterogeneity in the terrestrial subsurface and approaches for its description. The Microbiology of the Terrestrial Deep Subsurface. 6: 75-102.

Brusseau, M.L. 1995. The effect of nonlinear sorption on transformation of contaminants during transport in porous media. Journal of Contaminant Hydrology. 17: 277-291.

Brusseau, M.L. and Hu, M.Q. and Wang, J.M. and Maier, R.M. 1999. Biodegradation during contaminant transport in porous media. 2. The influence of physicochemical factors. Environmental Science Technology. 33(1): 96-103.

Brusseau, M.L. and Srivastava, R. 1997. Nonideal transport of reactive solutes in heterogeneous porous media: 2. Quantitative analysis of the Borden natural-gradient field experiment. Journal of Contaminant Hydrology. 28: 115-155.

Burgos, W.D., Berry, D.F., Bhandari, A., and Novak, J.T. 1999. Impact of soil-chemical interactions on the bioavailability of naphthalene and naphthol. Water Research. 33: 3789-3795.

Cerniglia, C.E. and Gibson 1977. Metabolism of naphthalene by cunninghamella elegans. Applied and Environmental Microbiology. 34: 363-370.

Cirpka, O.A. and Frind, E.O. and Helmig, R. 1999. Numerical simulation of biodegradation controlled by transverse mixing. Journal of Contaminant Hydrology. 40: 159-182.

Clement, T.P., 1997. A Modular Computer Code for Simulating Reactive MultispeciesTransport in 3-Dimensional Groundwater Systems. Battelle Pacific Northwest Laboratory, Richland,WA.

Clement, T.P., Sun, Y., Hooker, B.S., Petersen, J.N., 1997a. Modeling natural attenuation of contaminants in saturated groundwater, Proceedings of the Fourth International In situ and On site Bioremediation conference, New Orleans, *Bioremediation,* 4 (1), 37-42.

Clement, T.P, Peyton, B.M., Skeen, R.S., Jennings, D.A., Petersen, J.N., 1997b. Microbial growth and transport in porous media under denitrification conditions: Experiment and simulations, Journal of Contaminant Hydrology*,* 24, 269-285.

Clement, T.P. and Johnson, C.D. and Sun, Y. and Klecka, G.M. and Bartlett, C. 2000. Natural attenuation of chlorinated ethane compounds: model development and field-scale application at the Dover site. Journal of Contaminant Hydrology. 42: 113-140.

Connaughton, D.F. and Stedinger, J.R. and Lion, L.W. and Shuler, M.L. 1993. Description of time varying desorption kinetics: Release of naphthalene from contaminated soils. Environmental Science and Technology. 27(12): 2397-2403.

Domenico, P. A., and F. W. Schwartz. 1998. *Physical and Chemical Hydrogeology*, 2nd ed., John Wiley & Sons, New York.

Freeze, R.A. and Cherry, J.A. 1979. *Groundwater.* Prentice Hall, Englewood Cliffs, NJ.

Frind, E. O. 1982. The Principle direction technique: A new approach to groundwater contaminant transport modeling. Finite Elements in Water Resources. K.O. Holz et al., (eds.), Springer Verlag, Berlin: 13-41.

Gelhar, L.W. and Welty, C. and Rehfeldt, K.R. 1992. A critical review of data on field-scale dispersion in aquifers. Water Resources Research. 28(7): 1955-1974.

Ghosal, S. and Luthy, R.G. 1996. Bioavailability of hydrophobic organic compounds from nonaqueous-phase liquids: The biodegradation of naphthalene from coal tar . Environmental Toxicology and Chemistry. 15(11): 1894-1900.

Guerin, W. F., and Boyd, S. A. 1992. Differential bioavailability of soil-sorbed naphthalene of two bacterial species. Applied and Environmental Microbiology. 58(4): 1142-1152.

Guerin, W. F., and Boyd, S. A. 1997. Bioavailability of naphthalene associated with natural and synthetic sorbents. Water Resources. 31(6): 1504-1512.

Harbaugh, A.W. and McDonald, M.G. 1996. User's Documentation for MODFLOW-96, an update to the U.S. Geological Survey Modular Finite-Difference Ground-Water Flow Model. U.S. Geological Survey, Reston, VA, Open-File Report 96-485; 1-56.

Harms, H. and T.N.P. Bosma. 1997. Mass transfer limitation of microbial growth and pollutant degradation. Journal of Industrial Microbiology & Biotechnology. 18:97-105.

Heitkamp, M.A. and Freeman, J.P. and Cerniglia, C.E. 1987. Naphthalene biodegradation in environmental microcosms: estimates of degradation rates and characterization of metabolites. Applied and Environmental Microbiology. 53(1): 129-136.

Kapoor, V. et al. 1997. Bimolecular second-order reactions in spatially varying flows: Segregation induced scale-dependent transformation rates. Water Resources Research. 33:527-536.

Knapp, R.B. and B.D. Faison. 1997. A bioengineering system for in situ bioremediation of contaminated groundwater. Journal of Industrial Microbiology & Biotechnology. 18:189-197.

Knapp, R.B. and Faison, B.D. 1997. A bioengineering system for in situ bioremediation of contaminated groundwater. Journal of Industrial Microbiology & Biotechnology. 18: 189-197.

Krumholz L.R. 1998. Microbial Ecosystems in the Earth's Subsurface. ASM News. 64(4): 197-202.

Lapidus, L. and Amundson, N.R., 1952. The rate determining steps in radial adsorption analysis. Journal of Physical Chemistry. 56(3): 373-383.

MacIntyre, W.G. and Antworth, C.P. and Stauffer, T.B. and Young, R.G. 1998. Heterogeneity of sorption and transport-related properties in a sand-gravel aquifer at Columbus, Mississippi. Journal of Contaminant Hydrology. 31: 257-274.

MacQuarrie, K.T.B. and Sudicky, E.A. 1990. Simulation of biodegradable organic contaminants in groundwater. 2. Plume behavior in uniform and random flow fields. Water Resources Research. 26(2): 223-239.

MacQuarrie, K.T.B. and Sudicky, E.A. and Frind, E.O. 1990. Simulation of biodegradable organic contaminants in groundwater. 1. Numerical formulation in principal directions. Water Resources Research. 26(2): 207-222.

McCarty, P.L. 1975. Stoichiometry of biological reactions. Prog. Water Technol. 7:157-172.

Mihelcic, J.R. and Luthy, R. G. 1988. Microbial degradation of acenaphthalene and naphthalene under denitrification conditions in soil-water systems. Applied and Environmental Microbiology. 54(5): 1188-1198.

Mihelcic, J.R. and Luthy, R. G. 1991. Sorption and microbial degradation of naphthalene in soil-water suspensions under denitrification conditions. Environmental Science and Technology. 25: 169-177.

Miralles-Wilhelm, F. et al. 1997. Stochastic analysis of oxygen-limited biodegradation in three-dimensionally heterogeneous aquifers. Water Resources Research. 33:1251-1263.

Molz, F.J. and Widdowson, M.A. 1988. Internal inconsistencies in dispersion-dominated models that incorporate chemical and microbial kinetics. Water Resources Research. 22(8): 1207-1216.

Mravik, S.C. and Sillan, R.K. and Wood, A.L. and Sewell, G.W. 2003. Field evaluation of the solvent extraction residual biotreatment technology. Environmental Science and Technology. 37(21): 5040-5049.

Murphy, E. M., Ginn, T. R., Chilakapati, A., Resch, C. T., Phillips, J. L., Wietsma, T. W., and Spadoni, C. M. 1997. The influence of physical heterogeneity on microbial degradation and distribution in porous media, Water Resources Research. 33(5), 1087-1104.

Odencrantz, J.E. and Valocchi, A.J. and Rittmann, B.E. 1990. Modeling two-dimensional Solute Transport with different biodegradation kinetics. NWWA/API Petroleum Hydrocarbon Conference; Houston, TX; Oct. 31 – Nov. 2, 1990.

Odencrantz, J.E. 1992. Modeling the Biodegradation Kinetics of Dissolved Organic Contaminants in a Heterogeneous Two-Dimensional Aquifer. Ph.D. Dissertation, University of Illinois at Urbana-Champaign; Urbana, IL.

Oya, S. and A.J. Valocchi. 1997. Characterization of traveling waves and analytical estimation of pollutant removal in one-dimensional subsurface bioremediation modeling. Water Resources Research. 33:1117-1127.

Oya, S. and Valocchi, A.J. 1998. Analytical approximation of biodegradation rate for in situ bioremediation of groundwater under ideal radial flow conditions. Journal of Contaminant Hydrology. 31: 275-293.

Oya, S. and Valocchi, A.J. 1998. Transport and biodegradation of solutes in stratified aquifers under enhanced in situ bioremediation conditions. Water Resources Research. 34(12): 3323-3334.

Park, J. and Zhao, X. and Voice, T.C. 2001. Biodegradation of non-desorbable naphthalene in soils. Environmental Science and Technology. 35: 2734-2740.

Park, J. and Zhao, X. and Voice, T.C. 2002. Development of a kinetic basis for bioavailability of sorbed naphthalene in soil slurries. Water Research. 36: 1620-1628.

Pedit, J.A. and Miller, C.T. 1995. Heterogeneous sorption processes in subsurface systems. 2. Diffusion modeling approaches. Environmental Science and Technology. 29(7): 1766-1772.

Priddle, M.W. and MacQuarrie, K.T.B. 1994. Dissolution of creosote in groundwater: an experimental and modeling investigation. Journal of Contaminant Hydrology. 15: 27-56.

Quinodoz, H.A.M. and Valocchi, A.J. 1993. Stochastic analysis of the transport of kinetically sorbing solutes in aquifers with randomly heterogeneous hydraulic conductivity. Water Resources Research. 29(9): 3227-3240.

Ramaswami, A. and Ghosal, S. and Luthy, R.G. 1996. Biodegradation of naphthalene from coal tar and heptamethylnonane in mixed batch systems. Environmental Science & Technology. 30(4): 1282-1291.

Ramaswami, A. and Ghosal, S. and Luthy, R.G. 1997a. Mass transfer and bioavailability of PAH compounds in coal tar NAPL-slurry systems. 2. Experimental Evaluations. Environmental Science & Technology. 31(8): 2268-2276.

Ramaswami, A. and Luthy, R.G. 1997b. Mass transfer and bioavailability of PAH compounds in coal tar NAPL-slurry systems. 1. Model development. Environmental Science & Technology. 31(8): 2260-2267.

Ramaswami, A., and Luthy, R.G. 1997c. Measuring and modeling physicochemical limitations to bioavailability and biodegradation. In Manual of Environmental Microbiology. 78: 721-729.

Rifai, H. S., Bedient, P. B., and Wilson, J. T. 1989. BIOPLUME Model for Contaminant Transport Affected by Oxygen Limited Biodegradation, EPA/600/M-89/019.

Rifai, H. S., and Bedient, P. B. 1990. Comparison of biodegradation kinetics with an instantaneous reaction model for groundwater. Water Resources Research. 26 (4), 637-645.

Rittman, B.E. and Valocchi, A.J. and Odencrantz, J.E. and Bae, W. 1988. In situ bioreclamation of contaminated groundwater. WRC Report No. 209. 1-121.

Rockne, K..J. and Strand, S.E. 2001. Anaerobic biodegradation of naphthalene, phenanthrene, and biphenyl by a denitrifying enrichment culture. Water Resources. 35(1): 291-299.

Seagren, E.A., Rittmann, B.E. , and Valocchi, A.J. 1993. Quantitative evaluation of flushing and biodegradation for enhancing in situ dissolution of nonaqueous phase liquids. Journal of Contaminant Hydrology. 12(1-2), 103-132.

Seagren, E.A., B.E. Rittmann, and A.J. Valocchi. 1994. Quantitative evaluation of the enhancement of NAPL-pool dissolution by flushing and biodegradation. Environmental Science & Technology. 28(5), 833-839.

Severson, K.J. et al. 1991. Hydrogeologic parameters affecting vadose-zone microbial distributions. Geomicrobiology Journal. 9:197-216.

Shan, C. and Stephens, D.B. 1994. Recommendations for Usage of SURFER to Gridding Model Results. Groundwater. 32(3): 503-506.

Srivastava, R. and Brusseau, M.L. 1996. Nonideal transport of reactive solutes in heterogeneous porous media: 1. Numerical model development and moments analysis. Journal of Contaminant Hydrology. 24: 117-143.

Starr, R.C. and Gillham, R.W. and Sudicky, E.A. 1985. Experimental Investigation of Solute Transport in Stratified Porous Media. 2. The Reactive Case. Water Resources Research. 21(7): 1043-1050.

Starr, R.C. et al. 1985. Experimental investigation of solute transport in stratified porous media. 2. The reactive case. Water Resources Research. 21:1043-1050.

Sturman, P.J., Stewart, P.S., Cunningham, A.B., Bouwer, E.J., and Wolfram, J.H. 1995. Engineering scale-up of in situ bioremediation processes: A review. Journal of Contaminant Hydrology. 19(1):171-203.

Stringfellow, W.T. and Alvarez-Cohen, L. 1999. Evaluating the relationship between the sorption of PAHs to bacterial biomass and biodegradation. Water Resources. 33(11): 2535-2543.

Sun, Y. and Petersen, J.N. and Clement, T.P. and Hooker, B.S. 1998. Effect of reaction kinetics on predicted concentration profiles during subsurface bioremediation. Journal of Contaminant Hydrology. 31: 359-372.

Szecsody, J.E. and Brockman, F.J. and Wood, B.D. and Streile, G.P. and Truex, M.J. 1994. Transport and biodegradation of quinoline in horizontally stratified porous media. Journal of Contaminant Hydrology. 15(4): 277-304.

Tebes-Stevens, C. Valocchi, A.J. VanBriesen, J.M. and Rittman, B.E. 1998. Multicomponent transport with coupled geochemical and microbiological reactions: model description and example simulations. Journal of Hydrology. 209: 8-26.

Toride, N. and Leij, F.J. and van Genuchten, M.T. 1993. A comprehensive set of analytical solutions for nonequilibrium solute transport with first-order decay and zero-order production. Water Resources Research. 29(7): 2167-2182.

United States Environmental Protection Agency. 1996. Bioremediation of Hazardous Waste Sites: Practical Approaches to Implementation. Office of Research and Development. EPA/625/K-96/001. May 1996. 1-8.

United States Environmental Protection Agency. 2001. Use of Bioremediation at Superfund Sites. Solid Waste and Emergency Response. Office of Solid Waste and Emergency Response. EPA/542/R-01/019. September 2001. 1-9–1-12.

Valocchi, A., and others. 1998. FEREACT Draft user guide, personal communication to Dr. Eric Seagren, University of Maryland, College Park.

van Loosdrecht, M.C. M. and Lyklema, J. Norde, W. and Zehnder, A.J.B. 1990. Influence of interfaces on microbial activity. Microbiological Reviews. 54(1): 75-87.

van Genuchten, M.T. and Wierenga, P.J., 1976. Mass transfer studies in sorbing porous media I. Analytical solutions. Soil Science Society of America Journal. 40: 473-480.

Verschueren, K. 2001. Handbook of Environmental Data on Organic Chemicals. 4th edition, John Wiley & Sons Inc., New York.

Waterloo Hydrogeologic Inc. 2000. Visual MODFLOW v.2.8.2 User's Manual. 1-303.

Wilson, L.P. and D'Adamo, P. C. and Bouwer, E.J. 1997. Bioremediation of BTEX, naphthalene, and phenanthrene in aquifer material using mixed oxygen/nitrate electron acceptor conditions. National Risk Management Research Laboratory., U.S. Environmental Protection Agency. EPA/600/SR-97/120. 1-6.

Wood, B.D. and Dawson, C.N. and Szecsody, J.E. and Streile, G.P. 1994. Modeling contaminant transport and biodegradation in a layered porous media system. Water Resources Research. 30(6): 1833-1845.

Yabusaki, S.B. and Steefel, C.I. and Wood, B.D. 1998. Multidimensional, multicomponent, subsurface reactive transport in nonuniform velocity fields: code verification using an advective reactive streamtube approach. Journal of Contaminant Hydrology. 30: 299-331.

Yang, X., Erickson, L.E., and Fan, L.T. 1994. Dispersive-convective characteristics in the biorestoration of contaminated soil with a heterogeneous formation. Journal of Hazardous Materials. 38, 163-185.

Zheng, C. 1990. A Modular Three-Dimensional Transport Model for Simulation of Advection, Dispersion and Chemical Reactions of Contaminants in Groundwater Systems. S.S. Papadopulos & Associates, Inc., Bethesda, MD, Oct. 1990.